Master's thesis

NTNU
Norwegian University of Science and Technology
Faculty of Engineering
Department of Marine Technology

Andreas Isaksen

Estimating the replacement potential of offshore support vessels with zero-emission hydrogen solutions

Master's thesis in Marine Technology
Supervisor: Stein Ove Erikstad
June 2022

NTNU
Norwegian University of
Science and Technology

Andreas Isaksen

Estimating the replacement potential of offshore support vessels with zero-emission hydrogen solutions

Master's thesis in Marine Technology
Supervisor: Stein Ove Erikstad
June 2022

Norwegian University of Science and Technology
Faculty of Engineering
Department of Marine Technology

NTNU
Kunnskap for en bedre verden

NTNU | Department of Marine Technology

Master Thesis in Marine Systems Design

Estimating the replacement potential of offshore support vessels with zero-emission hydrogen solutions

Andreas Isaksen

Spring 2022

Background
To reach the zero-emission goal by 2050, a development in the offshore fleet is needed. *The end of the oil era* is regularly being brought up in the media. However, the offshore fleet will still be essential in many years. Unfortunately, most of today's offshore vessels run on fuels that produce significant emissions. Therefore, a change is needed to achieve the 2050 goals.

Overall aim and focus
The thesis will investigate the replacement potential of today's offshore support vessels running on MDO with zero-emission hydrogen solutions, and the corresponding impact on design, operational profile, and fuel infrastructure development.

Scope and main activities
The thesis will cover the following main points:

1. Provide a short overview of the status and essential development trends related to hydrogen as fuel.
2. Use AIS data to analyze the operational profiles of OSVs to map the demand placed on vessels in the offshore market.
3. Determine the theoretical sailing distances of various hydrogen solutions.
4. Develop a systematic approach to exhibit the applicability of hydrogen in OSVs by comparing demand with theoretical sailing distances.
5. Discuss and conclude if OSVs can operate with hydrogen propulsion.

Modus operandi
At NTNU, Professor Stein Ove Erikstad will be the responsible advisor. The work shall follow the guidelines given by NTNU.

Prof. Stein Ove Erikstad

Preface

This master thesis corresponded to 30 ECTs and was written in the spring of 2022. It is a part of the master's degree at the Department of Marine Technology, NTNU - Norwegian University of Science and Technology. A project thesis with the same topic was completed in 2021. A large part of the background study for the master thesis is based on this preparatory work.

The main objective of the thesis is to estimate the replacement potential of offshore support vessels with zero-emission hydrogen solutions. Ships are some of the most effective transportation methods and will be relevant for many years. Meanwhile, they contribute to the emission of undesirable greenhouse gases. Using hydrogen as fuel might be one of the solutions to reach the zero-emission goals by 2050.

After more than four years at the Institute of Marine Technology in Trondheim with Marine Systems Design as my specialization, I have gained an extra interest in zero-emission shipping and the decarbonization of the maritime industry. I believe there will be an immense development within this industry in the future. This made the subject exciting to work with, and I hope this can be reflected in the thesis itself.

I want to thank Professor Stein Ove Erikstad for his excellent collaboration throughout the writing process. Our discussions and conversations have contributed to several valuable objectives and key points towards the finishing of my thesis. Furthermore, I must express my gratitude to Ocean Hyway Cluster, who gave me access to some of their internal reports. In addition, I will highlight my friends in the office at the Marine Technology Centre as essential contributors to my thesis. Numerous obstacles have been solved jointly in office A2.011. At last, I would like to thank Solstad Offshore and YXNEY Maritime for letting me use values from their database.

Andreas Isaksen

Andreas Isaksen

Trondheim, 09.06.2022

Abstract

This thesis investigates the replacement potential of today's offshore support vessels (OSVs) with hydrogen fuel cell (FC) solutions to move towards a zero-emission society by 2050. The net-zero goal is crucial for reducing emissions and giving the world a fair chance of restraining the global temperature rise by 1.5 ℃. Ships are essential in today's globalization, thus also a vital part of the solution to achieving the zero-emission targets. However, shipping accounts for significant annual greenhouse gas emissions, and it is evident that amendments are necessary to turn the situation.

A systematic approach is established to analyze the demand placed on the vessels operating in the offshore market. Comparing this with a theoretical sailing range for various hydrogen FC solutions will exhibit applicability. The operating patterns are gathered using data from the automatic identification system (AIS), and the theoretical sailing range is calculated by analyzing power consumption, fuel efficacy, and storage characteristics. Assumptions regarding hydrogen infrastructure and vessel design are based on reasonable future scenarios from the literature review.

The results revealed a great potential for hydrogen FC propulsion for OSVs. Especially platform supply vessels (PSVs) emerged as one of the OSV types with the most significant potential, where liquid hydrogen (LH_2) stored at -252 ℃ proved to be the solution with the best applicability. This implies that the offshore vessels can make substantial emission reductions toward a zero-emission society by 2050, provided that the assumptions regarding infrastructure are applicable. Future research should look more into the hydrogen FC conversion cost, as the technology is immature and with several barriers to overcome. In order to make the transition profitable, it should be more cost-effective and practically feasible in the future.

Keywords: Offshore support vessels, offshore construction vessels, platform supply vessels, anchor handling tug & supply vessels, zero-emission, net-zero 2050, hydrogen, AIS

Sammendrag

Denne oppgaven undersøker erstatningspotensialet for dagens offshore skipsflåte med hydrogen brenselscelleløsninger, med det formål å gå mot et nullutslippssamfunn i 2050. Målet om netto nullutslipp i 2050 er viktig for å redusere utslippene og gi verden en realistisk sjanse for å begrense den globale temperaturøkningen til 1.5 ℃. Skip er helt essensielle i dagens globalisering og har dermed også en nøkkelrolle i løsningen mot å nå nullutslippsmålene. Skipsfarten står imidlertid for store årlige klimagassutslipp og det er åpenbart at endringer er nødvendig for å snu situasjonen.

For å svare på problembeskrivelsen ble det etablert en systematisk tilnærming for å analysere kravene som stilles til fartøyene i offshoremarkedet. Å sammenligne disse kravene med den teoretiske seilingsdistansen for ulike hydrogenløsninger vil gi en indikasjon på hvor realistisk det er å bruke hydrogen som drivstoff. Operasjonsmønstrene blir identifisert ved å bruke AIS data og den teoretiske seilingsdistansen blir beregnet ved å se på energiforbruket, drivstoffeffektiviteten og lagringsegenskapene til de ulike løsningene. Antagelser rundt infrastrukturen til hydrogen og fartøysdesign er basert på realistiske framtidsscenarier fra litteraturstudien.

Resultatene avslørte at det ligger et stort potensiale i å bruke brenselsceller og hydrogen som fremdrifstmiddel i OSV'er. Spesielt PSV'ene skilte seg ut som den typen som egnet seg best, og flytende hydrogen lagret på -252 ℃ viste seg å være den løsningen med høyest realiserbarhet. Dette betyr at offshorefartøyene kan bidra til store utslippskutt mot et nullutslippssamfunn i 2050, gitt at antagelsene om infrastruktur gjelder. Videre arbeid bør fokusere på økonomien knyttet til bruk av brenselsceller og hydrogen i skip. Siden teknologien er relativt ny og kompleks vil den mest sannsynlig være kostbar. For å gjøre overgangen til hydrogendrift lønnsom bør den bli billigere og mer praktisk anvendbar i fremtiden.

Table of Contents

List of Figures

List of Tables

Acronyms

AFC Alkaline Fuel Cell.

AH Anchor Handling.

AHTS Anchor Handling Tug and Supply.

AIS Automatic Identification System.

atm Atmospheric Pressure.

CAPEX Capital Expenditures.

CH_2 Compressed Hydrogen.

D_{max} Maximum Theoretical Sailing Distance.

DMFC Direct Methanol Fuel Cell.

DP Dynamic Positioning.

dwt Deadweight Tonnage.

ECA Emission Control Area.

FC Fuel Cell.

GHG Greenhouse Gas.

gt Gross Tonnage.

HFO Heavy Fuel Oil.

HHV Higher Heating Value.

HT-PEMFC High Temperature Proton Exchange Membrane Fuel Cell.

IEA International Energy Agency.

IMO International Maritime Organization.

LH_2 Liquid Hydrogen.

LHV Lower Heating Value.

LNG Liquefied Natural Gas.

MCFC Molten Carbonate Fuel Cell.

MDO Marine Diesel Oil.

MGO Marine Gas Oil.

MMSI Maritime Mobile Service Identity.

NOK Norwegian Kroner.

NOx Nitrogen Oxide.

OCV Offshore Construction Vessel.

OPEX Operational Expenditures.

OPS Onshore Power Supply.

OSV Offshore Support Vessel.

PAFC Phosphoric Acid Fuel Cell.

PEM Proton Exchange Membrane.

PEMFC Proton Exchange Membrane Fuel Cell.

PSV Platform Supply Vessel.

ROV Remote Operated Vehicles.

SDG Sustainable Development Goals.

sfc Specific Fuel Consumption.

SOFC Solid Oxide Fuel Cell.

SOG Speed Over Ground.

SOx Sulfur Oxide.

SWOT Strengths, Weaknesses, Opportunities and Threats.

USD U.S. Dollar ($).

Chapter 1

Introduction

Ships play a vital part in today's globalization. Unfortunately, the global fleet accounts for significant emissions. From 2007 to 2012, shipping accounted for 2.8 % of the annual global greenhouse gas (GHG) emissions [Jafarzadeh and Schjølberg, 2017]. Ships are some of the most effective transportation methods, and numerous worldwide operations depend on them [International Energy Agency, 2021]. Roughly 80 % of global trade by volume and 70 % by value is transported by sea [Concawe, 2016]. A fleet development is needed to reach the zero-emission goal by 2050. According to DNV [2020], maritime transport needs to reduce emissions by at least 95 % to contribute to a global net-zero by 2050. *The end of the oil era* is regularly being brought up in the media. However, the offshore fleet will still be essential for many years. Unfortunately, most of today's offshore vessels run on fuels that produce significant emissions. A change is needed to achieve the 2050 goals. Among the available solutions, hydrogen in combination with fuel cells (FCs) looks promising from an environmental point of view. This combination may be a valuable alternative to zero-emission transportation in the future. Burheim [2017] claims that hydrogen is one of the most compelling substances to be used as an energy carrier in the transportation sector. United Nations Industrial Development Organization [2018] states that hydrogen is still not fully recognized in the power industry but promotes hydrogen with three main sustainable development goals (SDGs) illustrated in Figure 1.1.

Figure 1.1: Sustainable development goals.

Source: [United Nations, 2022]

Some substantial obstacles need to be overcome for the hydrogen revolution to occur. Although hydrogen is the most abundant element in the universe, it is rare to see it in pure form on earth. Burheim [2017] summarizes three main problems when it comes to hydrogen as a fuel:

- *Getting hydrogen in its pure elemental form.*
- *Getting it on the vehicle in a storable form.*
- *Finding a way to convert it into power efficiently.*

In contrast to petroleum, which is an energy source, hydrogen is an energy carrier [Mazloomi and Gomes, 2012]. Energy is needed as input to create hydrogen and is often done by using methane or electricity. The word hydrogen comes from the two Greek words *hydro* and *genes*, meaning *water* and *generator* [Midilli et al., 2005]. The only byproduct of using hydrogen in a FC is pure water. This means that as long as the hydrogen is made from sustainable resources, it can play an important role in the decarbonization of the maritime industry [The Economist, 2021].

The thesis aims to investigate the replacement potential of today's offshore support vessels (OSV) running on marine diesel oil (MDO) with zero-emission hydrogen solutions. Oskar Levander, head of Kongsberg Maritime's work with zero-emission vessels for the future, states in Teknisk Ukeblad [2022] that none of today's zero-emission solutions stand out as better than others, and he understands that ship owners struggle to choose what investment strategy to use. The thesis intends to provide better insight into hydrogen's possibilities as a fuel.

Figure 1.2 summarizes the three main parts covered in this master thesis. First, the theoretical energy content of hydrogen is used to calculate the maximum theoretical sailing distances, which hereby will be denoted as D_{max}. Second, the power consumption of the various OSV types is mapped. A fleet containing offshore construction vessels (OCVs), platform supply vessels (PSVs), and anchor handling tug & supply (AHTS) vessels will be the main focus of the thesis. By distinguishing between these types, it may be possible to point out any differences when it comes to potential. At last, a comprehensive market analysis is performed, which is an essential factor before the execution of a potential conversion process. It is done by using data from an automatic identification system (AIS) to identify the operation pattern of each vessel. AIS data is often used as a tool in fleet analysis to streamline the routing in terms of emissions and efficiency [Sundvor et al., 2021].

Furthermore, the operational profile is used to map the demand placed on the vessels in the offshore market. According to Cambridge Dictionary [2022], demand is the need for something to be sold or supplied. At last, the need is compared with D_{max} and power consumption to see if it is possible to meet today's demand with vessels running on hydrogen.

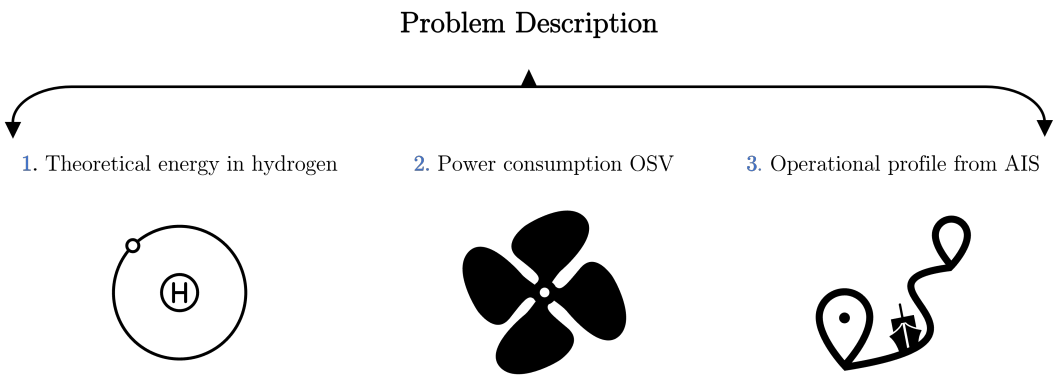

Figure 1.2: Illustration of problem description.

Chapter 2 describes the system boundaries used in the thesis, what assumptions were made in advance, and a quick introduction to the data used. Chapter 3 contains the background study, where a large part is taken from the project thesis that was written in the autumn of 2021. Chapter 4 describes the methods used to produce results to answer the problem description. Chapter 6 will be the part where the results are presented. Chapter 7 consists of a discussion and addresses the limitations and considerations for further work. At last, Chapter 8 presents a short and concise conclusion.

Chapter 2

Establishing system boundaries

This chapter summarizes the system boundaries with the purpose of clarifying the main focus of the thesis. The life cycle of hydrogen is large and complex, and hydrogen production could have been a field of study in itself. Therefore, it is crucial to establish some boundaries. As described in the introduction, the thesis will analyze the operational profiles of today's OSVs and evaluate if it is realizable to run these with hydrogen. This is done by investigating hydrogen's properties and examining if the demands from today's OSVs can be met with a hydrogen vessel.

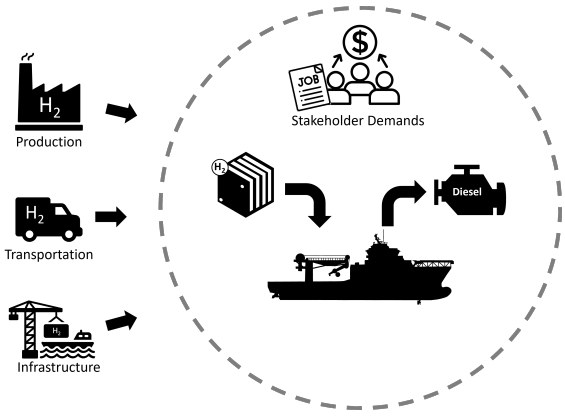

Figure 2.1: Illustration of system boundaries

The main focus of the thesis is visualized in Figure 2.1. Production, transportation, and hydrogen infrastructure are neglected and thus outside the system boundaries. For hydrogen ships to be completely emission-free, the hydrogen has to be made from renewable sources, so-called *green hydrogen*. Another assumption is that there will be no emissions from neither the transportation nor the infrastructure. The hydrogen-based energy process (energy to hydrogen, to energy again) consists of four main processes: production, storage, safety, and utilization [Dawood et al., 2020]. This study will not cover all these four stages. It will, as already mentioned, assume that both the production and safety aspect is fulfilled and only look at the final part (hydrogen to energy) taking place on the ship itself. In other words, from *tank-to-wake*.

Despite hydrogen being zero-carbon-emission energy at the end-use point, it depends on the cleanness of the production pathway and the energy used to produce it.
[Dawood et al., 2020]

Furthermore, the financial part is mainly set aside in the analysis. Hydrogen solutions today are complex, and the technology is relatively new. DNV [2019] states that if a transition to hydrogen ever will be profitable, it must become more cost-effective and practically feasible. The

background study in Chapter 3 will briefly introduce the most critical cost differences between hydrogen and diesel solutions. The results in Chapter 6 present the capital expenditures (CAPEX) and operational expenditures (OPEX). A list of vessels was gathered by using maritime mobile service identity numbers (MMSI) and further separated by using three different types of OSVs, OCV, PSV, and AHTS vessel. A total of 283 vessels were used in the mapping, 66 OCVs, 122 PSVs, and 95 AHTSs. The characteristics for the fleet was gathered from Vesselfinder [2022] by using a python code for web scraping, which was initially created by Associate Professor Ekaterina Kim for use in a previous course at the Department of Marine Technology, *TMR12 - Ocean System Simulation*. The vessel characteristics can be seen in Appendix A. Figure 2.2 shows the length and deadweight tonnage (dwt) distribution of the vessels in the database. The trend is that the OCVs are mainly larger than the PSVs and AHTS vessels. All ships were picked randomly from well-established shipping companies around the world. They are supposed to illustrate an average OSV, and by investigating their operational profiles, it is possible to get a good picture of how the average OSV operates. The vessel names and MMSI numbers are not listed with the purpose of keeping the vessels and shipping companies anonymous.

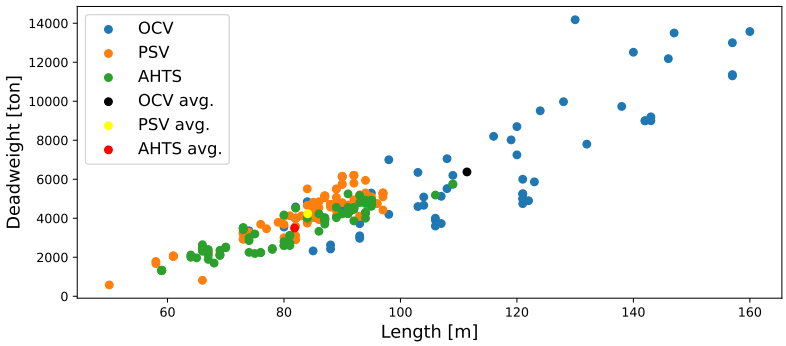

Figure 2.2: Characteristics of vessel database.

The primary input in python is the AIS data gathered from The Norwegian Coastal Administration through NTNU. The AIS data is of message type 1, consisting of time, position, speed, course, MMSI, and status. The data time window extends from 01.01.2020 to 31.12.2020, with a few exceptions where some vessel data is missing a few months. Figure 2.3 illustrates the area covered by the given AIS data. The data length has been chosen to take into account the seasonal variations within a year. It can be further discussed if 2020 was a bad year in the offshore market and if this can potentially lead to an imprecise picture of how the market is. The AIS data was given as a database (*.db*) file, and there was a significant variation in the data size for the different vessels. Some vessels had AIS data consisting of more than 200 000 lines, while others only had 64 lines. Therefore, the data quality had to be constantly evaluated and cleaned if necessary. Different hydrogen storage solutions in combination with FCs are used as examples when determining the potential energy content of hydrogen. Conventional diesel machinery running on MDO is used for comparison.

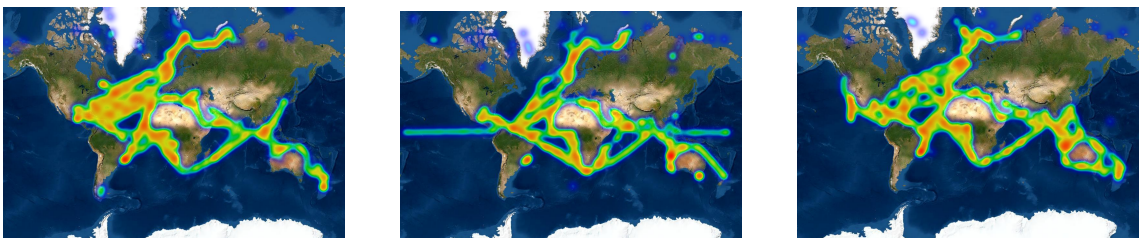

(a) OCV (b) PSV (c) AHTS

Figure 2.3: AIS data coverage.

Chapter 3

Background study

This chapter will provide insight into previous research and similar projects carried out with hydrogen as the main topic. The background study is presumed to gain knowledge about the subject and get a more extensive overview of the current hydrogen status. At last, the problem description will be answered using the insight obtained in this background study.

3.1 Hydrogen today

Hydrogen as a fuel is getting more and more attention as the years go by. Despite the destructive impact of the pandemic on the automotive industry, more FC-driven cars were shipped in 2020 than ever before [E4Tech, 2020]. In America, the California Energy Commission announced its largest investment in hydrogen infrastructure since 2015, funding 110 new stations over the next five years. FC-driven buses are becoming more and more popular all around the world. China has the world's largest bus market and the largest FC electric bus park, with around 3600 buses. Norway is also joining the hydrogen trend; Scania has supplied ASKO with four hydrogen-powered trucks of 26 tonnes. They are installed with 90 kW PEMFC. Hydrogen is considered in the maritime industry as well. Companies like Ballard, CMR Protech, Nedstack, PowerCell, and Proton Power have all received orders for hydrogen-based shipping applications for 2021.

In 2020, Enova decided to give 14.6 MNOK in support to the Norwegian ferry company Norled [Enova, 2020]. This project will be the first to rebuild a ferry from bio-diesel propulsion to hydrogen FC propulsion. It will also be the first ferry to use compromised hydrogen as an energy carrier. Enova calculated the emission reduction potential to be 1 647 114 CO_2 equivalents per year. Norled has several interesting projects related to hydrogen. MF Hydra, shown in Figure 3.1, will be the first ferry to use liquefied hydrogen as fuel in combination with FCs [Maritimt Forum, 2021]. The ferry will start with battery propulsion in the summer of 2021 before it moves over to hydrogen propulsion during the spring of 2022. Linde will deliver the hydrogen in addition to building and installing the storing facilities. The hydrogen is produced by the world's largest proton exchange membrane (PEM) electrolysis plant in Leuna, Germany, with a capacity of 24 MW. The ferry is equipped with two 200 kW FCwave modules and 80 m^3 liquid H_2 storage [E4Tech, 2020].

Figure 3.1: Norled's MF Hydra

Source: [Maritimt Forum, 2021]

Norway's first production plant for liquid hydrogen (LH_2) is planned to be built at Mongstad Industrial park [E24, 2021]. The plan is to start producing 6 tonnes of renewable hydrogen each year from 2024 using electrolysis. It will be a cooperation between BKK, Air Liquide, and Equinor. The main goal is to build a complete supply chain for LH_2 for the shipping industry. Additionally, Wilhelmsen plan to build two hydrogen cargo vessels to be used in this project [Wilhelmsen, 2020]. The main focus will be to distribute LH_2 along the west coast of Norway. The project is called Topeka and was awarded 219 MNOK by Enova in 2020. The vessels will transport both coastwise customer cargo and LH_2 to bunkering hubs along the coast, potentially removing up to 25 000 trucks from the road each year.

Figure 3.2: Wilhelmsen's Topeka hydrogen project

Source: [Wilhelmsen, 2020]

Havyard is another company that has taken part in the hydrogen revolution. They established a separate business called Havyard Hydrogen with the purpose of creating marine zero-emission energy systems. Havyard Hydrogen offers a propulsion system containing 3.2 MW FCs. This system is scalable and can be used by both large and small vessels [Havyard, 2021].

Back in 2019, according to [DNV, 2019], several initiatives were considering hybrid solutions with hydrogen in the shipping industry. They stated that the shipping segments with the most potential were the car and passenger ferries and high-speed vessels. But there was also potential in the offshore segment. However, due to the current economic situation of the offshore shipping companies, DNV expects negative growth. Still, DNV assumes that there will be hydrogen propulsion on four vessels by the end of 2030, with a total annual need of 2500 tonnes of hydrogen.

3.1.1 Hydrogen demand in the maritime sector

Arena Ocean Hyway Cluster [2020] published a report to map and estimate the potential future hydrogen demand in the Norwegian domestic maritime sector. The main focus of the report was hydrogen and ammonia, with offshore, domestic ferries, and high-speed passenger ferries as the main sectors. The article reveals, among other things, that there will be a significant demand for both ammonia and hydrogen in the domestic maritime sector in 2035, both liquid and compressed hydrogen (CH_2). DNV estimated that the Norwegian maritime sector alone had 4.8 million tonnes of CO_2 emission in 2017 Arena Ocean Hyway Cluster [2020].

The report concludes that CH_2 is the best technical and economical alternative in cases where it is possible to install the necessary equipment and bunkering solutions. Furthermore, they assume that this solution is best for vessels using less than 1000 kg hydrogen between bunkering operations. Figure 3.3a shows the estimated future demand for CH_2.

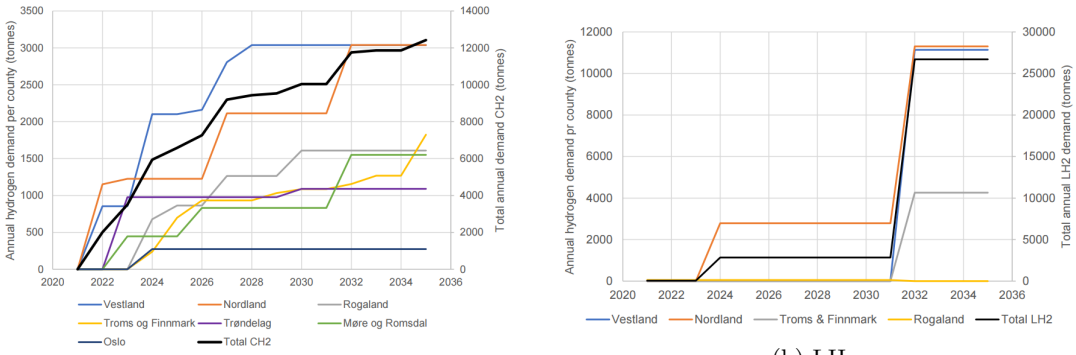

(a) CH_2

(b) LH_2

Figure 3.3: Estimated development of hydrogen demand.

Source: [Arena Ocean Hyway Cluster, 2020]

Moreover, the report concludes that LH_2 is the best hydrogen option in cases with space limitations, limited bunkering time, and other technical constraints. The estimated future demand for LH_2 can be seen in Figure 3.3b. In a report from 2020, *Pathway To Net Zero*, DNV [2020] states that hydrogen is a part of the net-zero strategy for the countries trying to decarbonize. The paper states that hydrogen will account for around 16 % of the energy demand in road transport within 2050. Furthermore, DNV claim that hydrogen and its derivatives may supply 75 % of the maritime fuel mix by 2050. Cluster [2020] claims that there are several complications regarding hydrogen as fuel. Table 3.1 summarizes the characteristics presented by Cluster [2020] and compares the hydrogen solutions with fossil fuels.

Table 3.1: Fuel ratings and predictions from Cluster [2020]

	MGO	**HFO**	**CH_2**	**LH_2**
Sustainability	Poor	Poor	Good	Good
Local Emission	Poor	Poor	Good	Good
Comfort	Fair	Fair	Good	Good
Cost	Good	Good	Poor	Poor
Storage Density	Good	Good	Poor	Poor
Availability	Good	Good	Fair	Poor
Safety	Good	Good	Fair	Fair
Maturity	Good	Good	Fair	Poor

3.1.2 Emission control areas

A large part of today's OSVs operate in emission control areas (ECAs), regions that are highly controlled with respect to emissions. Figure 3.4 illustrates both existing and possible future ECAs described by DNV-GL [2022]. The International Maritime Organization (IMO) limits the primary air pollutants contained in ship exhaust gas through MARPOL Annex VI [IMO, 2022]. Globally, the sulfur oxide regulations (SOx) were set to a maximum content of 0.5 % from 1st January 2020. Additionally, more strict regulations were set in the areas shown in Figure 3.4, where the SOx content must be less than 0.1 %. The ECAs also have strict regulations for nitrogen oxides (NOx), 3.4 g/kWh if the vessel has an engine speed lower than 130 rpm [International Maritime Organization, 2021].

Figure 3.4: ECAs.

Source: [Bø, 2016]

A CO_2 tax of 2.05 NOK/L (2.43 NOK/kg) must be expected when the vessel sails on MDO in 2022 [Finansdepartementet, 2022]. Additionally, vessels with installed propulsion systems of more than 750 kW have to pay a tax of 23.79 NOK per kilo NOx emissions [Skatteetaten, 2022]. The NOx taxes have risen by 8.4 % over the last five years, and it is expected to grow in the future. The development of the NOx taxes from 2018 to 2022 can be seen in Appendix C.

3.1.3 Potential emission reduction

More strict emission areas may be a solution toward a net-zero emission shipping industry by 2050 and can lead to shipowners having to take action. The predicted annual emissions from the world fleet, both IMO-registered and non-IMO, are 20.9 million tonnes of NOx and 831.3 million tonnes of CO_2 [Johansson et al., 2017]. Jafarzadeh and Schjølberg [2017] state that alternative fuels and power systems are required to reduce emissions in shipping. Hydrogen and FCs are some of the most promising alternatives [Dawood et al., 2020]. Figure 3.5 illustrates some of the most beneficial sides of hydrogen and FCs. Hydrogen will reduce air emissions directly by controlling the emission formation. In addition, the FC will indirectly reduce energy consumption through energy efficiency, thus also the emissions.

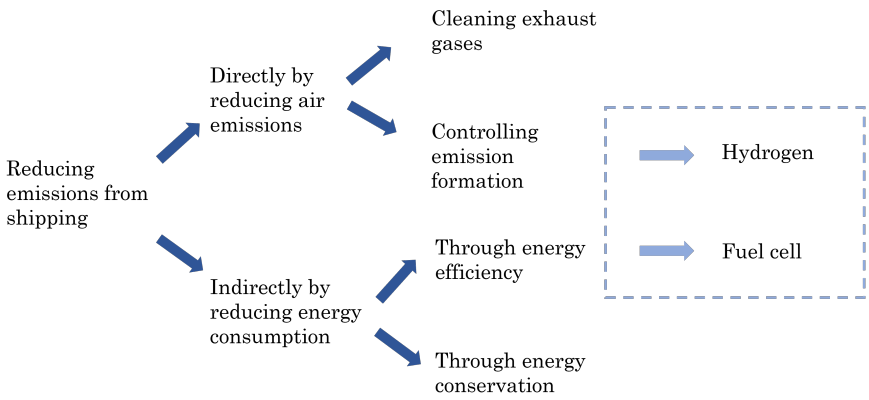

Figure 3.5: Emission formation and energy efficiency of hydrogen and FC.

Source: [Jafarzadeh and Schjølberg, 2017]

Risholm and Amon Maritime [2020] calculate the carbon dioxide reduction potential based on *tank-to-wake* and further assume that there are no emissions when operating on hydrogen. Due to high uncertainty in the future demand of the offshore sector, the calculations used a *low scenario* case. Arena Ocean Hyway Cluster [2020] estimates a CO_2 reduction potential of 728 661 tonnes per year for the offshore sector. For comparison, the carbon dioxide emissions from passenger cars and heavy transport in Norway were approximately 8.2 million tonnes in 2020 [SSB, 2021].

Table 3.2: Key characteristics of alternative fuels [Gilbert et al., 2018].

Fuel	**sfc** [g/kWh]	**Fuel Emission Factor** [g/kWh]			
		CO_2	CH_4	SOx	NOx
MDO	170	524	0.010	0.32	14.8
LH_2	57	0	0	0	0

Table 3.2 includes some relevant fuel characteristics gathered from Gilbert et al. [2018]. This article states that there are two main motivations for alternative fuels in shipping. The first one is to comply with current and future regulations, and the second one is to mitigate climate change by reducing GHG emissions.

3.2 Similar work

Many similar projects have been carried out in the past. In 2017 Ianssen et al. [2017] concluded that from a technological standpoint, the Norwegian fast ferry sector could become zero-emission in 2022. Aarskog and Danebergs [2020] estimates the energy demand in the Norwegian high-speed passenger ferry sector towards 2030, with the primary goal of mapping and assessing the potential hydrogen consumption. The energy consumption for each route is estimated based on the high-speed ferries' route length and fuel consumption. In conclusion, the study states a large potential for zero-emission operation. Out of 96 investigated routes, 51 of them could be hydrogen-powered, which would lead to an annual hydrogen consumption of 8710 tonnes and a reduction of fossil fuels by 93 % for the high-speed passenger ferry sector.

Another similar project is described by Sundvor et al. [2021], which also studied the potential of replacing today's high-speed passenger vessels with CH_2 solutions. The study uses AIS data from 2018 in combination with a modeled energy consumption. The AIS data is used to track vessel movements and provide a basis for a thorough fleet analysis. The paper concluded that 51 out of the 73 vessels were suitable for hydrogen propulsion. The Norwegian government plans that all public transport should be fossil-free by 2050 [Regjeringen, 2019], which includes high-speed passenger vessels.

A study from Strømgren et al. [2020] evaluates the economic feasibility of FC-powered high-speed crafts. It compares with today's diesel propulsion systems and future scenarios using real-world operation profiles. AIS data is used to map the position of the route and further combined with speed and power characteristics for a concept vessel. The study concludes that high-speed crafts with FC systems are 28 % more expensive than diesel alternatives. He claims that the first hydrogen driven high-speed ferry will not be cost-competitive with conventional technology, mainly because of the high development costs. By weight, the study assumes that the FCs installed in the high-speed ferry will weigh 150 kg per 100 kW FC module.

GKP7H2 is a pilot project part of DNV-GLs Green Coastal Shipping Program and is further described by Nygård and Strømgren [2017]. The story behind the name is that the project was taken up by DNV-GL as pilot project number seven and into *Grønt Kystfartsprogram*, with hydrogen as a primary fuel. The project is based on a high-speed ferry route between Florø and Måløy with a long-term goal of getting hydrogen established as an alternative energy carrier for passenger ferries. The concept vessel is designed by Brødrene Aa, with an installed engine power of 1200 kW, a speed of 28 knots, and a length of 30 meters. Figure 3.6 illustrates the concept design by Brødrene Aa. The three hydrogen tanks can be seen on the vessel's top deck, each tank with a pressure of 250 bar and a hydrogen capacity of 150 kg.

Figure 3.6: Sketch of the pilot project GKP7h2, with design from Brødrene Aa.

Source: [Nygård and Strømgren, 2017]

This section reveals that several studies focus on high-speed passenger ferries, mainly because they have the highest emissions of GHGs per passenger-km traveled [Sundvor et al., 2021]. Yet, these studies have many similarities with the topic in this thesis and can be used for comparison.

3.3 Theoretical energy content of hydrogen

Hydrogen is the most abundant element in the universe [McCarty et al., 1981]. However, practically none of it exists as free hydrogen gas [Zumdahl, 2009]. In 1981, McCarty et al. [1981] wrote that hydrogen was being seriously considered as a recyclable fuel substitute for petroleum and natural gas.

> *Considering a nonfossil fuel-based economy, we can engineer energy storage, distribution, and propulsion systems from less than a kW up to several MW using hydrogen systems.*
> *[Burheim, 2017]*

Even though hydrogen has a high energy density by weight and seems like a compelling choice for a future fuel, three main problems are associated with its use: costs of production, storage, and transport [Zumdahl, 2009]. The following sections will look more into the achievable energy output of hydrogen with FCs.

3.3.1 Thermodynamic properties of hydrogen

Dawood et al. [2020] summarize the results from more than 340 different sources. It claims that the energy content at higher heating value (HHV) of hydrogen is 141.8 MJ/kg at 298 K (25 ℃), and the lower heating value (LHV) is 120.0 MJ/kg. Compared to, e.g., gasoline, the hydrogen energy content is much higher by weight. Gasoline has a LHV of 42.5 MJ/kg [Bossel, 2003]. On the other hand, the volumetric energy density (J/m^3) of hydrogen is much lower compared to gasoline and other fossil fuels. 8 MJ/L and 32 MJ/L for hydrogen and gasoline [Dawood et al., 2020]. The difference between the variety of fuels can be seen in Figure 3.7, which clearly illustrates the low volumetric density of hydrogen compared to other alternatives. Low volumetric energy density may cause the hydrogen solutions to require more space than today's MDO solutions, especially when the range becomes longer.

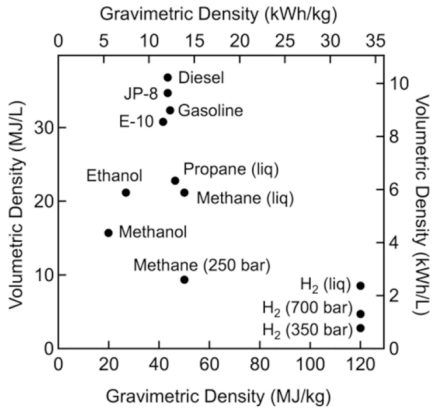

Figure 3.7: Gravimetric and volumetric energy densities of common fuels.

Source: [U.S Department of Energy, 2017]

The energy density of hydrogen is a major factor in investigating the theoretical sailing distances of ships using hydrogen as fuel. The LHV and HHV of hydrogen described in the previous section gives the energy output when hydrogen gas (H_2) reacts with oxygen (O_2) to form water (H_2O). The cell reaction in a classic FC can be seen in Equation 3.1 and Figure 3.8. Li [2006] states that although the reactions at anode and cathode may be quite different in different types of FCs, the overall cell reaction remains the same as in Equation 3.1. The heating value is defined as the absolute value of the standard enthalpy of combustion [Li, 2006]. However, there is no combustion in a FC. The heating value (LHV and HHV) of hydrogen is used as a measure of the total amount of energy that is put into the FC. In other words, it will be the maximum amount of thermal energy that may be extracted from the hydrogen gas [Barbir, 2005]. The thermal energy depends on the state of the water output in the chemical reaction. If the water is liquid, the thermal energy is HHV = 141.8 MJ/kg. If the water is steam, the thermal energy will be LHV = 120.0 MJ/kg. The difference between HHV and LHV is equal to the enthalpy of water condensation [Li, 2006].

$$H_2 + \frac{1}{2}O_2 \Rightarrow H_2O + Work + Waste\ Heat \tag{3.1}$$

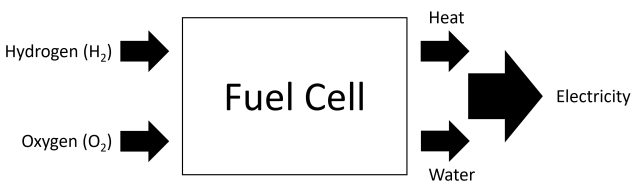

Figure 3.8: FC diagram

The reaction in Equation 3.1 is an exothermic process, which implies that energy is released and the change in enthalpy is negative ($\Delta H < 0$) [Khotseng, 2019]. A FC produces electricity. Unfortunately, not all the thermal energy can be converted into useful energy. Entropy change will often occur in a chemical reaction. Because of this, not all of the energy potential in the hydrogen can be converted into electricity. Entropy is the irreversible loss in the energy conversion [Zumdahl, 2009]. The electrical power output of a FC is calculated using the formula for Gibbs free energy shown in Equation 3.2, which represents the potential work from a chemical reaction [Burheim, 2017]. Khotseng [2019] describes H as the system's total thermal energy, S as the *unavailable* energy and G as the free energy, or the energy available to do useful work. The values used for calculating the free energy are shown in Table 3.3. The numbers are ideal gas properties and evaluated at one atmospheric pressure (atm) and 298 K (25 ℃).

$$\Delta G = \Delta H - T\Delta S \tag{3.2}$$

Table 3.3: Enthalpy and entropy values for reactants and products [Li, 2006]

	h_f $[kJ/mol]$	s_f $[J/(mol \cdot K)]$
Hydrogen, H_2 (g)	0.000	130.595
Oxygen, O_2 (g)	0.000	205.043
Water, H_2O (g)	-241.845	188.715

The enthalpy of a chemical reaction is the difference between the enthalpy values for the products and reactants. The product is assumed to be vaporized water for further calculations, as seen in Equation 3.3. The change in enthalpy, the total energy released as heat, can be seen in Equation 3.4.

$$H_2(g) + \frac{1}{2}O_2(g) \Rightarrow H_2O(g) \tag{3.3}$$

$$\begin{aligned}\Delta H &= \sum products - \sum reactants \\ &= (h_f)_{H_2O} - \left[(h_f)_{H_2} + \frac{1}{2}(h_f)_{O_2}\right] \\ &= -241.845\ kJ/mol - \left[0.000 + \frac{1}{2} \cdot 0.000\right] \\ &= -241.845\ kJ/mol\end{aligned} \tag{3.4}$$

Furthermore, the change in entropy is calculated in Equation 3.5, which is the irreversible losses in the energy conversion [Helbæk et al., 2006].

$$\begin{aligned}\Delta S &= \sum products - \sum reactants \\ &= (s_f)_{H_2O} - \left[(s_f)_{H_2} + \frac{1}{2}(s_f)_{O_2}\right] \\ &= 188.715\ J/(molK) - \left[130.595\ J/(molK) + \frac{1}{2} \cdot 205.043\ J/(molK)\right] \\ &= -44.4015\ J/(molK)\end{aligned} \tag{3.5}$$

The free energy is calculated using the enthalpy (ΔH) and entropy (ΔS) in Equation 3.2. As stated earlier, a negative value implies that energy is released.

$$\begin{aligned}\Delta G &= -241.845\ kJ/mol - 298\ K \cdot [-0.0444015\ kJ/(molK)] \\ &= -228.613\ kJ/mol\end{aligned} \tag{3.6}$$

3.3.2 The compressibility of hydrogen

The density of hydrogen changes a lot with both temperature and pressure. At high pressure, the deviation from ideality will increase [Helbæk et al., 2006]. This deviation can be expressed by using the ideal gas law combined with the *virial equation* shown in Equation 3.7. This is a function with pressure and density, where the polynomial degree will increase towards infinity. The constants will account for the intermolecular contraction forces as the hydrogen gas becomes denser [Burheim, 2017]. In other words, they are the correction factors for nonideality.

$$\frac{p}{RT} = \left[\frac{1}{v}\right] + A \cdot \left[\frac{1}{v}\right]^2 + B \cdot \left[\frac{1}{v}\right]^3 + \dots \tag{3.7}$$

The pressure p will be in Pascal (Pa), $\bar{R}$ is the molar gas constant ($\bar{R} = 8.3144598\ m^2kg/s^2Kmole$), T is the temperature in Kelvin (K), and v will be the molar volume ($m^3/mole$). The constants (A, B, C, ...) will depend on temperature. The expression in Equation 3.8 is valid for temperatures at 300 K.

$$\frac{p}{RT} = \left[\frac{1}{v}\right] + 1.438 \cdot 10^{-5} \cdot \left[\frac{1}{v}\right]^2 + 3.438 \cdot 10^{-10} \cdot \left[\frac{1}{v}\right]^3 + \dots \tag{3.8}$$

Table 3.4 summarize the results from the virial equation with two constants, as shown in Equation 3.8. Figure 3.9 illustrates how the molar volume varies with pressure. Both Hexagon Purus [2021] and UMOE Advanced Composites [2022] advertise hydrogen storage solutions for the maritime industry. The hydrogen characteristics for their storage solutions can be seen as red and black dots in Figure 3.9. The plot illustrates a small distinction between the virial equation and the numbers from UMOE and Hexagon Purus. This is probably because the virial equation calculates the molar volume for temperatures of 27 ℃, while Hexagon and UMOE use 15 ℃. The exact numbers presented by UMOE and Hexagon can be seen in Table G.1 in Appendix G. This data is retrieved for a 40 ft container.

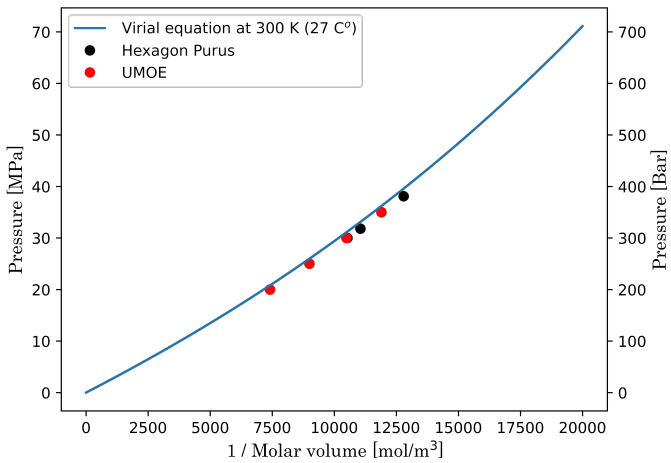

Figure 3.9: Solution to virial equation.

Table 3.4: Results from virial equation with given pressure and temperature of 298 K.

Pressure $[Bar]$	**Molar volume** $[mol/m^3]$
(1 atm) 1.01	41
10	401
100	3810
300	10200
400	13000
700	19900

3.3.3 Volumetric energy density of hydrogen

The volumetric energy density of hydrogen will depend on storage and energy conversion solutions. In addition to this, both storage and energy conversion are dependent on temperature and pressure. Section 3.3.1 described the theoretical energy output of a FC operating at one atm and 293 K. Section 3.3.2 depicted how the molar volume changed with storage pressure. Combining these results will obtain the volumetric energy density when hydrogen is used in FCs, presented in Table 3.6.

Table 3.5: Gibbs free energy of hydrogen reaction (Equation 3.2) with given temperature and pressure.

Pressure [Bar]	**Temperature** [K]	**Free Energy (G)** [kJ/mol]
1.01	298	-228.613

Table 3.6: Volumetric energy density with different storage pressures and temperature of 298 K.

Pressure [Bar]	**Molar Volume** [mol/m^3]	**Energy Density** [MJ/m^3]
(1 atm) 1.01	41	9.3
10	401	91.7
100	3810	871
300	10200	2340
400	13000	2970
700	19900	4540

3.3.4 Fuel efficiencies

Ianssen et al. [2017] state that the FC efficiency is about 50 %. However, it is possible to increase the efficiency by taking advantage of the heat loss. Aarskog and Danebergs [2020], Ianssen et al. [2017], Letafat et al. [2020], and Strømgren et al. [2020] all assume a LHV for hydrogen at 33.3 kWh/kg (120 MJ/kg) with an estimated average FC efficiency of 50 %, with the exception of Letafat et al. [2020], who assume a FC efficiency of 45 %. Compared with a diesel LHV of 11.86 kWh/kg (42.70 MJ/kg) and an estimated diesel engine efficiency of 37 %. By using a diesel density of 845 kg/m^3, the volumetric energy density of diesel will be 36 100 MJ/m^3. The hydrogen density will, as described above, depend on both pressure and temperature.

3.4 Hydrogen production

Today hydrogen is typically categorized in three different colors depending on how it is produced: grey, blue, and green, as seen in Figure 3.10. The color is set by which type of energy or additional technology is utilized to produce the hydrogen [Dawood et al., 2020]. Grey hydrogen is the most polluting type, the blue uses carbon capture and storage technologies to reduce the emissions, and the green is produced with 100 % renewable energy sources.

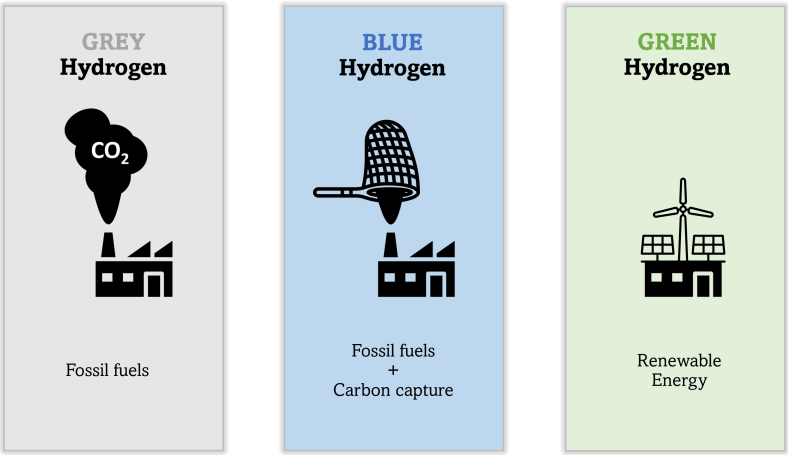

Figure 3.10: Color categorization of hydrogen production.

Jensen [2021] states that there are mainly three ways of producing hydrogen, either by biomass, natural gas, or electricity. Each of the production methods produces emissions of different extent. The most used process today is steam methane reforming. The carbon emissions from this method are relatively high, around 10-12 kg CO_2 per kg hydrogen produced. About 95 % of hydrogen production uses fossil fuels [Jensen, 2021]. Deloitte [2020] states that 48 % comes from natural gas, 30 % from hydrocarbons/crude oil products, 18 % from coal, and only 4 % from electrolysis. As mentioned earlier, hydrogen has to be made from renewable sources to reduce the life cycle emissions of hydrogen vessels, so called green hydrogen. Electrolysis is one example of a green hydrogen production method, given that the electricity used in the process originates from renewable sources. This method separates the hydrogen from the oxygen in water by using electricity.

The North Sea is known for its large waves and strong winds. The area holds a vast wind energy potential. Offshore wind is one of the key building blocks for the green transition of Europe and for meeting the Paris climate goals. This is reflected by the 2050 capacity target of 300 GW set by the European Commission [North Sea Wind Power Hub, 2021].

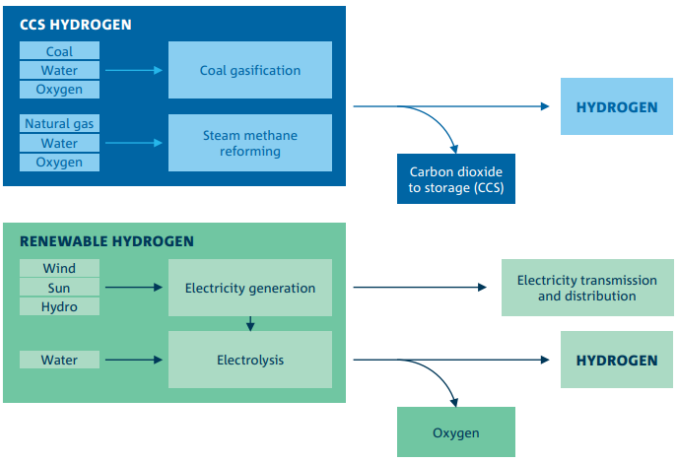

Figure 3.11: Various hydrogen production pathways.

Source: [Commonwealth of Australia, 2018]

Commonwealth of Australia [2018] states that alkaline electrolyzers are the most mature and widely used technology for creating renewable hydrogen through electrolysis. This type of electrolyzers use an alkaline water solution as an electrolyte. Another method to produce hydrogen is called PEM electrolyzers. This method uses a polymer membrane instead of an alkaline solution. PEM electrolyzers are more efficient in producing hydrogen, but they are also more advanced to operate

and more expensive. Figure 3.11 illustrates various methods to produce hydrogen.

Figure 3.12 estimates the world hydrogen production. DNV [2020] predict that the share of non-carbon-free hydrogen will be less than 5 % in 2050. A large share of hydrogen production is expected to come from offshore and onshore wind power. Electrolysis by using grid power is predicted to have the largest share by 2050.

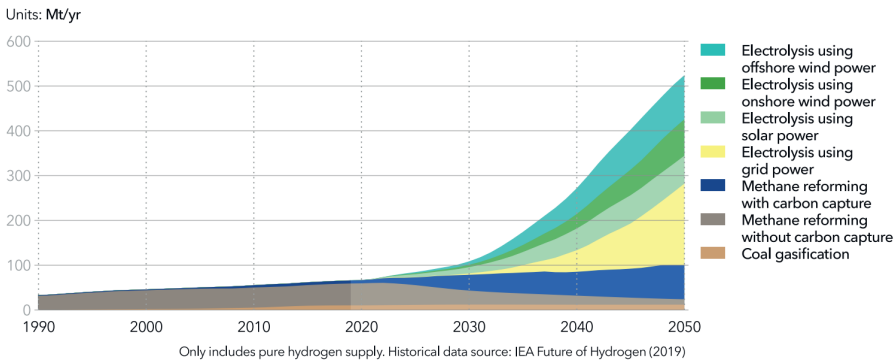

Figure 3.12: Prediction of world hydrogen production by source.

Source: [DNV, 2020]

3.4.1 Production costs

According to Elgohary et al. [2015], more than 50 % of a ship's operating expenses are fuel oil costs. This is why a large part of the shipowners use heavy fuel oil (HFO), as it is both easily accessible and inexpensive. If hydrogen is compared to HFO, it has low availability and is expensive. International Energy Agency [2021] (IEA) assumed a cost development for hydrogen production in the future, more specifically, 2060. The assumption neglected the most polluting methods because of the strict emission demands towards 2060. The price for hydrogen production in 2019 by using low-carbon electricity is claimed to be 3.2 - 7.7 U.S. Dollar (USD) per kg of hydrogen produced (2019 exchange rate: 28 - 68 NOK). IEA predicts a much lower cost for hydrogen in the future, from 1.3 - 3.3 USD per kg of hydrogen produced (2019 exchange rate: 11 - 29 NOK). According to Bruce et al. [2018], the CAPEX for producing and storing LH_2 is 10.63 USD/kg H_2/y, while the OPEX are assumed to be 0.92 USD/kg H_2/y. Ianssen et al. [2017] claimed in 2017 that the current development in hydrogen production could lead to prices of 25 NOK per kilogram of hydrogen, while Strømgren et al. [2020] claims that a hydrogen price below 45 NOK/kg only can be achieved by large scale production.

3.5 Hydrogen storage

Converting power to hydrogen may be a promising solution for storage of renewable energy. It can be the first step to achieving a 100 % renewable and sustainable hydrogen economy [Dawood et al., 2020]. Unfortunately, due to the relatively low ignition temperature of the hydrogen gas, there is a large portion of risk associated with it. In addition, hydrogen is capable of escaping through materials because of its small molecule size. This places even greater demands on the storage method. A hydrogen leakage can potentially lead to severe incidents.

As stated in Section 3.3.1, hydrogen has the highest energy per mass of any fuel. Still, its low ambient temperature density results in a low energy per unit volume [Office of Energy Efficiency and Renewable Energy, 2020]. By mass, hydrogen has almost three times larger energy content than gasoline, with 120 MJ/kg for hydrogen and 44 MJ/kg for gasoline. However, by volume, the advantage is swapped. LH_2 has a density of 8000 MJ/m^3, while the gasoline density is 32 000 MJ/m^3. This is why more advanced storage methods are necessary to have a potential for higher

energy density using hydrogen. Hydrogen can be stored as either a gas or a liquid. The boiling point of hydrogen at one atm is 20.28 Kelvin (-252.87 °C) [Mazloomi and Gomes, 2012].

Strømgren et al. [2020] depict that a tank from Hexagon of 250 bar, volume of 8500 liters, and a hydrogen capacity of 150 kg will cost around 720 USD per kg of stored hydrogen. With additional costs from valves and piping, bunkering interface, instrumentation, safety systems, class approval, and testing, the total cost is assumed to be 13 500 NOK/kg of stored hydrogen. Compared to maritime battery solutions, Aarskog et al. [2020] point out that a 250-350 bar hydrogen tank is about five times lighter than the battery solutions.

3.5.1 Compressed hydrogen

The progress in material science has led to a development within composite gas cylinders. By using composite plastic, reinforced glass, or carbon fiber, the cylinders can store hydrogen under pressures up to 350-700 bar [Tarasov et al., 2007]. Mazloomi and Gomes [2012] describe gas compression as the most time and energy-efficient method due to the efficiency, design, cost, and environmental advantages. The article also points out that storing the hydrogen under high pressure as CH_2 will have 4-5 times less cost than LH_2. However, Decker [2019] states that CH_2 requires 4 times more footprint than LH_2 as a rule of thumb. FC vehicles like Toyota Mirai and Hyundai Nexo use pressurized hydrogen at 700 bar [Commonwealth of Australia, 2018]. The weight of the hydrogen tank in the Toyota Mirai is 88 kg, and the FC weighs 56 kg [Toyota, 2022]. Compared to a Nissan Leaf with a battery pack of 24 kWh that weighs 294 kg [DNV, 2019]. According to Körner et al. [2015], storing CH_2 requires pressures from 18 MPa to 70 MPa to make it economically. Compression to 35 MPa will require 8-13 % of the original energy content of the hydrogen [DNV, 2019]. Sundvor et al. [2021] estimate 20 minutes for bunkering 450 kg hydrogen at 250 bar.

3.5.2 Liquid hydrogen

Hydrogen liquefaction is highly energy demanding because of the extremely low boiling temperature. Large amounts of energy are required to lower the temperature to -252 °C. This process alone consumes 20-30 % of the starting energy content of the hydrogen [Commonwealth of Australia, 2018]. This is slightly lower than assumed by Körner et al. [2015], who believe that between 25 % and 40 % of the energy is used for liquefaction. On the other side, Berstad et al. [2013] state that reducing the consumption to 19.2 % of the starting energy content is possible. Additionally, in a tank with a volume of 50 m^3 the evaporation rate will be approximately 0.4 % per day. For larger tanks up to 20 000 m^3, the evaporation will be less than 0.06 % per day [US Drive, 2016].

Figure 3.13: LH_2 tank from Linde.

Source: [Decker, 2019]

Linde is one of the largest industrial gas companies by market share and revenue [Research and Markets, 2021]. Figure 3.13 shows an example of a LH_2 tank from Linde. It is designed to fit into a 40 ft container, the inner volume of the tank is 11.5 m^3, and it has a design pressure of 6 bar (g). The storage capacity is 900 kg LH_2. The boil-off ratio in a tank like this will be less than 5.5 kg

per day [Decker, 2019]. According to Linde [2021], their most prominent liquid storage solutions have a capacity of 26 tonnes of LH_2 with a pressure of 12 bar (g).

3.5.3 Hydrogen containing liquid

At last, storing hydrogen in a hydrogen-containing liquid is also an opportunity. One of the most promising methods for this is using ammonia [Commonwealth of Australia, 2018]. This has a high hydrogen density and a higher boiling temperature (-33.4 °C) compared to hydrogen alone (-253 °C). Ammonia contains around 17.6 % hydrogen based on weight [DNV, 2019]. In addition to this, ammonia has a higher volumetric energy density than pure hydrogen. Unfortunately, it will still have low efficiency in the fuel production chain [Jensen, 2021].

3.6 Fuel cell types

A FC consists of an anode and a cathode, with an electrolyte between them. It is an electrochemical device that converts the chemical energy of reactants directly into electrical energy [Li, 2006]. A study on FCs in shipping by DNV in 2017 evaluated seven different FC technologies [Tronstad et al., 2017]:

- Alkaline fuel cell (AFC)
- Proton exchange membrane fuel cell (PEMFC)
- High-temperature PEMFC (HT-PEMFC)
- Direct methanol fuel cell (DMFC)
- Phosphoric acid fuel cell (PAFC)
- Molten carbonate fuel cell (MCFC)
- Solid oxide fuel cell (SOFC)

The seven FC technologies were rated based on relative cost, power level, lifetime, flexibility in fuel type, technological maturity, physical size, emissions, safety, and efficiency. Three different FC types stood out for marine use when the ranking was performed. These were SOFC, PEMFC and HT-PEMFC, and are further explained in Section 3.6.1, Section 3.6.2, and Section 3.6.3.

E4tech publishes a review of the FC industry every year. It is worth mentioning that this does not only apply to the maritime industry but the whole market. The bar chart in Figure 3.14 shows that the use of FCs has increased in recent years. Additionally, the green colors show that PEMFC is the most widely used FC type.

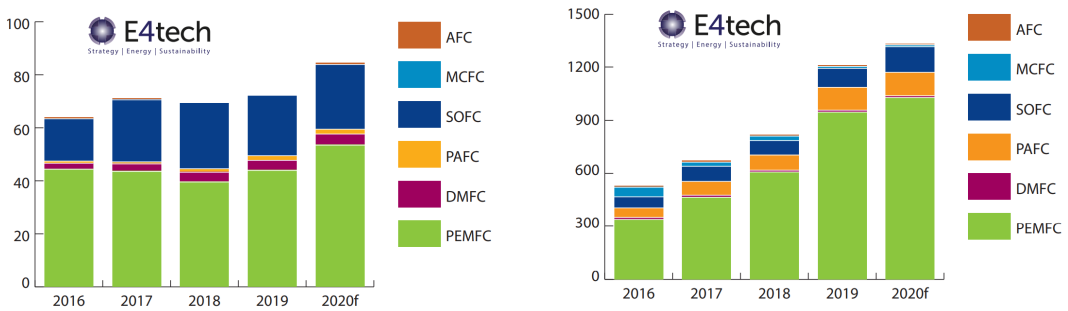

(a) Shipments by FC type 2016-2020 (1000 units) (b) Megawatts by FC type 2016-2020

Figure 3.14: Use of FCs from 2016 to 2020

Source: [E4Tech, 2020]

Figure 3.15 illustrates the prediction of future FC prices and lifecycle length made by Deloitte [2020]. The prognosis is made based on FC buses, but it can still be a good indication of the maritime market's pricing. The FC pricing is set to 1500 USD/kW in 2019 and is expected to decrease to 600 USD/kW in 2029. Furthermore, Deloitte [2020] expects the life cycle length of FCs to increase over the years, from about 25 000 hours in 2019 to 30 000 hours in 2029. In addition, a reduction of 60 % is expected for the maintenance cost of FCs in the next ten years.

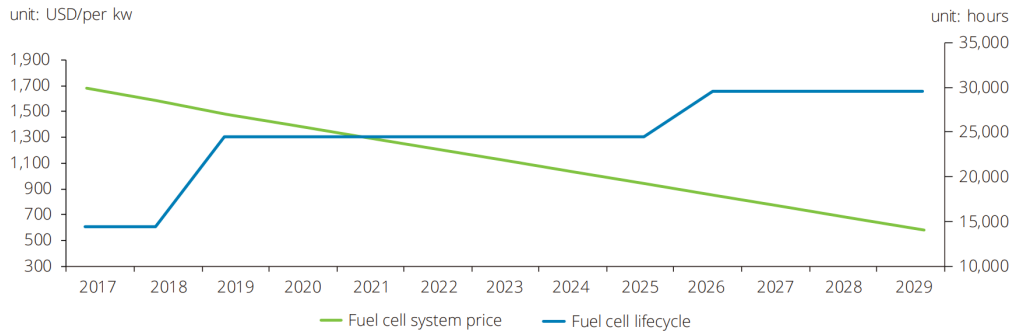

Figure 3.15: Prediction of future FC system prices and life cycle length.

Source: [Deloitte, 2020]

3.6.1 Proton exchange membrane fuel cell

The proton exchange membrane fuel cell (PEMFC) is a relatively mature technology used in marine and other high-energy applications [Tronstad et al., 2017]. This is also supported by Deloitte [2020], who depicts that PEMFC is the most commercialized type today, primarily because of its low operating temperature. The positive and negative aspects of PEMFC are summarized in Table 3.7. Figure 3.16 illustrates the flow chart of a PEMFC, both the input (hydrogen and oxygen) and output (electricity and water). Strømgren et al. [2020] and Aarskog et al. [2020] state that the price of a PEMFC is approximately 3000 USD/kW. However, Thompson et al. [2018] claim that if FCs are to become competitive with internal combustion engines, a significant cost reduction and durability are required. The 2025 FC targets set by the U.S. Department of Energy are 40 USD/kW and 5000 hours of durability. According to Jogchum Bruinsma, maritime application manager in Nedstack, their MT-FCPI-500 FC system will be a good choice for OSVs (personal communication, 02.04.2022). This is a low-temperature PEMFC with efficiency from 59 to 63 %, depending on the power output. The nominal power for the FC system is 500 kW, with a peak power of 626 kW [Nedstack, 2022].

Table 3.7: Positive and negative aspects of PEMFC from [Tronstad et al., 2017]

Positive [+]	**Negative** [-]
+ Mature technology	- Risk and safety related to use
+ Low cost	- Risk and safety related to storage
+ Low operating temperature [50-100 °C]	- Moderate efficiency (50-60 %)
+ Only water as byproduct	- Sensitive to impurities in hydrogen
+ Size up to 626 kW [Nedstack, 2022]	- Moderate lifetime
+ Small physical size	- Platinum catalyst has high cost
+ Low temperature makes it possible to cold start	
+ Highest score in DNVs ranking	

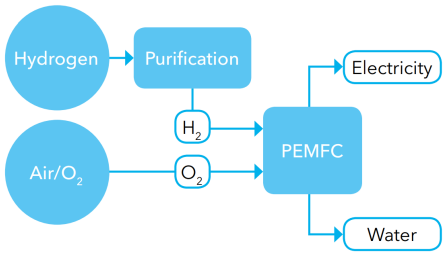

Figure 3.16: Flow chart of PEMFC

Source: [Tronstad et al., 2017]

3.6.2 High temperature proton exchange membrane fuel cell

The main characteristics of high temperature proton exchange membrane fuel cell (HT-PEMFC) are summarized in Table 3.8. Except for the temperature, the main difference between low-temperature PEMFC and HT-PEMFC is that the high temperature makes the FC less sensitive to impurities. This lowers the requirements for hydrogen quality, thus lower costs and simpler systems [Tronstad et al., 2017].

Table 3.8: Positive and negative aspects of HT-PEMFC from [Tronstad et al., 2017] and [Nerem, 2018].

Positive [+]	**Negative** [-]
+ Higher temperatures reduces sensitivity towards impurities	- Risk and safety related to use
+ Excess energy can be used for internal heating purposes	- Risk and safety related to storage
+ Only water as byproduct	- Moderate efficiency (50-60 %)
+ Size up to 90kW (3x30kW) (2017)	- Less mature than PEMFC
+ Small physical size	- Operational temperature of 200 °C
+ Tolerance for fuel impurities, simpler, lighter and cheaper reformers can be used to produce hydrogen	- Expensive catalyst
	- Impossible to cold start

3.6.3 Solid oxide fuel cell

Solid oxide fuel cell (SOFC) is another high-temperature FC. It operates at temperatures around 500-1000 °C [Tronstad et al., 2017]. This type of FC is flexible to fuel types. It can use hydrogen, liquefied natural gas (LNG), methanol, and hydrocarbons. However, some of these fuels will cause emissions of CO_2, thus not a zero-emission solution. Figure 3.17 shows a flowchart where LNG is used as input. It illustrates that the output is not only electricity and water but also CO_2. Additionally, this type of FC will have an option of a heat recovery system, which can be used to extract electricity and make it more effective.

Table 3.9: Positive and negative aspects of SOFC from [Tronstad et al., 2017] and [Nerem, 2018].

Positive [+]	**Negative** [-]
+ Moderately sized	- Risk and safety related to high temperatures
+ Flexible towards different fuels	- High operating temperatures [500-1000 °C]
+ Efficiency of 85 % with heat recovery	- Slow start up
+ Possible to increase life cycle by combining SOFC and batteries	- Moderate electrical efficiency (60 %)
+ Combining SOFC and batteries leads to faster start up	- High cost
+ Small physical size	- Strict material requirements

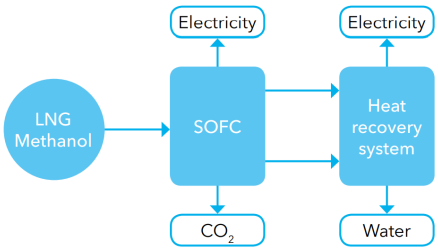

Figure 3.17: Flow chart of SOFC

Source: [Tronstad et al., 2017]

3.7 Hydrogen policy

DNV [2020] states that there are three fundamental key drivers needed to push the decarbonization in shipping:

- Regulations and policies
- Access to investors and capital
- Cargo owner and consumer expectations

Strømgren et al. [2020] depict that new technologies may lead to higher costs than conventional systems. Therefore, it is essential with incentives and public support to overcome these challenges. The Norwegian government stated in 2020 that Norway should have an increased focus on hydrogen and aim toward a low emission society [The Norwegian Government, 2020]. The government will pursue the development of new low emission technologies, and the goal is to have an internationally competitive business that addresses tomorrow's challenges. They state that *Hydrogen is an energy carrier with a significant potential for reducing local, national, and global emissions and creating economic value for Norwegian businesses.*

3.8 Risk assessment of hydrogen as fuel

As described in Section 3.5, with the low ignition temperature of hydrogen, great risk follows. In addition to this, the small molecule size makes the risk of escaping through materials very high. On the contrary, hydrogen is non-toxic and lighter than air [Dawood et al., 2020], making it disappear rapidly in case of leakage compared to other fuels. The main concern is if the leakage is not identified and the gas accumulates in enclosed spaces. In the worst case, a tiny spark will cause a large explosion. Placing the fuel tank in an open environment with adequate aeration can be a risk-reducing measure for this case. In 2019, an assembly failure caused a hydrogen tank at

an Uno-X gas station to explode at Sandvika [NRK, 2019]. The main cause of the accident was a human assembly error in the high-pressure storage unit which led to a hydrogen leak that ignited [NEL, 2019].

Some of the most critical findings from the safety assessment in Tronstad et al. [2017] are:

- Internal leakage in FC module
- High energy collision penetrating LH_2 tank
- Rupture of CH_2 tank containment system
- Leakage of hydrogen-rich gases

Proposed measures to reduce the risk are to let the distances between the hydrogen tanks reach the same safety level as conventional fuelled vessels, evaluate whether the hydrogen tanks should be placed away from the accommodation areas, and figure out where to place the hydrogen tanks with respect to collision probability. Sundvor et al. [2021] depict that hydrogen storage tanks need to be located on open deck due to safety. Table 3.10 summarize the most critical incidents and suggested mitigation measures identified by Tronstad et al. [2017]. The different scenarios and the associated risk are illustrated in the risk matrix in Table 3.11. This shows that incident (1) ends up in the red zone with high risk, indicating that the risk cannot be justified and mitigation measures have to be introduced. The incidents (2), (3), and (4) are all in the ALARP zone, which means that mitigation measures should be introduced to reduce the risk as low as reasonably practicable.

Table 3.10: Most critical FC and hydrogen related findings from Tronstad et al. [2017].

Num. Incident	**1**	**2**	**3**	**4**
Hazard	Internal leakage in FC Module	High energy collision penetrating LH_2 tank	Rupture of CH_2 tank containment system.	Leakage of hydrogen rich gases
Effect	Can lead to high stack temperatures and internal oxidation processes or internal fire. Shut down of stack.	Damage to the tank system. Potential immediate ignition.	Fatigue can lead to tank rupture. Potential damage the ship structure.	Mechanical failure, welding failure. Potential self ignition.
Mitigation	Evaluate amount of fuel in FC space. Minimize combustible material in FC.	Evaluate distance between tank and shipside. Assess hydrogen release scenarios in respect to ignition. Evaluate collision probability.	Install suitable pressure relief system.	Modules installed in protected FC space. Gas detection ventilation. Fire detection. Fire extinguisher.
Frequency (Oi)	4	2	2	3
Consequence (Si)	4	5	5	4
Risk Level	High	ALARP	ALARP	ALARP

Valland [2020] states that hydrogen can be stored as both CH_2 and LH_2, and the risks associated with these are high pressure and extremely low temperatures, respectively. Complex storage systems will be more prone to failure and leakages. Because of the low temperatures and high complexity, the bunkering should be performed with sufficient safety zones and strict rules. In cases where ammonia is used, the safety zones should be even larger due to the toxicity of ammonia.

Table 3.11: Risk matrix from Tronstad et al. [2017].

Consequence / Frequency	1. Negligible	2. Minor	3. Moderate	4. Major	5. Catastrophic
1. Improbable					
2. Remote					**(2), (3)**
3. Occasional				**(4)**	
4. Probable				**(1)**	
5. Frequent					

Cluster [2020] claims that the main hazards of using hydrogen as a fuel are explosive, flammable, and cryogenic. Hydrogen embrittlement is also highlighted as a major challenge. The small size makes hydrogen molecules able to permeate through materials. Cluster [2020] presents three safety zones to cope with the different risks. These are further described in Table 3.12. It is worth mentioning that the report emphasizes that the acceptable risk for all zones are substantially lower than the average risk for dying for other reasons, both natural causes and accidents, for any age group and gender.

Table 3.12: Description of safety zones from Cluster [2020].

Zone	Fatality risk [1/year]	Regulation
Inner Zone	1 x 10^{-5}	Should be within the facility property limits, however, exception exists for certain public areas with limited presence of people for shorter periods of time. A person spending all his/her time in this zone will die from a facility related accident once every 100 000 years.
Middle Zone	1 x 10^{-6}	Public roads, railway stations, quays, offices or industry can be within this zone. Private homes, guesthouses or accommodation should not be within the middle zone. A person spending all his/her time in this zone will die from a facility related accident once every 1 000 000 years.
Outher Zone	1 x 10^{-7}	Areas regulated for homes and general use by population can be within this zone. A person spending all his/her time in this zone will die from a facility-related accident once every 10 000 000 years.

De Groot [1982] describes the hazards associated with leakage in oil and gas pipelines and how this can damage the surrounding environment and wildlife. On the other side, Midilli et al. [2005] state that hydrogen can be transported safely in pipelines, and since hydrogen is a clean and non-toxic energy carrier, it will not affect the environment to the same extent. The main hazard of hydrogen leakage is, as described above, explosion.

At last, Strømgren et al. [2020] claims that the risk associated with hydrogen solutions is acceptable and comparable to conventional diesel systems. The risk assessment of Aarskog et al. [2020] also concludes that the risk related to the hydrogen systems is relatively low and much lower than the expected acceptable risk tolerance level of 0.5-1.0 fatalities per 10^9 passenger-km. This risk assessment was performed on a ferry, which usually is more crowded than an OSV.

3.9 OSV types and operational modes

This section will focus on the different types of OSVs (OCV, PSV, and AHTS) and their different operational modes:

- Transit
- Standby
- Dynamic positioning (DP)
- Anchor handling (AH), *AHTS*
- Towing, *AHTS*

A DP system is supposed to assist the vessel in maintaining its position when exposed to various hydrometeorological conditions. During positioning, the fuel consumption will be substantial because the thrusters work all the time [Łebkowski and Wnorowski, 2021]. Transit speed will vary with priorities and market situation. Lindstad et al. [2017] state that a speed around 10 knots is the best in terms of economy. Table 3.13 summarizes the average values for the vessels used in this analysis. The characteristics for all vessels can be seen in Appendix A. The average age of the vessels in the database is 10-12 years. Risholm and Amon Maritime [2020] state that the design lifetime for ships is 20-30 years. Total installed power is estimated using a graph from Erikstad and Levander [2012], where installed power is given as a function of gross tonnage (gt), which can be seen in Appendix B.

Table 3.13: Average values from vessel database. Installed power in italic is estimated by using power/gt graph from Erikstad and Levander [2012].

		OCV	**PSV**	**AHTS**
Year	[-]	2010	2012	2010
gt	[tons]	9264	3727	5149
dwt	[tons]	6375	4231	3498
Length	[m]	111	84	82
Width	[m]	23	18	20
Installed power	[kW]	*10000*	*8000*	*17500*

3.9.1 PSV

PSVs are used to supply and transfer goods, equipment, and people to offshore installations. They operate from a shore base and carry supplies to the offshore fields [Erikstad and Levander, 2012]. Valland [2020] states that they are installed with DP systems on various degrees and often installed with equipment related to oil spill recovery and fire fighting in case of secondary duties. Figure 3.18 illustrates the tank and void spaces for a normal PSV.

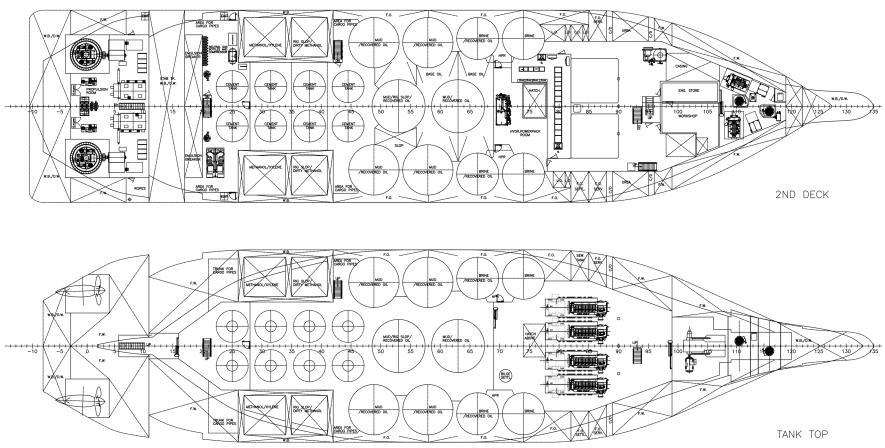

Figure 3.18: Tank top and 2nd deck of PSV.

Source: [Solstad Offshore, 2022]

3.9.2 AHTS

AHTS vessels usually have their area of use in installing and handling mooring equipment for large floating structures [Valland, 2020]. The vessels are installed with high bollard pull capabilities to move large offshore installations. The mooring chains are heavy for deep water operations and will require a high bollard pull from the vessel [Erikstad and Levander, 2012]. Ognedal [2021] depicts

the North Sea as an area with especially rough conditions compared to the US and Arabian Gulf and the vessels operating here are often equipped with even higher bollard pull. Myklebust and Ådnanes [2011] states that from 2007 to 2012, ABB installed electrical solutions for 24 hybrid propulsion AHTS vessels. The total installed propulsion power varied from 14 to 24 MW. Which is within what is estimated for the average AHTS vessel in Table 3.13. Some AHTS vessels can also operate in supply mode as a PSV. Table 3.14 presents the operational profile for an AHTS vessel identified by Strande [2018]. This analysis was based on 66 different AHTS vessels from various owners.

Table 3.14: Offshore operational profile for AHTS from Strande [2018].

	Time offshore [%]
AH	13
Towing	18
Transit	18
DP	13
Standby	38

3.9.3 OCV

OCVs are used for construction and maintenance at sea. Platforms, wellheads, under-water pumping units, pipelines, and power cables are typical tasks for an OCV, according to Erikstad and Levander [2012]. The deck is large and open to carry large structures at sea. The vessel is normally equipped with a large, heavy crane, moonpools for subsea work, remotely operated underwater vehicles (ROVs), and a helicopter deck for exchanging personnel at sea. Pettersen [2015] describes OCVs as multi-functional vessels.

3.10 OSV expenditures

This section will have a brief look into the different expenses associated with OSVs. The overall expenditures is used to compare the hydrogen FC solutions with today's conventional solutions. The costs in this study are primarily given in Norwegian Kroner (NOK), with an exchange rate of 9.83 NOK/USD [Norges Bank, 2022]. If some values are older, the exchange rate for the given year is used in combination with an average yearly inflation rate of 2.5 %.

3.10.1 CAPEX

According til Clarkson's Offshore Intelligence Network the newbuild price for a PSV built in Europe with a deck area larger than 900 m^2 will be around 480 MNOK (2022). The newbuild prices for all vessel types are summarized in Table 3.15. They are all from Clarkson's Offshore Intelligence Network and apply to vessels built in Europe. The CAPEX for OCVs was not found and is assumed to be a little more expensive than the largest AHTS vessels from Clarkson's network.

Table 3.15: CAPEX for different OSV types from Clarkson's Offshore Intelligence Network.

	CAPEX (2022) [MNOK]
OCV	790.7
PSV	478.9
AHTS	590.3

Lindstad et al. [2017] state that a typical OSV is installed with 8000 kW when built for operating in the North Sea. This is covered using four main conventional diesel engines with 2000 kW each,

where the price for one of these was estimated to be 7.0 mill USD in 2017. In today's worth, this will be 65.8 MNOK, which will give a price of around 8200 NOK/kW of installed machinery.

Table 3.16: Estimated investment cost of hydrogen driven high-speed ferry from Strømgren et al. [2020].

	Unit	**Value**
Total propulsion power	[kW]	1200
Cost of FC systems (permanent installations)	[MNOK] [NOK/kW]	12.6 10 500
Cost of FC systems (degradable components)	[MNOK] [NOK/kW]	12.6 10 500
Cost of hydrogen storage systems	[MNOK] [NOK/kW]	6.12 5100
Power electronics and electric motors	[MNOK] [NOK/kW]	6.12 5100
Total cost of FC system	[MNOK] [NOK/kW]	31.3 26 100

Table 3.16 describes the CAPEX for a high-speed ferry with installed FCs and hydrogen storage. The required propulsion power for the high speed ferry was assumed to be 1200 kW, which is much smaller than for an OSV, but it might give a reasonable prediction of the installation price for FCs per kW. Figure 3.19 illustrates the estimation of FC CAPEX made by Ianssen et al. [2017] in 2017. The estimated cost for 2020 is 79 % lower than what was estimated by Strømgren et al. [2020] in 2020. Because the assumption made by Strømgren et al. [2020] is the most recent, this will be used for further calculations.

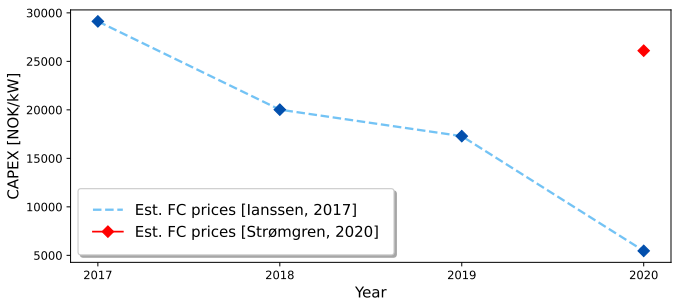

Figure 3.19: Estimated FC CAPEX cost from Strømgren et al. [2020] and Ianssen et al. [2017].

3.10.2 OPEX

OPEX are, according to Strømgren et al. [2020], normally divided into fuel, maintenance, and fees, where fuel costs are the dominant share. The different vessel types' operational profiles and energy demand are used to get an assumption of the fuel costs. Section 3.5 depicts several different assumptions for the price of hydrogen. Further in the thesis, a price for hydrogen is assumed between the estimate from Ianssen et al. [2017] (25 NOK/kg) and Strømgren et al. [2020] (45 NOK/kg), which indicates a price of 34 NOK/kg. According to Ship & Bunker [2022] the MDO cost is around 11.8 NOK/kg (12.05.2022), which is relatively high compared to developments in recent years.

Strømgren et al. [2020] state that due to the relatively low weight of FCs it can be assumed that service and maintenance mainly consist of replacing degraded FC modules. In addition, this can be performed while the vessel is in operation. The annual maintenance costs for the

high-speed ferry described by Strømgren et al. [2020] are assumed to be 0.675 MNOK and 1.130 MNOK for a hydrogen and diesel solution, respectively. Maintenance of deck accessories, cleaning of engine rooms, and annual lubricating oil consumption are also included in the maintenance costs for the conventional diesel machinery. The hydrogen FC concept adds additional costs for technical maintenance and safety systems, which have an annual cost of 0.45 MNOK. The values are summarized in Table 3.17 and made dimensionless by dividing the number of kW in the concept ferry (1200 kW).

Table 3.17: Estimated annual maintenance costs, hydrogen and diesel concept Strømgren et al. [2020].

	Unit	Hydrogen & FC	Diesel
Annual maintenance cost	[MNOK]	0.675	1.13
	[NOK/kW]	563	942
Technical maintenance and safety systems	[MNOK]	0.45	0.00
	[NOK/kW]	375	000

3.11 Hub utilization

Section 3.3.3 states that the volumetric energy density of hydrogen is significantly lower than other fuel types, e.g., MDO. This can make it more challenging to reach the same sailing distances with hydrogen as fuel. Introducing an offshore refueling and supply hub may solve this capacity problem. The definition of a hub is the effective center of an activity [Cambridge Dictionary, 2021]. For this case, the hub will most likely function as a refueling station. In addition, it may work as an offshore supply base. This will considerably reduce the required sailing distance and make it less dependent on large fuel tanks.

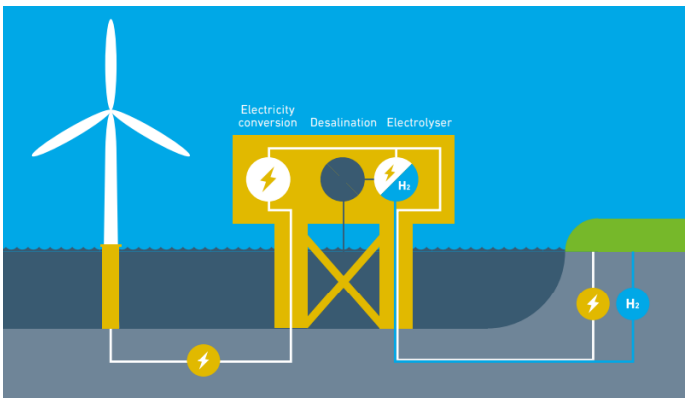

Figure 3.20: Hub solution from the North Sea Wind Power Hub Programme

Source: [North Sea Wind Power Hub, 2021]

North Sea Wind Power Hub [2021] is a project that investigates the possibilities of utilizing hubs. It is described as *a new approach to the challenge of integrating renewable energy* and that it is a solution for achieving the net zero-emission goals in 2050. Figure 3.20 illustrates one of the hub solutions described in the program. The hub will first and foremost act as a connection point between the offshore floating wind installations and the shore. In addition to this, it looks at the possibilities of producing green hydrogen by using energy from wind turbines.

Chapter 4

Methods

This chapter provides an overview of the methods used to analyze the potential of using hydrogen in today's OSVs. Figure 4.1 provides an overview of the model used to obtain the results. The primary purpose of the different methods is to get an overview of the demand and possibilities that lie in the OSV fleet. Section 4.1 briefly introduces the strengths, weaknesses, opportunities and threats (SWOT) of using hydrogen as fuel. Section 4.3 and Section 4.4 describes the methods used to highlight the power needed to propel a vessel. Furthermore, Section 4.5 outline the function used to calculate the maximum theoretical sailing distances (D_{max}) for the various fuel types. Section 4.6 gives a quick introduction of essential python codes made to solve the objective. At last, Section 4.7 presents two methods used to map the zero-emission potential.

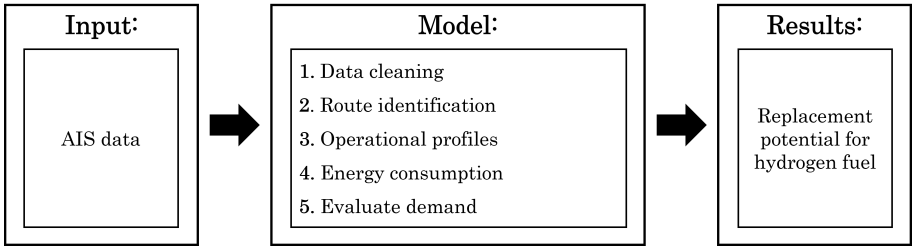

Figure 4.1: Model overview.

4.1 SWOT analysis of hydrogen as fuel in shipping

A brief SWOT analysis was performed before undertaking the thesis. It is a method used to examine the strengths, weaknesses, opportunities and threats of a field of interest, and can make it easier to identify the problems that need to be solved. In addition, it can bring out the positive aspects that can be used to push the project towards realization. The analysis is summarized in Table 4.1 and Figure 4.2.

Table 4.1: The process of pinpointing strengths, weaknesses, opportunities and threats.

Strengths	**1.** Only water as byproduct when using hydrogen. **2.** Low noise and vibration level. **3.** Hydrogen has high gravimetric energy density and high efficiency in FCs.
Opportunities	**4.** Ships running on hydrogen can operate in strict emission areas. **5.** Norway has good access to renewables to create green hydrogen. **6.** Today's renewables rely on weather, hydrogen can be used to store potential excess energy.
Threats	**7.** Limited lifetime of FC components, as well as a lot of doubts and concerns about the safety of using hydrogen. **8.** Today 96 % of the hydrogen production relies on fossil fuels. **9.** Lack of hydrogen refueling infrastructure.
Weaknesses	**10.** Hydrogen has low volumetric energy density, which may lead to large storage tanks. **11.** The various hydrogen systems have relatively high costs. **12.** Hydrogen has to be made from renewables in order to reduce emissions.

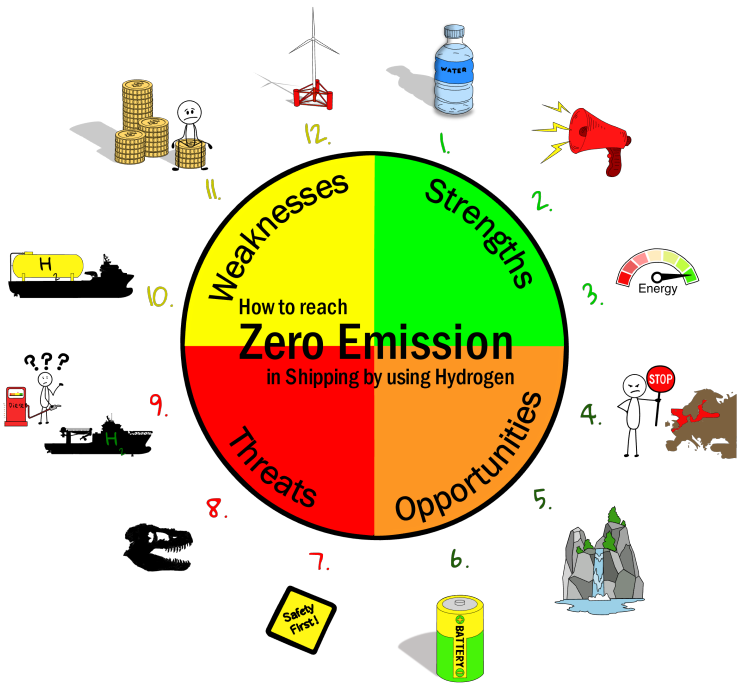

Figure 4.2: Illustration of SWOT process.

4.2 Operational profiles

According to Norwegian Shipowner's Association [2021], 542 OSVs operate in the Norwegian-controlled foreign-going fleet by July 1st 2021. Data from Clarkson's Offshore Intelligence Network 2022 presents 2023 PSVs, 1053 OCVs, and 2440 AHTS vessels in the global offshore market today (personal communication, 25.05.2022). Which will give an OSV fleet with a total of 5500 vessels.

A good overview of the operational profile of the offshore fleet is an advantage when analyzing the opportunities for hydrogen propulsion. Lindstad et al. [2017] state that the most common operational modes for PSVs in the North Sea are waiting in port, discharging in port, transit to

the oilfields, waiting at the oilfields, standby, and performing their intended work in DP mode. The duration of each mode will vary with operation and vessel type. AH and towing operations will also be introduced for the AHTS the vessels.

30 different vessels were used to investigate the operational profiles of OSVs. 10 OCVs, 10 PSVs, and 10 AHTS vessels. The operational patterns were mapped using a database from Solstad Offshore called MARESS. It includes both geospatial and temporal maritime data about the vessels owned by Solstad Offshore [2022]. Solstad offshore is among Norway's largest offshore shipping companies, a country with one of the world's biggest, most modern, and most advanced fleets [Norges Rederiforbund, 2015]. The vessels have been anonymized to satisfy the contracts and customers of Solstad Offshore. Table D.1 in Appendix D includes the obtained data from the 30 vessels for 2021. Figure 4.3 summarizes the average values for each vessel type. Time in port is not considered because it is assumed that the fuel consumption in port is negligible compared to the other modes of operation. This assumption is also supported by Strømgren et al. [2020] and Valland [2020], who state that onshore power supply (OPS) is used to prevent local emissions. The thesis will mainly focus on the parts where fuel is consumed since this is the segment that the hydrogen is to replace. Valland [2020] claims that PSVs usually spend more time in transit and standby, which is also pinpointed in Figure 4.3. The annual operational profile with time in port included can be seen in Figure D.1 in Appendix D. This shows that the vessels spend about a quarter of the time in port, 91 of 365 days.

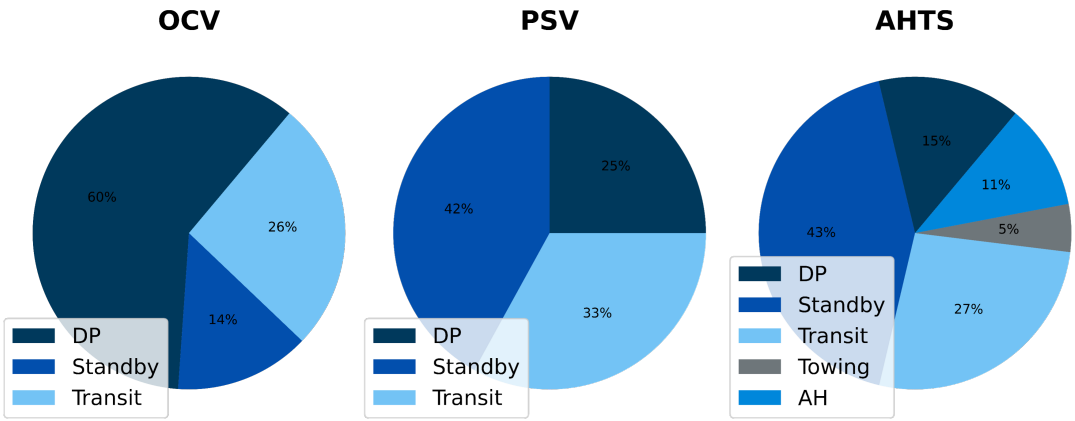

Figure 4.3: Analysis of operational profile from MARESS.

Source: [Solstad Offshore, 2022]

4.3 Power consumption of OSVs

The load profile of the vessel is vital when establishing the dimensions of the FCs and hydrogen storage systems. The operational profiles in Figure 4.3 from Section 4.2 highlighted some crucial differences between the various vessel types. It is essential to consider this when analyzing the operational pattern and power consumption. For instance, the operational profile identified that an OCV, on average, only spent about 26 % in transit. Therefore, it is necessary to include the power consumption for both DP and standby to get a realistic load profile. Typically an OCV will be less in transit than a PSV, and an AHTS vessel will spend less time in DP. As stated in Section 4.2, negligible fuel consumption is assumed in port because the vessel will connect to the OPS. Samferdselsdepartementet [2019] affirms that the majority of the largest domestic ports have OPS today and states that Enova will provide financial support to build even more in the future.

$$sfc\,[kg/h] \cdot LHV\,[kWh/kg] \cdot \eta_{diesel}\,[\%] = P\,[kW] \tag{4.1}$$

The MARESS database from Solstad Offshore was used to find the power requirement in the various modes of operation. Solstad Offshore stores all data from their ships, and the vessel

statistics include, among other things, the average fuel usage in tonnes per hour for a specific mode of operation. Together with the diesel LHV (11.86 kWh/kg) and diesel engine efficiency (37 %) described in Section 3.3.4, the power was calculated by using Equation 4.1. This is presented with rounded numbers in Table 4.2. The values will be the power needed at the different modes of operation, regardless of the type of fuel used. The specific fuel consumption (sfc) from 12 AHTS vessels, 17 PSVs, and 15 OCVs were used to identify the load profile. The full dataset can be seen in Table E.1, Table E.2, and Table E.3 in Appendix E. The vessels have been anonymized, but they are all part of the database that constitutes the system boundaries described in Chapter 2. The average fuel consumption in transit applies to speeds of 11 knots. A minority of the vessels used dual-fuel engines with both LNG and MDO. Then, for the sake of simplicity, it was assumed that both fuel types had the same LHV and efficiency. Furthermore, the vessel statistics from MARESS were mainly made up of more than two years of data, from 2020 to 2022, except for a few vessels that had data from 2017 to 2022. Figure 4.4 illustrates the differences in power for vessel type and operational mode. The trend is that OCV generally has higher power consumption in the various modes of operation.

Table 4.2: Load profiles of OSVs for various modes of operation [Solstad Offshore, 2022].

	Mode	**Time [%]**	**Power [kW]**
OCV	DP	60	2300
	Standby	14	1700
	Transit (11 kn)	26	4000
PSV	DP	25	1100
	Standby	42	740
	Transit (11 kn)	33	2000
AHTS	DP	15	2200
	Standby	43	1200
	Transit (11 kn)	27	3800
	Towing	5	4700
	AH	11	3500

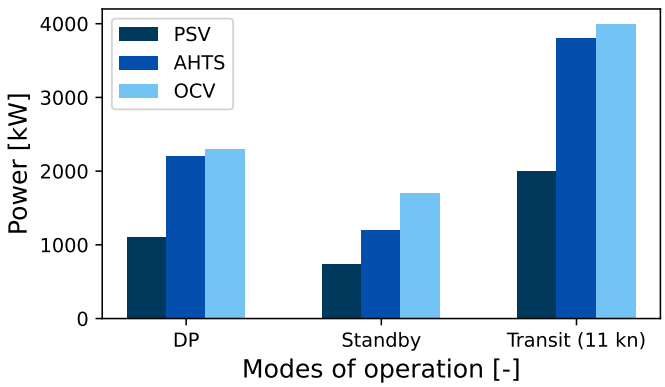

Figure 4.4: Load profile for different OSV types.

4.4 Resistance estimates

A variety of methods have been developed to estimate ships' resistance and powering requirements. The methods are mostly based on a few geometric properties in addition to speed. Some methods are also using data from model tests. Section 4.3 described the average power used by the various vessel types in transit with a speed of 11 knots. The empirical methods depicted in this chapter are used to estimate the variation in power consumption for different transit speeds. Three different methods are used to get an estimate of the power variation. It is important to clarify that

assumptions had to be made to adopt the empirical methods. Section 4.4.1, Section 4.4.2, and Section 4.4.3 describe the methods and Section 4.4.4 presents the variety in power consumption at different transit speeds.

4.4.1 Hollenbach's method

A Matlab code was made using the theory from *Fundamentals of Ship Hydrodynamics*, chapter 51 [Birk, 2019]. This method was developed in the 1990s and is based on test data from Schiffbau Versuchsanstalt in Vienna, Austria. The range of applicability is narrower compared to Holtrop and Mennen's method. However, the results seem to be more reliable and with less standard deviation, especially for twin-screw vessels, which is often the case for OSVs.

Table 4.3: Required and optional input for Hollenbach's method.

Required Parameters		
Parameter	*Symbol*	*Remarks*
Length between perpendiculars	L_{PP}	
Length in waterline	L_{WL}	check def. for ballast cond.
Length over wetted surface	L_{OS}	check def. for ballast cond.
Molded beam	B	
Molded draft at aft perpendicular	T_A	
Molded draft at forward perpendicular	T_F	
Propeller diameter	D	
Block coefficient (Based on L_{PP})	C_B	
Transverse vertical area above waterline	A_V	for air resistance
Number of rudders	$N_{rudders}$	1 or 2
Number of shaft brackets	$N_{brackets}$	0, 1 or 2
Number of shaft bossings	$N_{bossings}$	0, 1 or 2
Number of side thrusters	$N_{thrusters}$	between 0 and 4
Optional Parameters		
Wetted surface (hull)	S	
Wetted surface of appendages	S_{APP_i}	bilge keels, stabilizer fins, bossings
Diameter(s) of transverse thruster tunnels	d_{TH}	for appendage resistance fins etc.

4.4.2 Guldhammer Harvald's method

The theory for this method was gathered from *Fundamentals of Ship Hydrodynamics*, chapter 31 [Birk, 2019]. This method was developed in the late 60s when most ships did not have a bulbous bow. To make it applicable for ships with a bulbous bow, they later implemented the *computational length,* L_c. The required and optional input for this method is presented in Table 4.4.

Table 4.4: Required and optional input for Guldhammer and Harvald's method.

Required Parameters		
Parameter	*Symbol*	*Remarks*
Length between perpendiculars	L_{PP}	
Length of aft overhang in waterline	L_{aft}	usually $L_{WL} = L_{PP} + Laft$
Extension of S beyond fore perpendicular	L_{fore}	
Computation length	L	total extension of wetted surface (usually equal to L_{OS}.)
Maximum molded beam in waterline	B	
Molded draft	T	
Block coefficient	C_B	or volumetric displacement V
Prismatic coefficient	C_P	or midship section area A_M
Transverse cross section area of bulb	A_{BT}	at forward perpendicular
Optional Parameters		
Propeller diameter	D_P	for propulsion analysis
Longitudinal center of buoyancy	LCB	or assume optimum position
Wetted surface (hull+rudder)	S	
Wetted surface of appendages	S_{APP}	bilge keels, stabilizer fins, bossings
Form factors for fore and aft body	$F_F,\ F_A$	$-3 \leq F_A,\ F_F \leq +3$

4.4.3 Holtrop and Mennen's method

The theory for this method was also gathered from *Fundamentals of Ship Hydrodynamics*, chapter 50 [Birk, 2019]. This method is based on a regression analysis of model tests and trial data from MARIN, the model basin in Wageningen. Holtrop and Mennen's method is one of the most popular methods for estimating the resistance and powering of ships. The required and optional parameters for this method can be seen in Table 4.5.

Table 4.5: Required and optional input for Holtrop and Mennen's method.

Required Parameters		
Parameter	*Symbol*	*Remarks*
Length in waterline	L_{WL}	
Molded beam	B	
Molded mean draft	T	typically $T = \frac{1}{2}(T_A + T_F)$
Molded draft at aft perpendicular	T_A	
Molded draft at forward perpendicular	T_F	
Volumetric displacement (molded)	V	alternatively use the block coefficient as $C_B = V/(BTL_{WL})$
Prismatic coefficient (Based on L_{WL})	C_P	
Midship section coefficient	C_M	or use $C_M = C_B/C_P$
Waterplane area coefficient	C_{WP}	may have to be estimated in early design
Longitudinal center of buoyancy	l_{CB}	positive forward; with respect to $L_{WL}/2$ in percent of L_{WL}
Area of ship and cargo above waterline	A_V	projected in direction of v_s
Immersed transom area	A_T	measured at rest
Transverse area of bulbous bow	A_{BT}	measured at forward perpendicular
Height of center of A_{BT} above basis	h_B	has to be smaller than $0.6T_F$
Propeller diameter	D	
Propeller expanded area ratio	A_E/A_0	
Stern shape parameter	C_{stern}	
Optional Parameters		
Wetted surface (hull)	S	
Wetted surface of appendages	S_{APP_i}	bilge keels, stabilizer fins, bossings, etc.
Half angle of waterline entrance	i_E	
Diameter of bow thruster tunnel	d_{TH}	

4.4.4 Power consumption as a function of transit speed

As described above, simplified methods for ship powering were used to estimate how the power requirement changed with transit speed. Guldhammer-Harvald, Holtrop and Hollenbach are all empirical prediction methods [Dale, 2020]. Figure 4.5a shows the results from the three methods for an OCV. The average result from all methods is plotted as a dotted red line. The same plots for the other vessel types can be seen in Appendix H. The plots show that the empirical power is much lower than the power described in Section 4.3. This is probably because the empirical calculations assume calm sea and focus exclusively on the energy needed to push the hull through the water. Dr. Elizabeth Lindstad stated that the difference was mainly because of the lack of added resistance from waves. This could, in many cases, play an essential role (personal communication, Nov. 16. 2021). In addition, the vessel will also require power to operate cranes, bow- and aft thrusters, accommodation, etc.

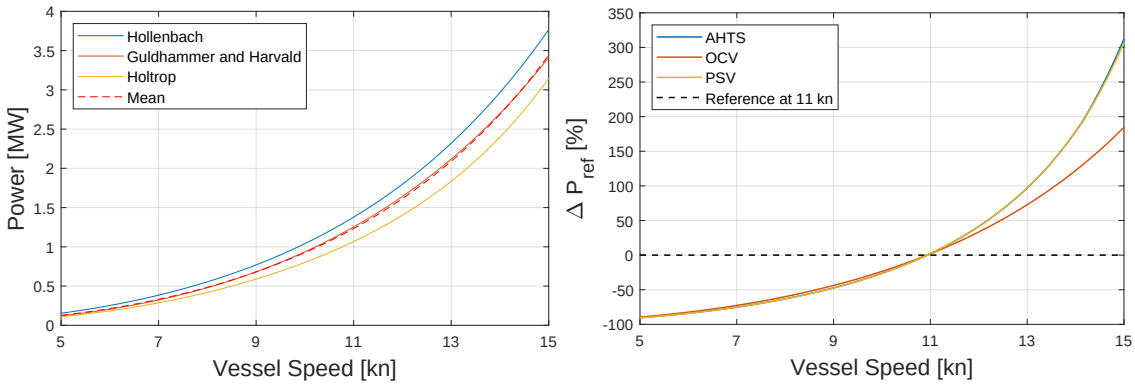

(a) Empirical power for OCV in transit. (b) Power variation from reference power at 11 knots.

Figure 4.5: Estimated transit power from empirical methods.

Figure 4.5b shows how the estimated mean power alters with transit speed for each vessel type. The change is based on a reference speed of 11 knots, as this is the speed used in Section 4.3 to investigate the power consumption. An extended load profile is estimated assuming that the empirical methods give a suitable picture of the change in power for different transit speeds. For instance, Figure 4.5b shows that the power for a PSV with a transit speed of 13 knots will be around 100 % more than the power at 11 knots. The original load profile is extended to contain more transit speeds, as shown in Table 4.6, with the reference speed (v = 11 knots) seen in italic.

Table 4.6: Load profile at different transit speeds with v = 11 kn as reference.

Speed [kn]	**Transit Power OCV** [kW]	**Transit Power PSV** [kW]	**Transit Power AHTS** [kW]
5	400	190	360
7	1100	490	930
9	2200	1000	2000
11	*4000*	*2000*	*3800*
13	6800	3900	7300
15	11 000	8000	15 000

4.5 Theoretical sailing distances for various fuel types

The load profiles from Table 4.2 and the load profile at different transit speeds from Table 4.6 are used to calculate the achievable sailing distances for the various fuel types. Equation 4.2 is used to calculate D_{max}. V_{Tank} is the size of the fuel tank for different vessel types. It is based on average values from numerous chosen vessels. The analysis can be seen in Appendix F, and the average values can be seen in Table 4.7. The energy densities for the different fuel types (E_{fuel} [MJ/m^3]) are based on the background study in Section 3.5, Section 3.3.3, and Section 3.3.4 and can be seen in the second column of Table 4.8. η_{lhv} is the efficiency with respect to the LHV of the fuel used. Section 3.3.4 depicts the efficiency of hydrogen FC as 50 % and MDO with a conventional machine as 37 %.

$\eta_{storage}$ shall take into account the loss of energy when storing hydrogen. From Section 3.5, *Hydrogen Storage*, it was clear that there are significant losses when storing hydrogen. The loss of keeping MDO is assumed to be zero compared to hydrogen. The losses can be seen in the third column of Table 4.8. v is the transit speed of the vessel. Furthermore, T_T, T_{SB}, and T_{DP} are the percentages in which the vessel operated in a given mode of operation, gathered from the operational profiles. For AHTS vessels, two additional time variables are added for AH (T_{AH}) and towing (T_{tow}). At last, P_T, P_{SB}, and P_{DP} are the power requirements in the various modes of operation, described in Table 4.2 and Table 4.6. P_{AH} and P_{tow} are added for AHTS vessels.

$$D_{max} = \frac{V_{Tank} \cdot E_{fuel} \cdot \eta_{lhv} \cdot (1 - \eta_{storage}) \cdot v \cdot T_T}{[P_t \cdot T_T + P_{SB} \cdot T_{SB} + P_{DP} \cdot T_{DP}] \cdot (60 \cdot 60)} \tag{4.2}$$

When Equation 4.2 is used with the parameters described above, different values for D_{max} based on transit speed, vessel type, fuel type, fuel storage technology and volume of fuel tank are gathered.

Table 4.7: Average tank sizes from analysis of 33 vessels.

	V_{Tank} $[m^3]$
OCV	2100
PSV	1200
AHTS	1300

Table 4.8: Energy densities and storage loss of various fuel types. All with temperature of 293 K.

Fueltype [-]	**Energy density** [MJ/m^3]	**Energy loss storage** [$\eta_{storage}$ %]
Hydrogen, 1 bar	9.3	0
Hydrogen, 10 bar	91.7	5
Hydrogen, 100 bar	871	5
Hydrogen, 300 bar	2340	10
Hydrogen, 400 bar	2970	11
Hydrogen, 700 bar	4540	15
Hydrogen, liquid	8000	30
MDO	36 100	0

4.6 Python implementations

Python was used to handle the AIS data from the vessel fleet described in Chapter 2. The main task of the python code is to analyze the AIS data, give an overview of the operation pattern of each OSV type, and evaluate if an OSV can run on hydrogen. The different functions are developed in python using well-established libraries like Pandas, matplotlib.pyplot, NumPy, Folium and Scikit-Learn. In addition to some slightly lesser known ones as SQLite3, Functools, BeautifulSoup, GeoPy, and Global-Land-Mask.

4.6.1 Speed profile and data cleaning

The AIS database contains a column with the speed of the vessel in each position. This is called speed over ground (SOG). However, by looking closer at the given data, it was possible to identify several unexpected and unnatural numbers. In some positions, the AIS data stated that the vessel had speeds of 100 knots. Because of this, a code to calculate the speed profile was created. This uses the *geopy.distance* package in python to find the distance between each data point (latitude and longitude). Furthermore, it uses the *to_datetime* characteristics of the *panda dataframes* to find the corresponding time between each data point. At last it calculates the speed as distance divided by time. The code can be seen in Appendix I.2. Figure 4.6 shows two speed profiles of the same AHTS vessel with data from 01.01.2020 to 18.12.2020. Calculating the vessel's speed using position and time removes the unnatural numbers in the SOG column from the AIS data. Figure 4.6a illustrates how this 100 kn recording damages the speed profile and how it is fixed in Figure 4.6b.

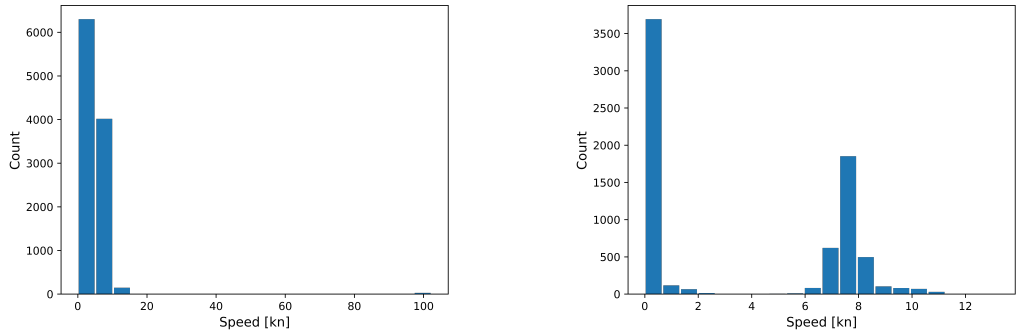

(a) SOG from AIS data.

(b) Calculations in python code.

Figure 4.6: Speed profile differences by using two different methods for speed collection in AIS data for AHTS vessel, before data cleanup.

The unnatural values from Figure 4.6a demonstrate the importance of data cleanup when using AIS data. This is done by introducing different constraints in the code. The *cleanSpeedDataframe(listDF)* function (Appendix I.3) combined with the *removeLargeTimeIntervals(routeDF)* (Appendix I.4) function is used to clean the data. It will drop data points with speeds larger than 25 knots and lower than zero knots. The *removeLargeTimeIntervals* function will go through the data and drop already identified routes if they contain points that have intervals of more than 12 hours between each measurement. The 12 hours limit is selected with respect to a common AIS measurement frequency. Further inspection of the AIS data revealed that intervals of 6 and 12 hours were often used. If the limit had been set just under 12 hours, a lot of data would have been neglected. Listing 4.1 shows how the cleaning of large time intervals works.

Listing 4.1: Drop data points with intervals of more than 12 hours.

```
def removeLargeTimeIntervals(routeDF):
    removeDataframe = False
    s = routeDF['dt'].diff().apply(lambda x: x/np.timedelta64(1, 's')).
    fillna(0).astype('int64')
    if (s > 43200).any():  # 12 hours = 43200 s
        removeDataframe = True
    return removeDataframe
```

More data cleanup is performed in the *readDatabase(dbName)* function (Appendix I.1). Data points with latitude values lower than -90 and higher than 90 degrees are removed, in addition to longitude values lower than -180 and higher than 180. Duplicates and empty data points are also removed. Table 4.9 summarizes the main effects of the data cleaning.

Table 4.9: Impact of AIS data cleaning.

	Dataset length (Data pts)	**Num. neglected rows (0 <kn <25)**		**Neglected rows (duplicates, zero-values, lat, lon)**		**Num. datapoints identified as routes**	
Units	*[pcs]*	*[pcs]*	*[%]*	*[pcs]*	*[%]*	*[pcs]*	*[%]*
OCV	3 088 072	7782	0.25	11	0.00	2 317 219	75
PSV	5 846 524	18 658	0.32	192	0.00	2 724 396	47
AHTS	5 911 315	17 514	0.30	1061	0.02	3 830 121	65
Total	**14 845 911**	**43 954**	**0.30**	**1264**	**0.01**	**8 871 736**	**60**

4.6.2 Classification of data points

The functions *classifyPoints(df)* (Appendix I.5) and *isOnLand(lat, lon, r, n)* (Appendix I.6) will take the data frame from *readDatabase(dbName, vesselIn)* (Appendix I.1) as input, loop through it and identify nearshore and offshore points. Nearshore is defined using a circle with a radius of 0.25 degrees, as seen in Figure 4.7. In this case, n = 8 points will be created in a circle around the data point, and one by one, they are evaluated by the *globe.is_land(lat, lon)* function. If one of the points on the circle is on land, the original point will be defined as a nearshore point. Listing 4.2 shows a simple-pseudo code on how the *isOnLand(lat, lon, r, n)* function works. The output is an updated data frame with an extra column where the classification is added, nearshore or offshore. This column is later used to pick out routes in the given dataset. Figure 4.8 shows how each AIS point is classified as either a nearshore (green) or offshore (blue) point.

Listing 4.2: Verify if point is a nearshore or offshore point.

```
def isOnLand(lat, lon, r=0.25, n=8):
    isNearShore = False
    dTheta = np.pi * 2 / n
    startTheta = 0

    for i in range(n):
        if globe.is_land(lat+np.sin(startTheta)*r, lon+np.cos(startTheta)*r):
            isNearShore = True
            break
        startTheta += dTheta

    return isNearShore
```

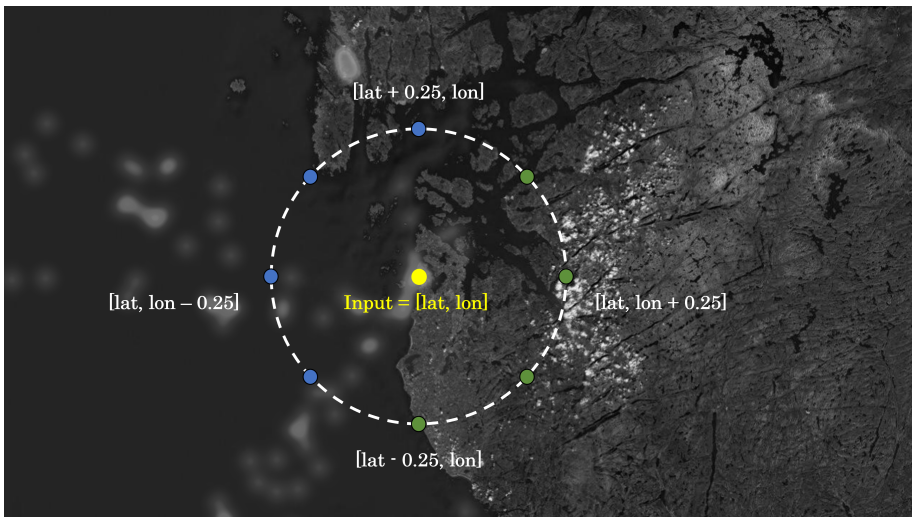

Figure 4.7: Identify nearshore points with n = 8.

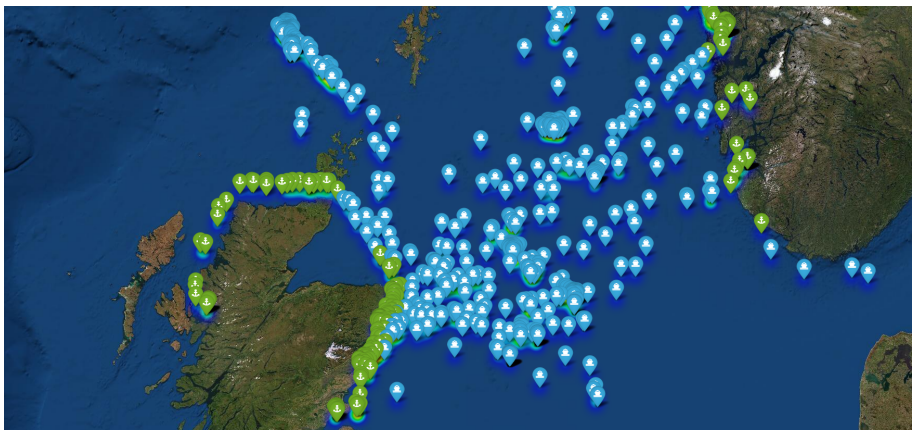

Figure 4.8: Pinpointing nearshore (green) and offshore (blue) points from AIS dataset.

4.6.3 Establish routes

The next step is to use the classification described in Section 4.6.2 to point out the routes traveled by each vessel. The function *findRoutes(df)* will take in a data frame and loop through all points. When the data frame is sorted by date, the function will reveal all intervals starting and stopping on a nearshore point. Table 4.10 is an example of a route that starts on 03.01.2020 and ends on 31.01.2020. One can see from the *class* column that the route both starts and stops at a nearshore point. The output from the function will be a list of data frames where each data frame represents a route. The total distance and speed are also calculated for every route. Figure 4.9 illustrates how the route in Table 4.10 is identified by the code. The colored lines represent the transit speed of the vessel with intervals defined in Table 4.11.

Table 4.10: Example of route construction in python code.

dt	lat	lon	Class	Route
03/01/2020 20:37	-22.6498	-41.6938	Nearshore	1
03/01/2020 20:44	-22.6692	-41.6920	Offshore	1
03/01/2020 20:46	-22.6739	-41.6915	Offshore	1
03/01/2020 21:28	-22.7891	-41.6808	Offshore	1
03/01/2020 21:56	-22.8583	-41.7141	Offshore	1
03/01/2020 22:55	-23.0034	-41.7959	Offshore	1
⋮	⋮	⋮	⋮	⋮
30/01/2020 23:53	-22.2713	-40.5032	Offshore	1
30/01/2020 23:57	-22.2723	-40.5148	Offshore	1
31/01/2020 00:28	-22.2803	-40.6068	Offshore	1
31/01/2020 01:56	-22.3046	-40.8655	Offshore	1
31/01/2020 03:09	-22.3349	-41.0755	Offshore	1
31/01/2020 05:24	-22.3963	-41.4602	Nearshore	1

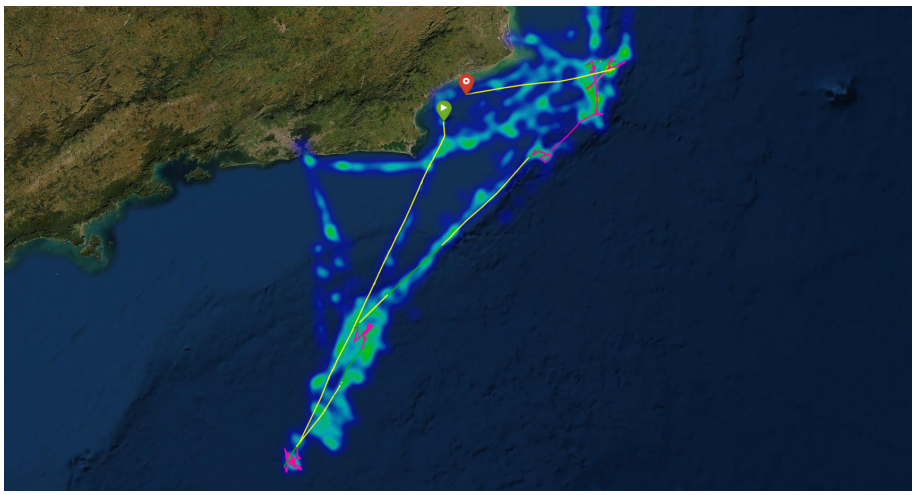

Figure 4.9: Example route for AHTS vessel outside Brazil.

Table 4.11: Defined color intervals for route plotting [kn].

	From [kn]	**To** [kn]
	0	5
	5	9
	9	12
	12	15
	15	∞

4.6.4 Theoretical sailing distances

Equation 4.2 was used to create the *sailingDistance()* function in python (Appendix I.8). It calculates D_{max} for different fuel and vessel types at different transit speeds. All assumptions made in the function are the same as in Section 4.5. The different characteristics used as input are stored as csv-files imported by the function itself. The content of the csv-files can be seen in Appendix J.

4.7 Mapping zero-emission potential

Two different methods were formulated to map the zero-emission potential. Each method compares the demand from AIS data with D_{max} from Section 4.5. The only difference is how the demand is mapped. Figure 4.10 illustrates the main differences between the two approaches. The green points represent the start of a route and the red points represent the ending. Method 1 will only focus on the longest route identified for each vessel. The longest route will be the threshold for what the vessel has to be able to cover with the given fuel type. For instance, the vessel will not be able to run on LH_2 if D_{max} is shorter than the longest route, which means that the potential will be zero. However, method 2 will focus on all routes identified in the AIS data for each vessel. D_{max} will be compared with each route, and it will be stored whether the vessel can cover the distance or not. Instead of checking only one route as in the first method, method 2 will give a percentage of how many of the yearly routes the vessel is able to cover.

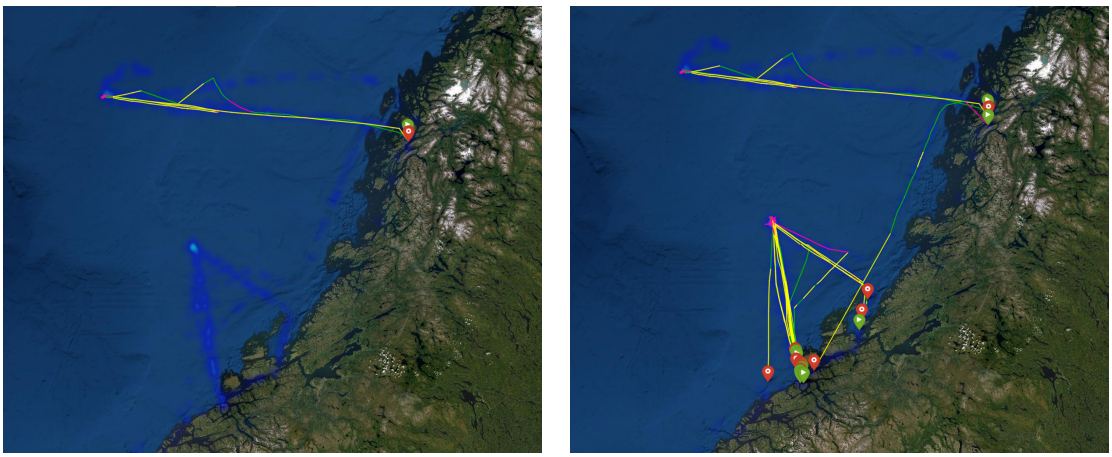

(a) **Method 1**: analyzing only the longest route. (b) **Method 2**: analyzing all routes.

Figure 4.10: Method 1 and 2 used to map zero-emission potential.

Chapter 5

Case

This chapter will focus on one year of AIS data for a chosen vessel. It will go through the process step by step, use one vessel as an example and illustrate how the analysis has been carried out.

5.1 Properties of selected vessel

The vessel selected for this case is a relatively large OCV with a length of 124 meters, a width of 28 meters, and a dwt of 9511. The vessel's AIS data consists of 99 978 lines with data points from 01.01.2020 to 29.12.2020. The speed profile of the vessel can be seen in Figure 5.1. It is essential to point out that the y-axis has been limited to a count of 5000 for better visualization of transit speeds. Originally, there were almost 70 000 measurements for speeds between 0 and 0.5 knots. The average speed for all measurements is 1.69 knots, which indicates that the vessel spends much of its time at rest. The transit speed seems to have two peaks, one from 6.5 to 7.0 knots and one from 9.0 and 9.5 knots.

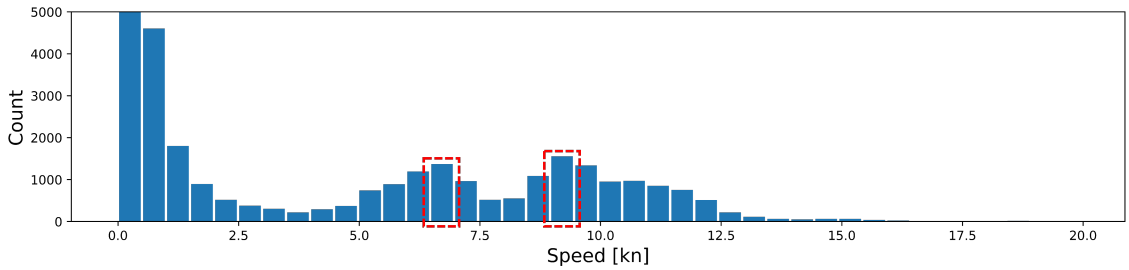

Figure 5.1: Speed profile of case vessel (OCV).

5.2 Identify routes

A total of 21 routes were identified from the AIS data. 91 733 lines of data points were used to build the routes. In other words, 91 733 out of 99 978 lines of data were linked to a route. The main characteristics of the identified routes can be seen in Table 5.1. The routes have been sorted by length. Some of the routes have been neglected due to constraints, which is the reason for the inconsistent numbering. All in all, three routes had to be neglected because there were too large time steps between some points. As described in Section 4.6.1, the time step could not exceed 12 hours. If so, the route was dropped from further analysis. One of the dropped routes can be seen in Figure 5.2. The AIS system was turned off for more than 12 hours, and thus the time interval became so large that the route was neglected. The main reason for this constraint is the uncertainty associated with such large time intervals. If not ignored, it may lead to false data.

Table 5.1: Routes identified for case OCV from one year of AIS data.

Route num.	**Length** [nm]	**Avg. Speed** [kn]	**Duration** [dd,hh]
25	3780	10.4	14 days, 16 hours
2	1340	10.6	5 days, 6 hours
5	1330	8.1	6 days, 18 hours
16	687	6.5	4 days, 12 hours
23	668	1.7	14 days, 22 hours
22	666	1.6	17 days, 13 hours
20	655	1.4	21 days, 19 hours
4	454	0.5	39 days, 9 hours
1	333	1.9	8 days, 10 hours
3	299	0.3	43 days, 20 hours
14	212	3.5	2 days, 9 hours
24	178	4.4	1 days, 22 hours
8	153	6.5	0 days, 23 hours
7	151	5.7	1 days, 2 hours
10	150	5.4	1 days, 3 hours
12	100	6.3	0 days, 15 hours
11	47	6.0	0 days, 7 hours
15	25	1.3	15 days, 2 hours
9	15	2.6	0 days, 12 hours
13	14	4.1	1 days, 3 hours
6	12	0.9	1 days, 6 hours

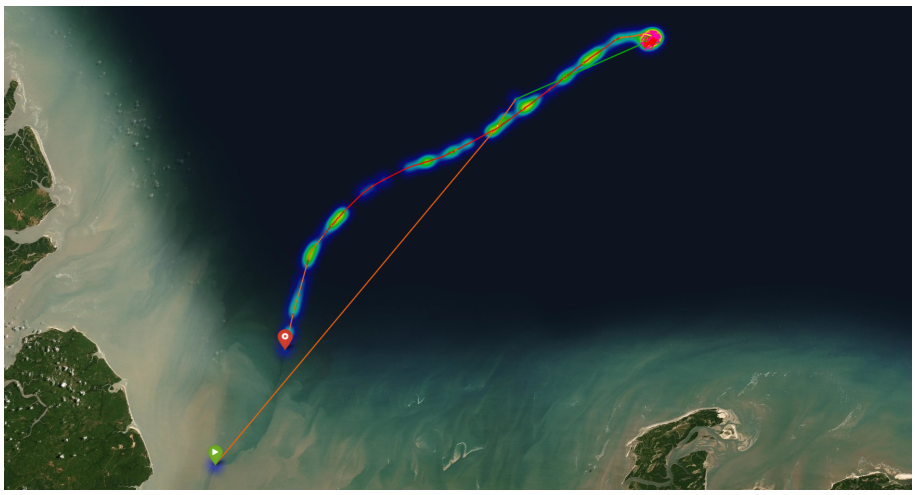

Figure 5.2: Dropped route because of too large time steps.

Figure 5.3 and Figure 5.4a illustrates the problem related to the poor quality of the AIS data. One of the points abruptly ends up outside Greenland. For the ship to be able to reach there at the specified time, it is necessary to sail at more than 140 000 knots. This is, naturally enough, not realistic for a ship. Section 4.6.1 describes how the AIS data is cleaned for unnatural speeds. This will remove the point causing these problems, and as long as the new time step to the next point satisfies the constraints ($<$ 12 hours), the route will be saved. Figure 5.4b shows how the final route appears after being cleaned.

Figure 5.3: Overview of bad data point.

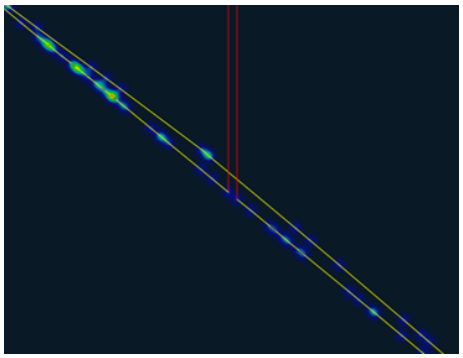

(a) Bad data point.

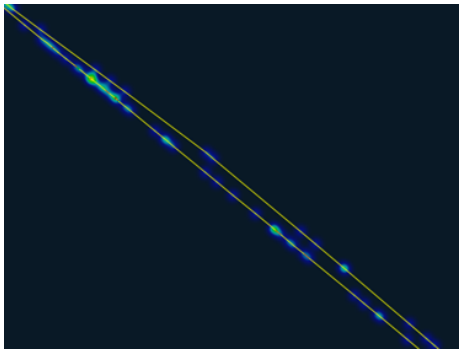

(b) Fixed data point.

Figure 5.4: Close up of how code is fixing bad data.

Figure 5.5 exhibits the two longest routes identified in one year of AIS data for the case vessel. The longest route is 3780 nautical miles (route 25 in Table 5.1), and crosses the Atlantic Ocean from Bridgetown of Barbados to Boulogne of France. The mean speed across the Atlantic Ocean is 10.4 knots, and the route duration is 14 days and 16 hours. Veson Nautical [2022] and Sea-web were used to evaluate the quality of the analysis. This maritime portal calculates the sea distance between international ports based on transit speed. The result from Sea-web can be seen in Table 5.2. Compared to the AIS analysis, Sea-web predicts 3723 nm instead of 3780 nm. Furthermore, a duration of 16 days and 10 hours is assumed. This is a few days longer than the AIS analysis. However, Sea-web assumes a weather factor of 10 % as default, which may be the reason for the long duration. If the 10 % weather factor is added to the duration from the AIS analysis, the new sailing period will be 16 days and 3 hours. This is not far from the Sea-web prediction, which indicates a good correlation between the AIS analysis and Sea-web. Additionally, it may be that the weather was calm when the AIS data was logged.

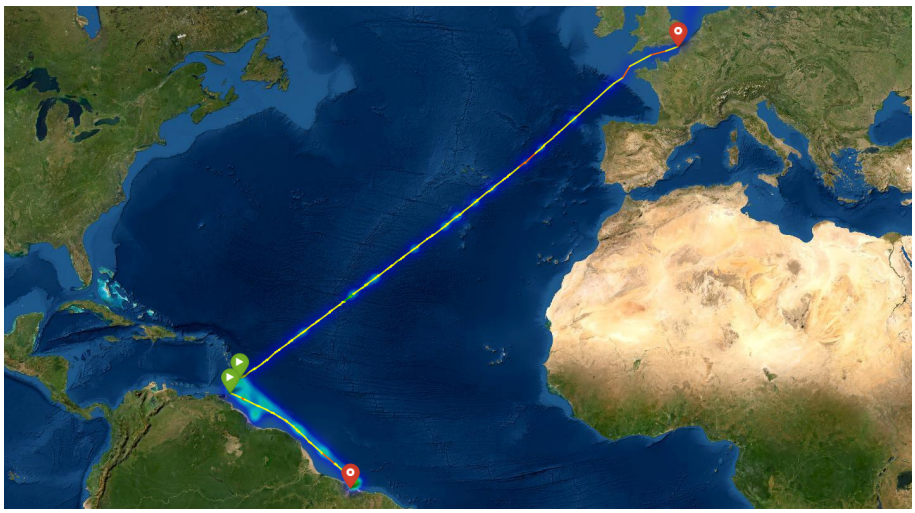

Figure 5.5: The two longest routes identified in one year of data.

Table 5.2: Sea distance from Bridgetown (Barbados) to Boulogne (France) Veson Nautical [2022].

From port		Bridgetown
To port		Boulogne-Sur-Mer
Weather factor	[%]	10
Mean speed	[kn]	10.4
Distance	[nm]	3723
Duration		16 days, 10 hours

Route number three is another trail that stands out from Table 5.1, with a duration of 43 days and 20 hours. A close-up of the route where the vessel spent most of the time can be seen in Figure 5.6. The operation pattern shows that the vessel was relatively stationary during this period. As summarized in Table 4.11, a pink line indicates that the vessel had speeds from 0 to 5 knots. This may explain the low average speed identified in the yearly speed profile above. If the duration of all routes from the AIS analysis is summed together, the total duration will be 203 days and 9 hours. This implies that the vessel spent roughly 60 % of the time at sea in 2020.

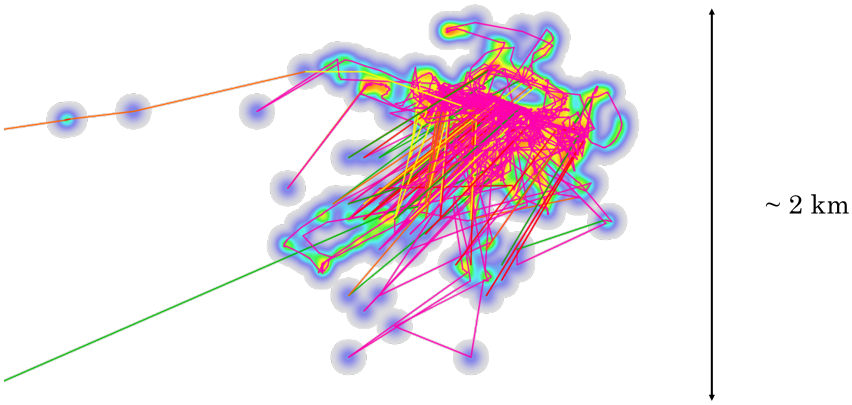

Figure 5.6: Route 3 with duration of 43 days and 20 hours.

5.3 Compare demand against theoretical sailing distance

The routes identified in the previous section are presumed to represent the demand from the offshore market. It will indicate the expectations set for an offshore vessel. Perhaps one vessel does not represent it thoroughly, but the coverage will hopefully be adequate when more vessels are analyzed in the results. Figure 5.7a shows how the length of the transatlantic crossing (route 25) is compared with D_{max} for different fuel types. D_{max} is calculated as described in Section 4.5, with a given tank size and a transit speed of 11 knots. The bar plot reveals that MDO is the only fuel with sufficient range.

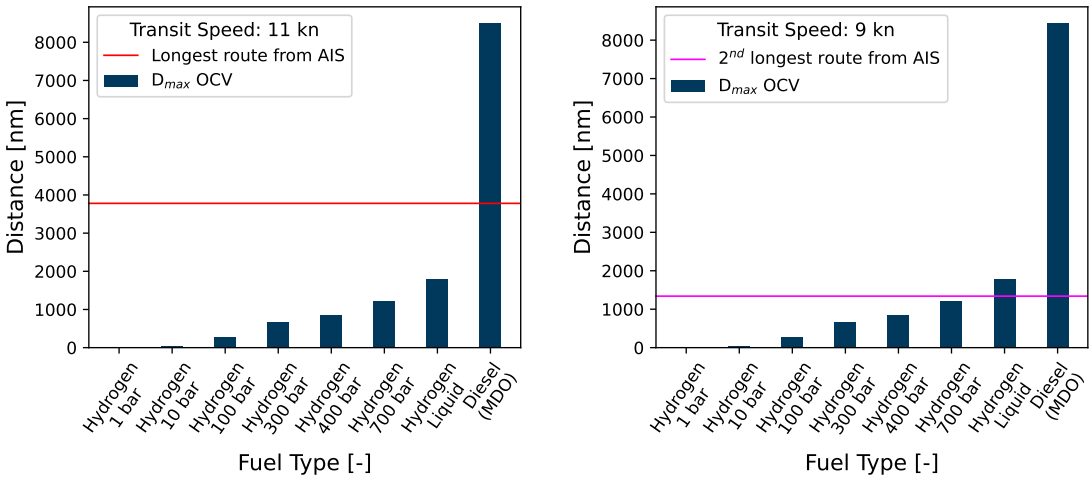

(a) Longest route.

(b) Second-longest route.

Figure 5.7: AIS demand compared with D_{max} for various fuel types and transit speeds.

Figure 5.8 illustrates D_{max} for LH_2 as a function of transit speed and vessel type. By looking further into the effect of transit speed, it seems like a speed of 9 knots would maximize the range. The red line still indicates that LH_2 does not have sufficient range to cover route 25. However, for further inspection, it could be interesting to see which fuel types are sufficient if the transatlantic crossing is removed and the second-largest route is compared with D_{max}. This implies that the vessel can not operate internationally, but perhaps this could be a distinct step toward streamlining the use of the offshore fleet. The pink line in Figure 5.7b will now represent the second-largest route, compared with D_{max} for a transit speed of 9 knots. This is the second-largest route from Table 5.1 (route 2), with a length of 1340 nm. Now one can see that LH_2 also has sufficient range. In addition, one can see that hydrogen stored at 700 bar is almost enough for OCVs.

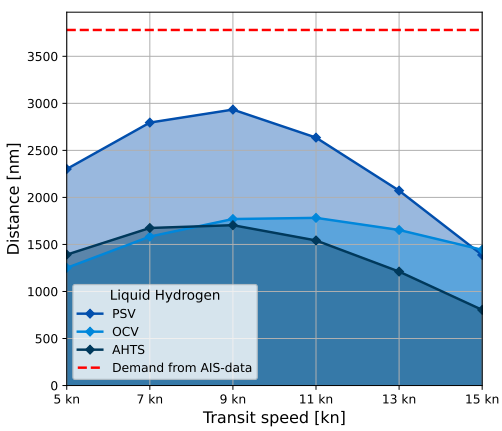

Figure 5.8: D_{max} for LH_2 as a function of transit speed.

5.3.1 Method 1

Chapter 4 described two different methods for mapping the zero-emission potential. The first method used only the longest route, which in this case will be the transatlantic crossing from Barbados to France, seen as route number 25 in Table 5.1. Figure 5.7a showed that MDO was the only fuel able to cover this distance, and the potential for hydrogen propulsion will, in this case, be zero according to method 1.

5.3.2 Method 2

The second method used all routes to map the potential. Figure 5.7a already illustrated that the longest route was not realistic to be run on hydrogen. However, Figure 5.7b showed that the second-longest route was sufficient with LH_2, thus also the other shorter routes. In other words, 20 out of 21 routes will be sufficient to be run on LH_2. For comparison, as method 1 mapped the potential to be zero, method 2 will map the potential to be 95 % for this particular vessel.

5.3.3 Effect of changing fuel capacity

Figure 5.9 demonstrates how D_{max} changes with tank size for an OCV. When the size of the tank is increased with 50 % CH_2 at 700 bar will also be sufficient when the transatlantic route is neglected. However, with LH_2, the vessel is able to cross the Atlantic if the fuel capacity is increased by 200 % from the average tank size of 2100 m^3. A more comprehensive analysis of the effect of changing the tank size is presented in Chapter 6, *Results*.

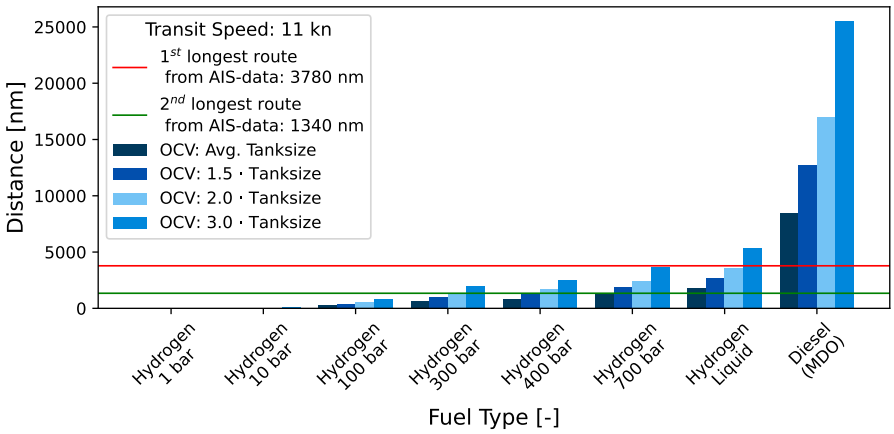

Figure 5.9: D_{max} tank size dependency for OCV at 11 knots.

Chapter 6

Results

This chapter contains the results from the calculations made to evaluate the use of hydrogen in today's OSVs. The values gathered from the methods in Chapter 4 are put up against the demand gathered from the AIS data to evaluate the applicability of hydrogen as fuel in OSVs.

6.1 Average sailing speed

The code described in Section 4.6.1 is used to calculate the speed profile of each vessel investigated. Adding all speed profiles together will give a good overview of which transit speeds are most common. The speed profile for all AHTS vessels can be seen in Figure 6.1. The other vessel types can be seen in Appendix K. The speed profiles have been cleaned as described in *Methods* and built up by all the routes identified in the given database. A route is defined from one nearshore point to another nearshore points. Therefore, the speed profiles will apply to vessels in offshore operation, not laying in port.

A total of 3 805 575 lines of data points were used to build the speed profile in Figure 6.1. It shows that the vessels sail at relatively low speeds even when offshore. The first bar with speeds from 0 knots is, without a doubt, the highest. Table 6.1 displays the average speeds on all routes identified for each vessel type. This shows that the vessels, on average, have a very low speed when offshore. Once again, it is worth mentioning that these speed profiles are built up by the routes identified by the python code. In other words, the time the vessel leaves the quay until it returns. A total of 3122, 3968, and 1049 routes were found for AHTS, PSV and OCV, respectively.

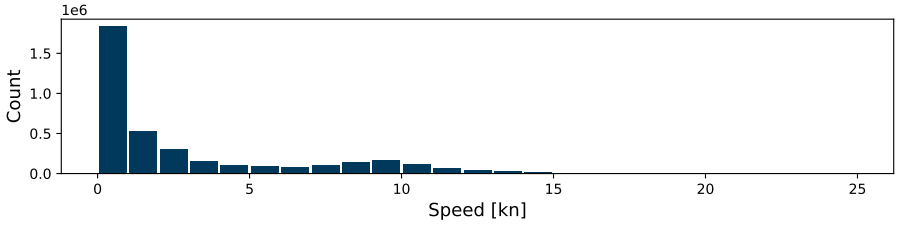

Figure 6.1: Total speed profile of all AHTS vessels in the database.

Table 6.1: Average speed of OSVs in database.

	Avg. Speed [kn]
OCV	2.38
PSV	3.00
AHTS	2.93

The speed profiles are further cleaned with an interval from 4 to 20 knots to get a better insight into the transit speed of the various vessel types. The interval length is chosen to eliminate the lowest speeds where the vessel is most likely in standby or DP. The three new speed profiles can be seen in Figure 6.2. It seems like the most frequent transit speeds are 10.5 knots for OCVs, 9.0 knots for PSVs, and 9.5 knots for AHTS vessels.

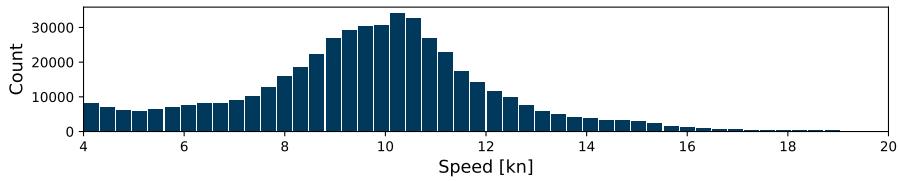

(a) OCV

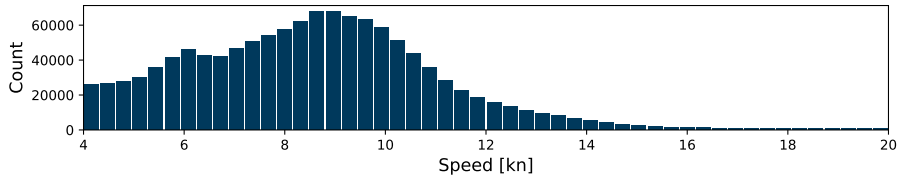

(b) PSV

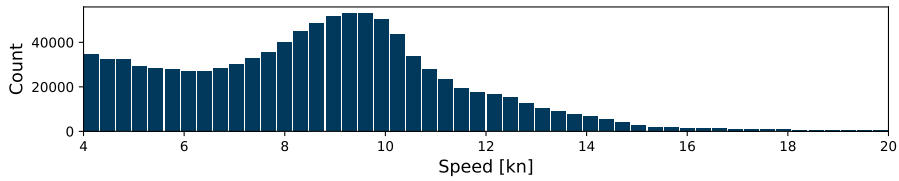

(c) AHTS

Figure 6.2: Transit speed profiles for the OSVs.

6.2 Theoretical sailing distances

The maximum theoretical sailing distances (D_{max}) are determined using the method described in Section 4.5 and python functions described in Section 4.6.4. The sailing distances are compared for different fuel and storage methods and set up against the demand identified in the AIS data. Figure 6.3 is an example of the output. In this case, the transit speed was set to 11 knots. It shows how D_{max} changes with both fuel and vessel type. Additional plots for other transit speeds can be seen in Appendix L.

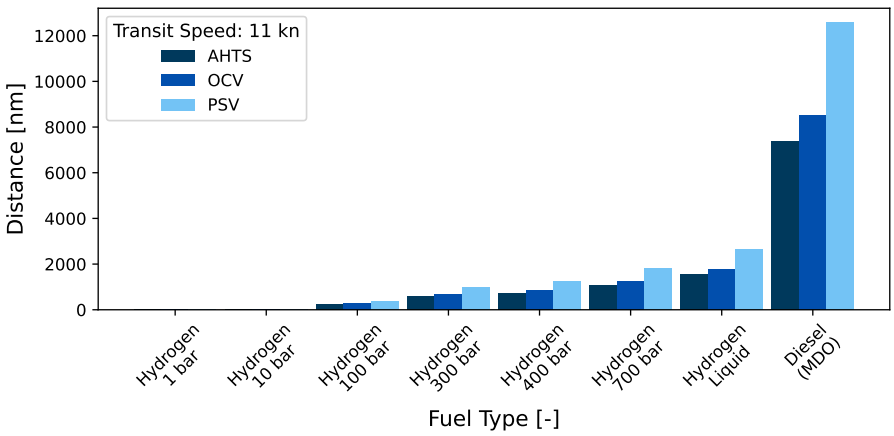

Figure 6.3: D_{max} with transit speed of 11 kn.

Figure 6.3 shows that PSVs generally have larger D_{max} than the two other vessel types, although the average tank size of PSVs was assumed to be almost half of OCVs (Seen in Table 4.7). This is mainly because the power consumption is much lower for PSVs compared to OCVs and AHTS vessels, both in transit and the other modes of operation (Seen in Table 4.2 and Table 4.6). In addition, it is possible to see from Figure 6.3 that D_{max} is much larger for MDO than all hydrogen solutions. This is mainly because of the low volumetric energy density of hydrogen and the losses associated with storage. It is worth discussing that this method assumes that the average tank size for each vessel type is the volume available for fuel and that this is the same for all types of fuel. However, this is further analyzed in Section 6.5, *Effect of changing fuel capacity.*

Figure 6.4 illustrates how D_{max} varies with transit speed and vessel type. Figure 6.4a presents D_{max} when the tank is filled with LH_2 and Figure 6.4b with MDO. D_{max} for the other fuel types can be seen in Appendix M. The trend is that D_{max} increases from five to nine knots, even though the vessel needs more power to run at nine knots compared to five. The reason for this is probably that the consumed energy in *Standby* and *DP* is expressed as a percentage of the total route duration. When the vessel's transit speed is too low, the total route duration will be longer, and the time in *Standby* and *DP* becomes longer. Hence the power consumption in *Standby* and *DP* plays a larger role. Whether this is a reasonable assumption is further discussed in Chapter 7, *Discussion.*

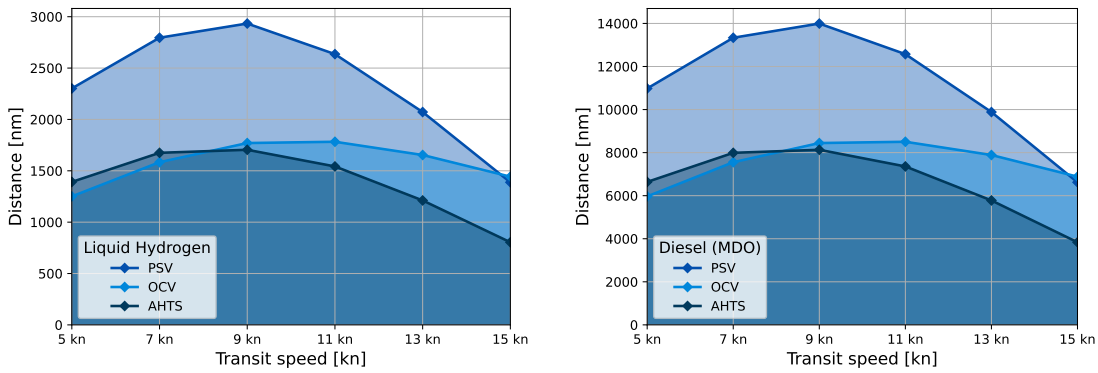

(a) LH_2 (b) MDO

Figure 6.4: D_{max} as function of transit speed.

6.3 Sailing distances from AIS

All vessels in the AIS database have been investigated using the python functions described in Section 4.6, *Python Implementations.* Some vessels had to be dropped because of the lack of data points. In addition, some vessels had to be neglected due to poor data quality. 66 OCVs, 122 PSVs, and 95 AHTS vessels have been analyzed. As described in Section 6.1, 1121 routes were found for OCVs, with an average of 17 routes identified for each vessel. 4226 routes were identified for PSVs, with an average of 35 routes per vessel. At last, 3125 routes were identified in the AHTS database, with an average of 33 routes per vessel.

Table 6.2 presents some average values from the AIS analysis. It shows, among other things, that OCV, on average, travels longer distances than the other two vessel types. The average route length for a PSV is 272 nm compared to an OCV with 590 nm. The largest route for each vessel was also stored. The average maximum route lengths were identified as 1558, 816, and 1155 nm for OCV, PSV, and AHTS vessels, respectively.

Figure 6.5 compares the mapped demand from AIS data with D_{max} for a transit speed of 11 knots. The red, green and blue lines illustrate the average longest route identified for each vessel type. It shows that to cover the longest routes from the AIS data, the OCV could run on either LH_2 or MDO. For PSVs, hydrogen at 700, 400, and 300 bar will also be sufficient. It is important to point out that the y-axis in Figure 6.5 has been limited to 4000 nm to illustrate the main focus more

clearly. The sailing distance for MDO is longer than demonstrated in the figure.

Table 6.2: Average values from vessel database and AIS analysis.

		OCV	**PSV**	**AHTS**
Age vessels	[year]	2010	2012	2010
gt	[m^3]	9536	3719	5149
dwt	[tons]	6567	4221	3498
Length	[m]	113	84	82
Width	[m]	23	18	20
Num. vessels analyzed	[pcs]	66	122	95
Avg. database size	[Num. lines]	46 789	47 922	62 224
Avg. num. of routes identified	[pcs/vessel]	17	35	33
Avg. route length	[nm]	590	272	346
Avg. largest route	[nm]	1558	816	1155
Avg. duration largest route	[dd, hh]	15 d, 12 h	8 d, 8 h	11 d, 5 h

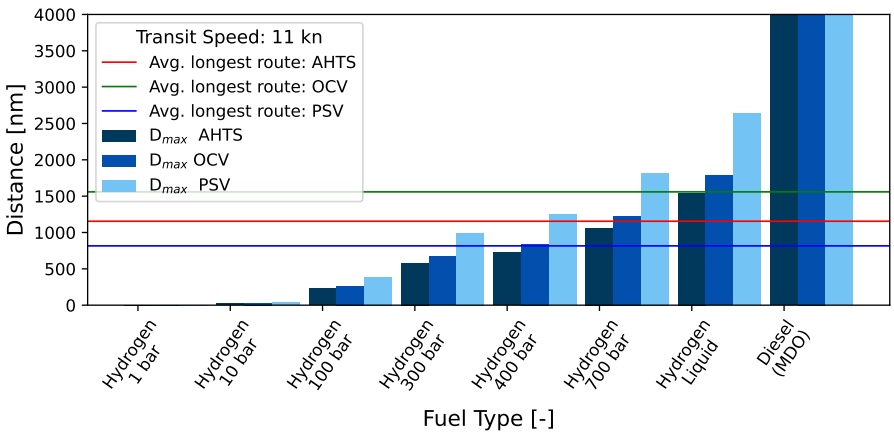

Figure 6.5: Demand from AIS data compared to D_{max} at 11 knots.

6.4 Zero-emission potential

As described in Section 4.7, Method 1 will highlight only the longest route identified for each vessel throughout the year. If D_{max} is larger than the longest route, it will also be sufficient for the other shorter routes identified for the vessel. While Method 1 focused only on the longest route identified for each vessel, Method 2 will, as described in Section 4.7, investigate each individual route found for every vessel.

6.4.1 Method 1

The longest route identified for each vessel will for this method serve as a threshold for what the ship must be able to sail to meet the needs of the offshore market. Comparing it with D_{max} gives an overview of which fuel types are adequate. Figure 6.6 shows the percentage of vessels analyzed that fulfilled the demand from AIS data with a transit speed of 11 knots and the corresponding fuel. In other words, it illustrates the percentage of vessels that manage to cover their longest route with a given fuel type. Naturally enough, all vessels manage to cover the distance with MDO. 71.2 % of the OCVs examined can run on LH_2, 74.7 % of the AHTS vessels, and as much as 95.1 % of the PSVs. The trend from the plot is that the PSVs generally have a much higher

acceptance of alternative fuels than the other ship types. The results for the other transit speeds are presented as tables in Appendix N.

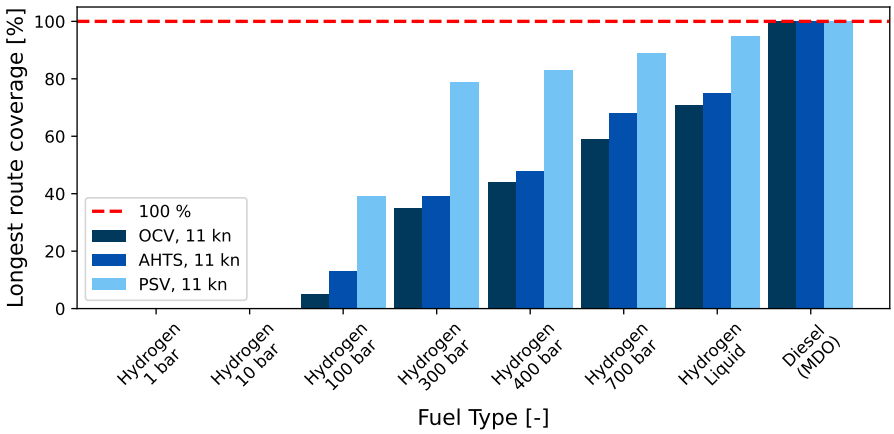

Figure 6.6: AIS data coverage with transit speed of 11 knots.

Suppose the fuel types are divided into two groups, zero-emission and fossil fuels, and the different vessel types are disregarded. In that case, 84 % of the 283 vessels investigated could sail their longest route by running on hydrogen, as illustrated in Figure 6.7. This is a strong indicator that it is possible to move towards a zero-emission shipping industry.

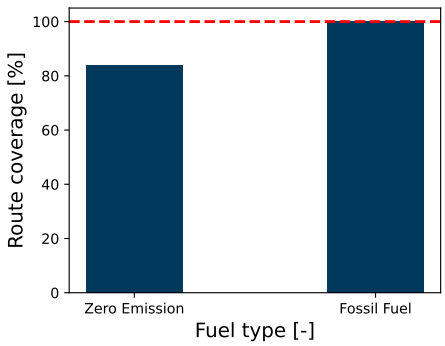

Figure 6.7: Route coverage for entire OSV fleet by using Method 1.

6.4.2 Method 2

Figure 6.8 shows how the route coverage depends on different hydrogen storage solutions. Each bar represents one AHTS vessel from the database, and the height of the bar is the percentage of identified routes that can be covered with the given fuel type. The transit speed in Figure 6.8 was set to 11 knots, and the three highlighted hydrogen storage solutions are hydrogen at 100 bar, 300 bar, and LH_2.

By illuminating the bars that reach the 100 percent line, it can be seen that roughly 20 vessels are not able to cover all their routes for a year running on LH_2. Furthermore, if the vessel is running on CH_2 at 300 bar, roughly 50 vessels are not able to cover all routes. At last, with hydrogen at 100 bar, only four vessels reach the 100 percent line. Table 6.3 presents the average route coverage percentage for all vessel and fuel types with a transit speed of 11 knots.

Figure 6.6 from Method 1 presented that as low as 40 % of the AHTS vessels were able to cover the longest route with a transit speed of 11 knots and hydrogen stored at 300 bars. Yet, Figure 6.8 reveals that many of the vessels managed to cover a majority of the routes by running on hydrogen stored at 300 bar. In fact, Table 6.3 shows that the average coverage for AHTS vessels running on

hydrogen at 300 bar is 86.5 %. The plots for OCVs and PSVs with additional fuel types can be seen in Appendix O.

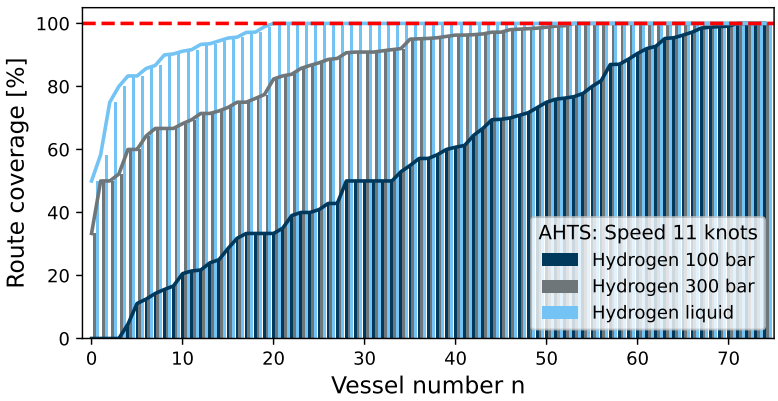

Figure 6.8: Route coverage percentage for AHTS vessels with three different fuel types and transit speed of 11 knots.

Table 6.3: Route coverage percentage for all fuel and vessel types with transit speed of 11 knots. Values represented in Figure 6.8 are highlighted in blue.

	OCV [%]	**PSV** [%]	**AHTS** [%]
Hydr. 1 bar	0.9	1.4	3.3
Hydr. 10 bar	6.2	11.8	16.6
Hydr. 100 bar	40.7	84.6	56.0
Hydr. 300 bar	79.9	97.4	86.5
Hydr. 400 bar	84.3	98.1	89.0
Hydr. 700 bar	88.6	99.4	92.5
Hydr. liquid	92.6	99.7	94.5
MDO	100.0	100.0	100.0

All calculations made in this section are so far based on the vessel having the opportunity to bunker between each route. Situations may arise where the vessel is not given the opportunity to bunker. Where it must sail straight into port, demobilize and mobilize, and then on to the next route, as illustrated in Figure 6.9. Assuming that each vessel must cover two routes before it can refuel, the new data coverage plot will look like Figure 6.10. The overall coverage has decreased compared to when the AHTS vessel could bunker between each route (Figure 6.8), especially for hydrogen at 100 and 300 bar.

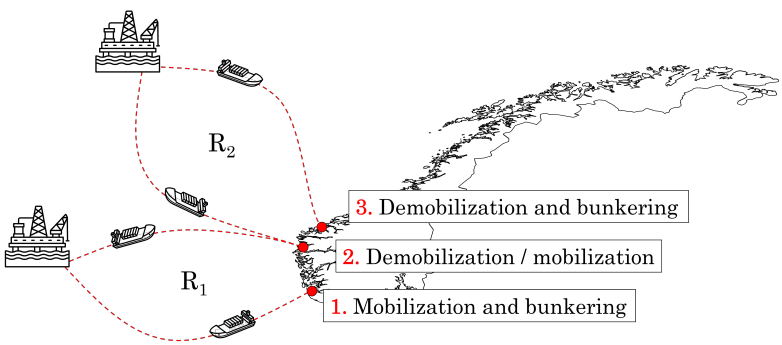

Figure 6.9: Vessel restricted to cover two routes before bunkering.

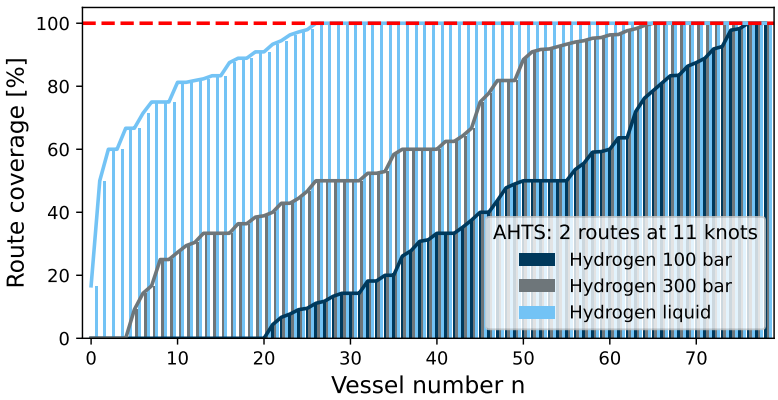

Figure 6.10: Route coverage percentage for AHTS vessels with restriction to complete two routes before bunkering.

6.5 Effect of changing fuel capacity

For the AIS analysis in the previous sections, the size of the fuel tank has been assumed to be equal to the average of some chosen vessels (see tank size analysis in Appendix F) and set constant through the calculations. Method 1 in Section 6.4.1 stated that roughly 85 % of the vessels investigated could satisfy the demand with hydrogen as fuel. By experimenting with different tank sizes, it is possible to observe the effect of changing the fuel capacity. Figure 5.9 from Chapter 5, showed that by increasing the tank capacity of an OCV by 50 %, D_{max} would increase by 50 % as well. In other words, D_{max} is proportional to the tank size.

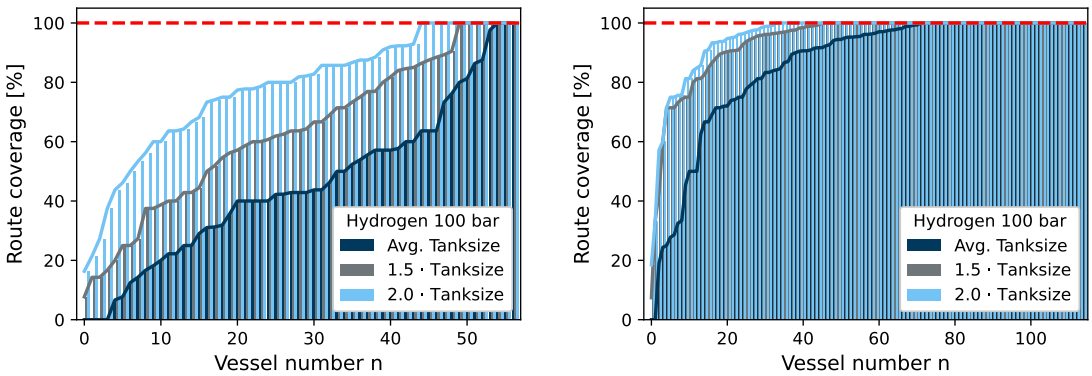

(a) OCV (b) PSV

Figure 6.11: Route coverage percentage and tank size dependency for OCV and PSV with hydrogen at 100 bar and transit speed of 11 knots.

Figure 6.11a shows how the tank size affects the route coverage for an OCV running on hydrogen at 100 bar and a transit speed of 11 knots. With the average tank size, it can be seen that a majority of the vessels cover less than 60 % of their routes. However, if the tank capacity increases by 100 %, most vessels will swiftly be above 60 % coverage. On the other hand, Figure 6.11b illustrates that the route coverage is much greater for PSVs when running on hydrogen at 100 bar. By increasing the tank size of PSVs, most vessels will even reach the 100 % coverage limit. How much a change in tank size will affect the mode of operation, vessel design, and competitiveness will be further discussed in Chapter 7, *Discussion*.

6.6 Seasonal variations in AIS data

As described in Chapter 2, *System boundaries*, one year of AIS data was used with the intention of covering the seasonal variations within the offshore market. Figure 6.12 illustrates the distribution of the starting month for all routes identified for all vessels in the database. Section 6.3 presented that 1121, 4226, and 3125 routes were found from the OCV, PSV, and AHTS database respectively. Hence the bar chart in Figure 6.12 consists of 8472 routes and their start month. It is apparent that most of the routes start in the summer months and early fall. With the two least busy months being November and December.

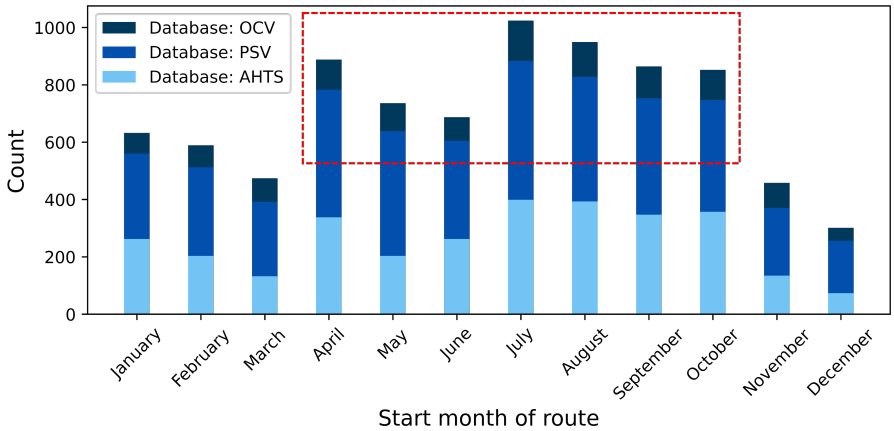

Figure 6.12: Starting month of all routes identified in vessel database.

6.7 Cost analysis

The average annual energy demand in Table 6.4 is estimated by combining the load profile from Section 4.3 with the annual operational profiles (time in port included) presented in Figure D.1 in Appendix D. The average yearly energy demand is further used to calculate the annual cost for the different fuel solutions. The cost differences between the various hydrogen storage methods are neglected. Hence this section will only focus on the overall cost distinction between hydrogen FC solutions and conventional machinery running on MDO using the values presented in Section 3.10, *OSV expenditures*.

Table 6.4: Annual energy consumption OSVs.

	DP [MWh]	Standby [MWh]	Transit [MWh]	Port [MWh]	Towing [MWh]	AH [MWh]	**Total** [MWh]
OCV	9170	1580	6760	0	N/A	N/A	**17 500**
PSV	1760	2040	4330	0	N/A	N/A	**8130**
AHTS	2020	3220	6490	0	1400	2360	**15 500**

6.7.1 CAPEX

It is assumed that CAPEX for hull, task-related equipment, and accomodation areas are identical for both hydrogen and MDO-driven vessels. To reduce the complexity of the calculations, the only difference in CAPEX is expected to be the price difference between hydrogen and diesel solutions. Section 3.10.1 in the *Background study* stated that a cost of 8200 NOK/kW installed diesel machinery was realistic for an OSV. Moreover, the cost of FC systems is mentioned in Section 3.10.1, where it is assumed that the cost per kW will be the same for OSVs as for high-speed ferries. Table 6.5 shows the differences in CAPEX for the two types of energy systems when

the installed power presented in Table 3.13 is used for each vessel type.

Table 6.5: Difference in CAPEX for conventional diesel machinery and hydrogen FC solution.

		OCV	**PSV**	**AHTS**
Installed power	[kW]	10000	8000	17500
Cost conventional diesel machinery	[MNOK]	82.3	65.8	143.9
Cost FC systems	[MNOK]	261.0	208.8	456.8
Cost difference hydrogen & diesel	[MNOK]	- 178.8	- 143.0	- 312.8

6.7.2 OPEX

As stated in Section 3.10.2, OPEX consists of fuel, maintenance, and fees. For this part, the fees are assumed to be so small in relation to the other costs that it is negligible. Yearly fuel consumption can be found by dividing the annual energy demand from Table 6.4 by the LHV for hydrogen (33.3 kWh/kg) and MDO (11.86 kWh/kg) multiplied by the efficiency. Furthermore, the annual fuel cost is calculated by using the fuel prices described in Section 3.10.2. 34 NOK/kg for hydrogen and 11.8 NOK/kg for MDO. Moreover, Section 3.1.2 mentions a CO_2 tax of 2.43 NOK/kg MDO and a tax of 23.79 NOK/kg NOx emissions. Table 3.2 in Section 3.1.3 assumes emissions of 14.8 g NOx per kWh. Maintenance costs are estimated using the dimensionless numbers (NOK/kW) presented in Table 3.17 in the *Background study*.

Table 6.6: Annual OPEX for OSVs with hydrogen and diesel solutions.

		OCV		**PSV**		**AHTS**	
		Hydrogen	*Diesel*	*Hydrogen*	*Diesel*	*Hydrogen*	*Diesel*
Annual fuel consumption	[tons]	1051	3988	488.3	1853	930.9	3532
Fuel cost							
Annual fuel cost	[MNOK]	35.7	47.1	16.6	21.9	31.7	41.7
Annual NOx tax	[MNOK]	0	6.16	0	2.86	0	5.46
Annual CO2 tax	[MNOK]	0	9.69	0	4.50	0	8.58
Maintenance cost							
Annual maintenance cost	[MNOK]	5.63	9.42	4.50	7.54	9.85	16.5
Annual technical maintenance and safety system cost	[MNOK]	3.75	0	3.00	0	6.56	0
Total OPEX	**[MNOK]**	**45.1**	**72.3**	**24.1**	**36.8**	**48.1**	**72.2**

6.7.3 Total cost

The cost analysis highlighted that the CAPEX was found to be 178.8 MNOK, 143.0 MNOK, and 312.8 MNOK more for a hydrogen solution than a conventional diesel solution for OCVs, PSVs, and AHTS vessels, respectively. However, the OPEX seems lower for the hydrogen solution with the given assumptions. On average, hydrogen solutions have 35 % less OPEX than conventional diesel solutions, primarily due to higher fuel costs and emission taxes. This illustrates a potential for cost savings by introducing zero-emission solutions, and the vessels will no longer have any restrictions related to the ECAs. The assumptions linked to the annual fuel consumption and costs will be further discussed.

The sensitivity of the different cost assumptions for a PSV is illustrated in Figure 6.13. It is assumed that the sensitivity will be approximately the same for the other vessel types. Six different variables were adjusted to assess the OPEX sensitivity for a conventional diesel machinery solution on board a PSV (Figure 6.13a). A change in annual energy demand seems to impact OPEX significantly. Increasing the diesel efficiency for LHV from 37 % to 47 % could decrease the OPEX by 8 MNOK per year. The OPEX study in Section 3.10.2 assumed a MDO cost of 11.8 NOK/kg, which was relatively high compared to recent years. Figure 6.13a reveals that OPEX can be reduced by almost 8 MNOK if the MDO cost is reduced by 30 %. The hydrogen FC solution seems to be most sensitive in terms of FC LHV efficiency and hydrogen cost. If the efficiency is reduced to 20 % (60 % reduction), it could double OPEX. The annual energy demand is not included in the hydrogen FC case because it is proportional with the hydrogen cost and will therefore have the same slope.

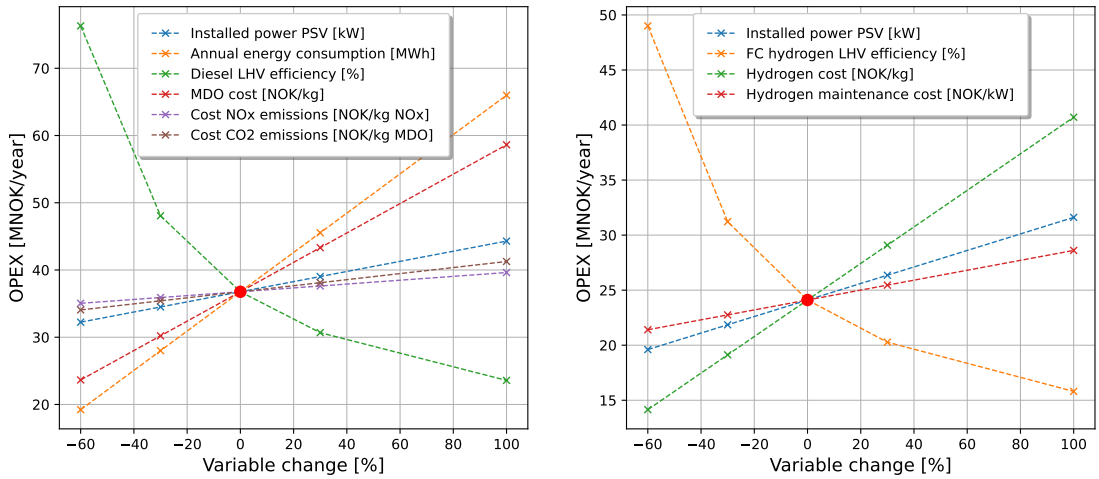

(a) Conventional diesel machinery.

(b) Hydrogen FC solution.

Figure 6.13: OPEX sensitivity analysis for PSV.

6.8 Potential emission reduction

The estimate of annual fuel consumption can be further used to calculate the potential emission reduction by replacing the conventional diesel machinery with hydrogen FC systems. This section will use the results from Method 1 to evaluate the emissions. Figure 6.6 revealed that 71 %, 75 %, and 95 % of OCVs, AHTS vessels, and PSVs, respectively, were able to meet the demand from the offshore market by running on LH_2. Assuming that these percentages were introduced in today's OSV fleet, it is possible to make a simple estimate of the potential emission reductions. The fuel emission factors from Table 3.2 is used to calculate the emissions based on the annual fuel consumption from Table 6.6. Table 6.7 summarizes the annual emissions for the various OSV types. The values will represent the average annual emissions from one vessel.

Table 6.7: Annual OSV emissions.

Vessel type	**CO_2** [$10^3 \cdot$ tons]	**NOx** [tons]
OCV	24.8	700
PSV	11.5	325
AHTS	22.0	620

Section 4.2 claimed that there were 5516 OSVs in service in 2021, 1053 OCVs, 2023 PSVs, and 2440 AHTS vessels. Table 6.8 displays the total emission reduction potential of the world's OSV

fleet. These numbers will be valid if there are sufficient FC solutions for LH_2 capable of operating the mapped share of vessels. In that case, it could be a major step towards the zero-emission target in 2050. With an annual emission reduction of 80.8 million tonnes of CO_2 and 2.2 million tonnes NOx for the world's OSV fleet.

Table 6.8: Annual emission reduction potential for OSV fleet.

	Proportion of vessels that satisfy AIS demand [LH_2, 9 kn] [%]	**Annual emission reduction potential for world's OSV fleet** CO_2 [$10^3 \cdot$ tons]	NOx [$10^3 \cdot$ tons]
OCV	71	18 500	523
PSV	95	22 100	625
AHTS	75	40 200	1100
Total	**N/A**	**80 800**	**2248**

Chapter 7

Discussion

This chapter discusses the results, assumptions, and methods used to exhibit the applicability of hydrogen. The results from Chapter 6 indicate that it is possible to reduce emissions considerably by switching to hydrogen propulsion systems, given that the assumptions are appropriate. These uncertainties and their quality is further discussed. Additionally, the limitations and considerations for future research are addressed.

7.1 Database relevance

The database used to evaluate the requirements set for the OSV fleet consisted of 283 vessels, 66 OCVs, 122 PSVs, and 95 AHTS vessels. It is assumed that it gives a good overview of the world's offshore fleet and can be used to represent the average offshore ship. As described in Chapter 2, the vessels were picked randomly from well-established shipping companies worldwide. Through the analysis of AIS data, it emerged that the vessels operated all across the globe, which may support the hypothesis that the database provides a good representation of the entire offshore fleet. There can often be large differences in the vessels' sizes and operational patterns from continent to continent. The fact that the database covers the whole world will most likely strengthen the quality of the analysis. Additionally, it is assumed that the demand identified for the different vessel types remains unchanged. In reality, the demand and need for different vessel types can change from year to year. The analyzed database consists of data from 2020 only. To make a more comprehensive analysis, the database could be extended to include data from further back in time, in addition to more vessels.

Most calculations in the analysis are based on comparison vessels, and the relevance of the chosen ships can be discussed. Table 6.2 presented the average age of the OSVs in the database as 11 years (2011). Some of the oldest were built in 2001. In recent years, the machinery systems and ship hulls have developed a lot. Whether it would have been better to pick out a few of the newest ships and use them as comparison ships can be debated. Sundvor et al. [2021] argue that the hydrogen ferries used in their analysis will likely be newbuilds. When an *old* fleet is used for comparison, it may lead to unrealistic results because newbuilds will likely be more efficient than the vessels built 11 years ago. In other words, the current fleet is used as a scale for future needs, and it is assumed that the current needs will be the same in the future. Whether the OSVs in this study will be newbuilds or whether the existing vessels will be retrofitted has not been explored thoroughly enough to draw a conclusion.

Risholm and Amon Maritime [2020] stated that the design lifetime for ships is 20-30 years. The average age of the vessels used in this thesis is 10-12 years, indicating that in a few years, a large part of the fleet will most likely need to be upgraded or replaced. For further work, it may be interesting to find the turning point for when it pays off to replace the entire vessel or to upgrade it. Then it would be necessary to get a more detailed view of the hydrogen systems and look more into how extensive the conversion to hydrogen operation is.

7.2 Analysis of operational profiles

The operational profile for AHTS vessels mapped in Section 4.2 is compared with the values from Strande [2018] to make a brief quality check. This can be seen in Table 7.1. There is some interaction between the two datasets. The Pearson's correlation coefficient is 0.84, which indicates a certain correlation. Towing is the operation that stands out the most, with a difference of 13 %. The study from Strande [2018] is based on 66 different AHTS vessels with various owners. For comparison, the analysis in this thesis used only 10 AHTS vessels to identify the operational profile. Therefore, the values related to *towing* could have been analyzed more thoroughly since this is an energy-consuming form of operation and may have a significant impact on both annual fuel and energy consumption.

Table 7.1: Comparison of AHTS operation profile, Strande [2018] against the MARESS database.

	AH	**Towing**	**Transit**	**DP**	**Standby**
Numbers from [Strande, 2018] [%]	13	18	18	13	38
MARESS database [%]	11	5	27	15	43
Diff. [|%|]	2	-13	10	2	5

As described in Section 4.5, time in standby and DP is expressed as a percentage of total route duration. After further consideration, it has been discussed whether this might give a wrong picture of reality. If a vessel has a transit speed of four knots, the duration in transit will naturally become longer. However, according to the model, the time in standby and DP will also be longer. In reality, the ship would possibly spend the same time in both standby and DP, regardless of the transit speed.

As already mentioned, the operational profiles were gathered using the MARESS database. Through discussion, it emerged that there were several uncertainties associated with the method. It is not certain that the vessels used for analyzing the operational profiles have the same characteristics as those explored in the AIS data. As further work, the code could be extended to identify the operation profile itself by using the AIS data from each vessel. Each mode of operation has a particular characteristic that makes it possible to recognize the pattern using the info contained in the AIS data. For instance, *time in port* can be stored as the duration from the ship arrives in port until it leaves again. Moreover, if more accurate numbers for filling a hydrogen tank are obtained, it is possible to compare this with the time spent in port for each vessel. This could strengthen the analysis and make it more robust.

7.3 Seasonal variations within a dataset

Section 6.6 investigates the seasonal variations within a year. The AIS data range is from January 2020 to December 2020 with the intention of representing potential seasonal variations. The overall seasonal trend is that the summer months are busier than the rest. The number of routes mapped in July is three times as many as in December. Ideally, the analysis should have been carried out for more years to see if the pattern recurred. It may be that 2020 was a unique year. Nevertheless, it still indicates that it was acceptable to include data for an entire year with such large seasonal variations.

The power consumption is assumed to be constant throughout the whole year. In reality, the weather is often harsher during the winter months, placing higher demands on the DP systems and thus increasing power consumption. For future research, it could be interesting to expand the code by merging AIS data with weather data to include the seasonal variations in the power consumption.

7.4 Tank size and bunkering options

The average tank sizes were found by doing a brief analysis of 33 vessels and further used to calculate D_{max} for a given vessel and fuel type. Tank volume was found by using web scraping with the keyword *fuel oil*. On second thought, this may have been too large compared to the actual size of the fuel tanks. This was brought to attention when reading Risholm and Amon Maritime [2020]. Here the tank size for fuel was separated between *own use* and *transportation use*, which means that the tank sizes in the thesis may be too large compared to a realistic scenario. However, the values can still be used to estimate how much space the hydrogen systems occupy to cover a given distance. For example, an average PSV with 1200 m^3 available for hydrogen systems can serve offshore contracts with a sailing range of up to 3000 nautical miles on one tank of LH_2 and a transit speed of 9 knots.

Section 6.5 presents the effect of changing the fuel capacity. The results revealed that even with CH_2 at 100 bar, it is possible to achieve almost 100 % route coverage for the analyzed PSV fleet by doubling the tank capacity. However, the tank arrangement drawings in Figure 3.18 illustrates limited available space inside a PSV. Increasing the fuel capacity can cause the ship to have less room to carry payload and, in the worst case, weaken its competitiveness. The size available for hydrogen systems on board the vessel will eventually be a trade-off between the maximum sailing range and cargo capacity. This could develop into a vicious circle, as illustrated in Figure 7.1. Therefore, it is important to carry out a good market analysis before starting a project.

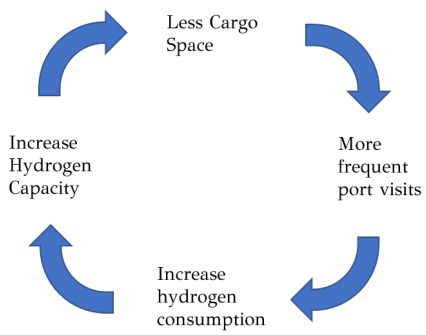

Figure 7.1: Trade-off between cargo capacity and sailing distance.

Furthermore, the analysis does not consider whether it takes more time to fill a hydrogen tank than a standard diesel tank. Section 3.1.1 stated that LH_2 was the best hydrogen option when space limitations and limited bunker time became relevant. Section 3.5 depicts a time of 20 minutes to fill 450 kg CH_2 at 250 bar. The PSV described above would need roughly 47 tonnes of hydrogen, stored in a 1200 m^3 tank at 250 bar, to travel 3000 nautical miles. By using the value of 450 kg per 20 min the PSV will require a bunkering time of 34 hours and 49 minutes. The background study revealed many ongoing projects related to the use of hydrogen. It can be speculated if this will lead to more efficient hydrogen bunkering in the future. Bunkering of larger volumes will also most likely make it more efficient.

In addition, the methods used in this study map all routes for all vessels and use this to identify the requirements set for today's offshore vessels. This implies that each port should have the option of bunkering hydrogen for the analysis to be realistic. Today's infrastructure cannot offer the necessary accessibility of hydrogen refueling facilities, but it may be possible to do so in the future. The background study addressed that Norway is planning to build a production plant for LH_2, with a long-term goal of building a complete supply chain for the shipping industry.

7.5 Risk of using hydrogen

The average tank size from the analysis is used as a measure of how much space that is available for hydrogen storage systems. However, the location of these has not been taken into account concerning risk and probabilistic damage stability. Section 3.8 briefly overviews the different risks associated with hydrogen as fuel. It reveals that many hazards must be taken into account. Today's fuel tank location has been determined based on MDO as fuel. A more thorough risk analysis must be carried out if the exact location is used for hydrogen, as it is common for MDO tanks to be located inside the ship. Placing the hydrogen tanks in the same locations as today's MDO tanks can expose the ship to much higher risk. When estimating the hydrogen replacement potential for high-speed ferries, Sundvor et al. [2021] state that the hydrogen tanks should be located on an open deck due to safety. Whether this requirement will apply to a much less populated OSV should be further investigated together with the safety zones described by Cluster [2020]. Suppose hydrogen has to be stored on an open deck. In that case, it may affect the profitability and competitiveness of the vessel because the deck area is an essential attribute.

7.6 Power and fuel consumption

When power consumption was estimated, many assumptions had to be made. Three different empirical methods were used to identify the power variation for different transit speeds, Hollenbach, Guldhammer Harvald's, and Holtrop & Mennen's method. Which of the three methods predicts the effect best is hard to say. Therefore, the average value was assumed to be the best approach. Characteristics from one OCV, one PSV, and one AHTS were used as input. Normand Vision, Normand Arctic, and Normand Prosper, respectively. In retrospect, it might have been better to use the average values from the vessels used in the analysis.

The power consumption for the various modes of operation was found by using sfc data from MARESS. All in all, 15 OCVs, 17 PSVs, and 12 AHTS vessels were used. Ideally, data from even more vessels should be used, but it seemed that the average number converged towards a reasonable estimate. Using the average sfc from Table E.2 (Appendix E) in combination with the operational profile, the sfc for a PSV will be 8.16 m^3 MDO/day in this analysis. Risholm and Amon Maritime [2020] claim that a PSV use from 7 to 10 m^3 MDO/day, which fits reasonably well with the assumptions.

The background study highlighted that Strømgren et al. [2020] used multiple FCs of 100 kW to assess the replacement potential of hydrogen in high-speed ferries. MF Hydra is equipped with two 200 kW FC modules. Jogchum Bruinsma stated that the MT-FCPI-500 FC system is the best option from Nedstack to be used in an OSV. This system can provide a nominal power output of 500 kW. Section 3.9 presented the installed power for the various OSV types. An average AHTS vessel is installed with 17 500 kW because towing and AH require a lot of power. Barcellos [2013] stated that some of the biggest AHTS vessels with up to 300 metric tons of bollard pull would need a propulsion system with 20 MW. If the 500 kW FCs were to be used as a propellant, 40 of these would have to be installed. This would most likely take up a lot of space and entail high costs. A larger and more efficient FC system must be created before it can be relevant to install on board an OSV without compromising the competitiveness of the ship. However, Havyard Hydrogen promotes a scalable hydrogen FC propulsion system able to give 3200 kW, making FCs in OSVs much more relevant. Additionally, Burheim [2017] stated that it is possible to engineer hydrogen storage, distribution, and propulsion systems up to several MWs. Strømgren et al. [2020] discuss if moderate technology improvements can make FC systems competitive with diesel in the future.

Risholm and Amon Maritime [2020] claimed that CH_2 was the best option for vessels using less than 1000 kg hydrogen between each refueling. A simple estimate of fuel consumption between each refueling can be obtained by dividing the annual fuel consumption by the number of routes per year. The average annual fuel consumption is taken from Table 6.6, and the number of routes per year is obtained from Table 6.2. For simplicity, the numbers are summarized in Table 7.2 below. It shows that a PSV has the lowest average consumption per trip with 14 tonnes of hydrogen,

regardless of storage method. If CH_2 is best for vessels using less than 1000 kg hydrogen between each refueling, it might be that LH_2 is a better option for offshore vessels.

Table 7.2: Average amount of fuel consumption between each refueling.

			OCV	**PSV**	**AHTS**
Avg. num. routes per year	[pcs/vessel]		17	35	33
Annual fuel consumption	[tons]	Hydrogen	1051	488	931
		MDO	3988	1853	3532
Avg. amount fuel each refueling	[tons/route]	Hydrogen	**61.8**	**14.0**	**28.2**
		MDO	**235**	**52.9**	**107**

One of the hypotheses in the project's initiation phase was that hydrogen and FCs would be a better zero-emission alternative than batteries. Mainly because the high energy demand in shipping would require large and heavy batteries to be zero-emission, which would negatively affect the efficiency of the ship, especially if the vessel is critical in terms of weight. Aarskog et al. [2020] point out that a 250-350 bar hydrogen tank is about five times lighter than the battery solutions. However, after conducting a literature study on the subject, it seems like hydrogen systems may be large and complex as well, especially when hydrogen is stored at high pressure or extremely low temperatures. For instance, the total weight of the hydrogen systems in a hydrogen-driven Toyota Mirai was 144 kg compared to a battery-driven Nissan Leaf with a battery pack of 294 kg. Whether the weight of battery solutions for the offshore industry will be 100% heavier than FC solutions is hard to tell, but it is perhaps worth looking into as further work.

As further research, it can be discussed whether it is possible to introduce offshore hubs as described in Section 3.11. This is a measure to cope with hydrogen's low volumetric energy density by shortening today's sailing distances and lowering fuel capacity requirements. However, introducing a hub will most likely entail a large investment cost and place great demands on the infrastructure. Anyway, before utilizing the hub idea, a thorough market analysis should be carried out beforehand.

The profitability of introducing hubs can be highlighted by formulating a basic optimization problem. An example can be seen in Figure 7.2, where the offshore hub is placed far out on the Norwegian continental shelf (Figure 7.2b). It will perhaps be more relevant for a PSV sailing from platform to platform with supplies, but the hub can also be used as a natural operation center for OCVs and AHTS vessels.

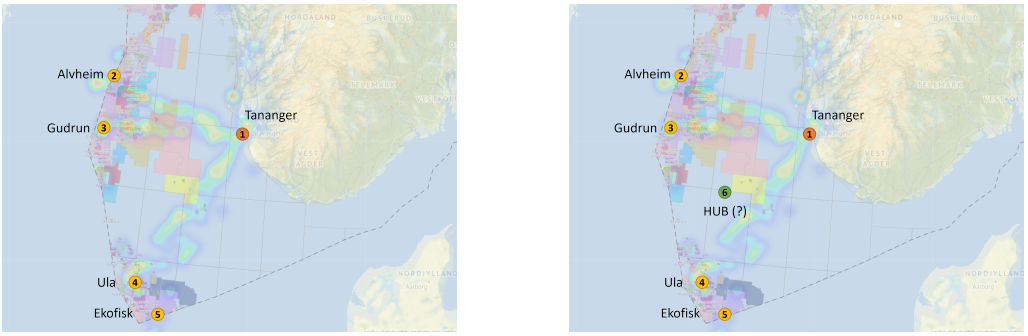

(a) Example of route without hub.

(b) Example of hub solution.

Figure 7.2: Hub implementation case.

Introducing a hub should make the hydrogen vessel able to refuel at the offshore field, which makes it capable of visiting more platforms if the range was not long enough in the first place. The optimization problem shown in Figure 7.3 can be used to identify the potential gains in terms of emissions and costs. However, even though a hub is introduced, it will still be a need for a filling solution for the hub itself.

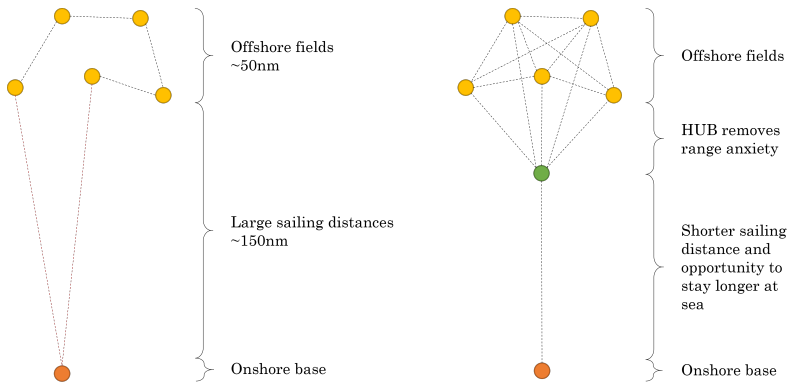

Figure 7.3: Optimization problem with hub.

7.7 Calculate energy densities

The energy density calculation was performed to better understand the principle of a FC and get a value on the energy content for different hydrogen storage methods. While there is low uncertainty related to the energy output for hydrogen in a FC per kilo, there is greater uncertainty to the energy output per cubic meter. Gibbs free energy (kJ/mol) for hydrogen was calculated using chemistry's well-established and well-known tabulated values. Furthermore, gibbs energy was multiplied by the molar volume (mol/m^3), which changed with pressure and temperature. This gave the volumetric energy density (kJ/m^3) used in this analysis. As already mentioned, Khotseng [2019] states that gibbs free energy is the energy available to do useful work. In addition, the plot in Figure 3.9 shows that the molar volume from the industry agrees well with the assumptions made. The final volumetric energy density corresponds well with the values from Aarskog and Danebergs [2020], which conducts a similar analysis for high-speed ferries. Since the assumptions for calculating energy density agree well with multiple other sources, it is assumed that the values used in this analysis will give a realistic result.

7.8 Estimate fuel efficiency

The efficiency of conventional diesel machinery and FCs was assumed to be the same for all vessels when calculating the theoretical sailing range. The uncertainty surrounding this efficiency plays a major role in the calculations. In the worst case, an incorrect value can lead to large errors and unrealistic results. It can be discussed if 50 % was the best choice to represent the efficiency of a FC. Most likely, the efficiency will depend on the type of FC used. Additionally, Strømgren et al. [2020] state that the efficiency of a FC depends on the power output. However, after doing a thorough background study, it seemed that a 50 % efficiency for FCs was widely used. Furthermore, a value of 37 % was often applied to the efficiency of conventional machinery.

Additional energy loss will be associated with various fuel storage methods, especially hydrogen. For example, an energy loss of another 30 % is assumed when hydrogen is stored in a liquid phase. Commonwealth of Australia [2018] assumes an energy loss of 20 - 30 %, while Berstad et al. [2013] assume a loss between 25 and 40 %. Therefore, 30 % seemed to be a reasonable estimate. Although LH_2 has more energy loss in storage than CH_2, Figure 6.3 shows that LH_2 is the hydrogen solution with the largest D_{max} for all vessel types. It is challenging to discuss which hydrogen solution is the best, especially when FCs are relatively new and there is little test data from the maritime industry. However, in terms of range, LH_2 seems to be the best solution. As mentioned in the background study, Mazloomi and Gomes [2012] described CH_2 as the most time and energy-efficient hydrogen solution. In addition, hydrogen storage at high pressure will have 4-5 times less cost compared to LH_2.

7.9 Data cleaning

Data cleaning is an essential tool for neglecting unrealistic and invalid results. The description of the methods in Chapter 4 shows that many assumptions must be made. Some data points had transit speeds that were very high, much higher than the vessel's maximum speed, and were thus neglected. In retrospect, it was perhaps unnecessary to neglect them. Instead of deleting the data points with high speeds, Strømgren et al. [2020] chose to lower the measured speeds to the vessel's maximum speed, which meant they did not miss the data points. In this study, 43 954 data points (0.3 %) were neglected due to unrealistic speeds.

Moreover, data points with more than 12 hours between each measurement were neglected. A widely used measurement frequency was observed as 6 hours. Tolerating up to 12 hours between each tracking allowed one measurement to be skipped, which meant that the analysis could identify more routes. It can be discussed how much a ship can do in 12 hours and to what extent this can affect the operational profile. In total, 8 871 736 data points were identified as part of a route, corresponding to 60 % of the input data. Whether this says anything about the quality of the python code used in the analysis or the data quality is difficult to say. If all data points were categorized into a route, the code would have been able to detect all routes traveled by the vessels and thus also represent the reality perfectly. Figure 7.4 illustrates an example where a large part of the data was not categorized as a route because the AIS tracking was turned off before reaching Europe. Because the code defines a route as coast to coast, it relies on two measurements near shore at each end of the route to store it. Therefore, the data for this vessel was deleted from the analysis along with other similar cases where the code gave a wrong picture of reality.

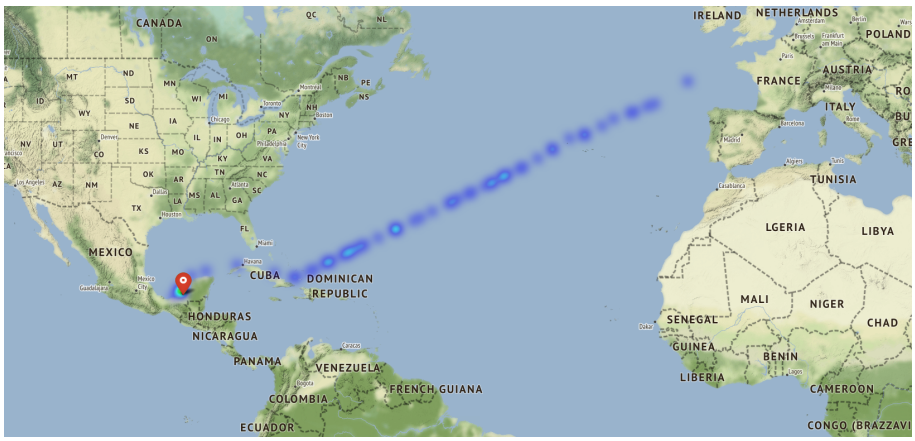

Figure 7.4: Transatlantic route not identified by code.

7.10 Route identification

In the categorization of nearshore and offshore points, the python code used a circle with a given radius to evaluate the distance from shore. The length of the radius had to be chosen carefully. It could lead to inaccuracies if it became too long or too short. Figure 7.5 illustrates which factors must be considered when defining the radius. Figure 7.5a shows the consequence of choosing a search radius that is too long. The start of the route will be defined in the middle of the Strait of Gibraltar, even though the route runs straight through. Figure 7.5b illustrates a case where the length of the search radius is appropriate. The start of the route will be when the vessel leaves the port of Las Palmas, and when it returns, the code manages to detect that the route goes past Las Palmas and further on to Europe. If the search radius had been larger, the route would have stopped at Las Palmas on the way back as well.

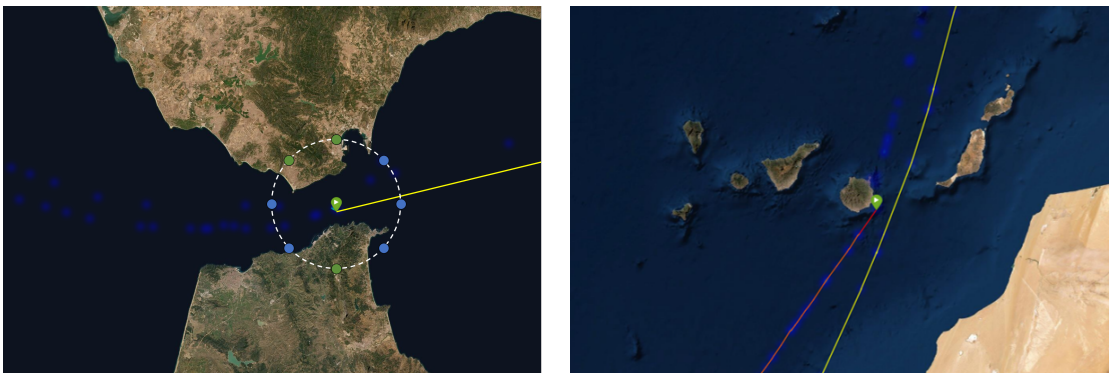

(a) Too large radius. (b) Sufficient length of radius.

Figure 7.5: Selection of radius to categorize AIS points.

For further work, it could be interesting to expand the python code to be able to handle the problems described above. The search radius at each point makes it hard to detect routes sailing parallel and close to shore. Usually, these points were categorized as *nearshore* points and thus not included as a route. Introducing a constraint that the speed must be 0 knots to be categorized as a *nearshore* point could enable the code to identify more of these *nearshore* routes.

7.11 Cost and emission estimation

Many assumptions were made to generate a brief cost analysis. The sensitivity analysis performed in Section 6.7 revealed that the annual energy consumption greatly influenced OPEX. There are several ways to change the annual energy consumption. For example, improving hull efficiency or optimizing the vessel's operational pattern. The annual energy consumption was estimated using the load and operational profiles identified in Chapter 4, *Methods*. As discussed above, the analysis is based on comparison vessels, some very old. It can be argued if these values will give the best representation of fuel consumption today or whether they are too old. The same applies to the cost of hydrogen. As presented in the background study, previous articles presented different values for the hydrogen cost. Furthermore, it is questionable whether the average was the most appropriate to use, especially given the fact that a significant price reduction for hydrogen is expected. It is worth mentioning that OPEX was calculated using the energy per kilogram and not per cubic meter, which means that the storage losses for hydrogen were neglected in this section. After further consideration, the results could have been more realistic by using the energy per cubic meter for LH_2 and the energy losses due to storage. The results from Table 6.6 showed that the annual fuel consumption of hydrogen was almost a quarter of the annual MDO consumption by weight. The energy per kilogram is much higher for hydrogen (33.30 kWh/kg) compared to MDO (11.86 kWh/kg), in addition to higher efficiency (50 %/37 %). However, it is more complicated and energy-demanding to store hydrogen. It should be further analyzed if this should have been taken into account in the OPEX calculations.

The results revealed that CAPEX was greater for a hydrogen vessel than a conventional diesel vessel. The cost of FC systems was 217 % higher than conventional machinery. To compare, Strømgren et al. [2020] concluded that the cost of the FC solutions was 28 % higher than diesel alternatives for high-speed crafts. Some uncertainty is associated with the assumption of 8200 NOK per kW of installed machinery. The same applies to the FCs. It can be questioned if the cost per kW is the same for high-speed ferries as for OSVs. Figure 3.19 illustrates how Ianssen et al. [2017] expect a decrease in the FC price. Additionally, there are good opportunities to obtain financing for these kinds of future-oriented projects. Enova awarded the Topeka project described in Section 3.1 219 MNOK in 2020, and the MF Hydra project received 14.6 MNOK, also from Enova. Furthermore, Section 3.7 mentioned that the Norwegian government would have an increasing focus on hydrogen and aim toward a low-emission society in the future.

At last, the emissions were calculated using the characteristics of alternative fuels and the fuel emission factors from Section 3.1.3. The uncertainty surrounding these numbers is difficult to determine, but they will give a good indication of the extent of the emission reductions. When calculating the emission reductions, it was assumed that all vessels initially used MDO. This is mainly true, but some OSVs also use dual-fuel engines with, for instance, LNG. DNV [2020] states that *the world fleet is mostly powered by diesel engines running on marine fuel oils.* The results showed that the total annual emission reduction potential by using LH_2 on today's OSVs was 81 million tonnes of CO_2. Arena Ocean Hyway Cluster [2020] states that the Norwegian maritime sector alone had emissions of 4.8 million tonnes of CO_2 in 2017. In addition, Johansson et al. [2017] presented an annual emission from the world fleet of 20.9 million tonnes of NOx and 831.3 million tonnes of CO_2. In other words, the results of this study show that the emission reduction from the OSV fleet alone can help reduce the total emissions from the world fleet by roughly 10 %.

7.12 Determination of hydrogen potential

When determining the hydrogen potential, it is difficult to say which of the methods is best. Method 1 in Section 6.4.1 used the largest route for each vessel as a threshold, and Method 2 in Section 6.4.2 used all routes identified for each vessel. For the first method, when converting to zero-emission propulsion, the vessel must be capable of covering the longest route. If not, it could reduce its competitiveness and lose contracts to diesel vessels. At the same time, if the vessel manages to cover the longest route, it will also be able to cover all the smaller routes. For the second method, D_{max} was compared against all routes mapped in the AIS data. This made it possible to investigate the average route coverage for each vessel. By looking at the average values, the zero-emission potential became higher. Method 1 focuses exclusively on whether the vessel can cover the longest route. In contrast, Method 2 can identify if there is still potential even if it cannot cover the longest route. For instance, the case vessel in Chapter 5 got zero potential when using Method 1. But Method 2 was able to detect that as much as 20 of 21 identified routes could be sailed with LH_2 as fuel, giving a potential of 95 %. To finish off, what coverage method that should be used as an argument for initiating hydrogen operation of ships is difficult to say. It depends on the preference of the shipping companies and shipowners. How they prefer to arrange their fleet, have the highest average route coverage, or build the ships always to be able to take on all contracts, even those with the longest distances.

Chapter 8

Conclusion

The main scope of the thesis is to investigate the replacement potential of OSVs with zero-emission hydrogen solutions. The background study revealed that development in the offshore fleet is needed to reach the zero-emission goals in 2050, and hydrogen as fuel stood out as a promising alternative. One main concern related to hydrogen is the low volumetric energy density, leading to major challenges regarding capacity and storage options.

The maximum theoretical sailing distance (D_{max}) for a PSV with a transit speed of 11 knots running on MDO was calculated to be around 12 500 nm. With LH_2, the hydrogen solution with the highest volumetric energy content, it was able to cover 2600 nm. An AHTS vessel with a transit speed of 11 knots running on MDO was calculated to have a D_{max} of 7200 nm, while it was 1500 nm with LH_2. At last, an OCV with a transit speed of 11 knots running on MDO D_{max} was calculated to be around 8500 nm, while it was 1800 nm with LH_2. These values reveal that D_{max} with hydrogen is considerably lower than with MDO, given that both solutions have the same volume limitation.

By analyzing 283 vessels and 15 million data points, it appeared that the most frequent transit speeds are 10.5 knots for an OCV, 9.0 knots for a PSV, and 9.5 knots for an AHTS vessel. Furthermore, the AIS analysis detected that the average route length was almost twice as long for an OCV compared to a PSV. Additionally, the background study revealed that it could be challenging to find FCs large enough to meet the power demand of an AHTS vessel.

Two different methods were formulated to determine the zero-emission potential of using hydrogen as fuel. The first route coverage method disclosed that 71.2 % of the OCVs, 74.7 % of the AHTS vessels, and 95.1 % of the PSVs could cover their longest route with transit speed of 11 knots and LH_2 as fuel. The second method identified an average route coverage of 92.6 % for the OCVs, 94.5 % for the AHTS vessels, and 99.7 % for the PSVs with a transit speed of 11 knots and LH_2 as fuel. The route coverage should be as high as possible to not affect the vessel's competitiveness.

In conclusion, the results show great potential in converting OSVs to hydrogen propulsion, with an annual emission reduction potential of 80.8 million tonnes of CO_2 and 2.2 million tonnes NOx. Although Method 1 detects less than 75% coverage for both OCV and AHTS vessels, Method 2 still reveals that a majority of the routes can be completed with zero-emission fuel. However, both methods point out PSV as the vessel type with the highest replacement potential. The results show that it is possible to cover the demand with hydrogen FCs running on LH_2 without affecting the competitiveness and design of the ship. 16 FCs of the type MT-FCPI-500 from Nedstack will be sufficient to cover the need for installed power in a PSV. A zero-emission conversion will place great demands on the infrastructure and it may challenge today's risk-related hydrogen regulations. Using green hydrogen will make shipping 100 % zero-emission, contribute to clean energy, and significantly impact the three SDGs. In addition to being a climate action, the hydrogen revolution may act as a catalyst, contribute to innovations, and create new industries and infrastructure for the future.

Bibliography

Aarskog, F. G. and Danebergs, J. (2020). Estimation of energy demand in the norwegian high-speed passenger ferry sector towards 2030. *IFE/E*.

Aarskog, F. G., Hansen, O. R., Strømgren, T., and Ulleberg, Ø. (2020). Concept risk assessment of a hydrogen driven high speed passenger ferry. *International Journal of Hydrogen Energy*, 45(2):1359–1372.

Arena Ocean Hyway Cluster (2020). 2030 hydrogen demand in the norwegian domestic maritime sector. *OHC HyInfra*, 19:1–19.

Barbir, F. (2005). *PEM Fuel Cells - Theory and practice*. Elsevier Academic Press, University of California (USA).

Barcellos, R. (2013). The hybrid propulsion system as an alternative for offshore vessels servicing and supporting remote oil field operations. In *OTC Brasil*. OnePetro.

Berstad, D., Walnum, H. T., Decker, L., AG, L. K., and Quack, H. (2013). Integrated design for demonstration of efficient liquefaction of hydrogen (idealhy). *Fuel Cells and Hydrogen Joint Undertaking (FCH JU)*.

Birk, L. (2019). *Fundamentals of Ship Hydrodynamics, Fluid mechanics, Ship Resistance and Propulsion*. Wiley, New Orleans, LA.

Bø, T. I. (2016). Scenario-and optimization-based control of marine electric power systems. *ISBN: 978-82-326-1434-9*.

Bossel, U. (2003). *Well-to-wheel studies, heating values, and the energy conservation principle*. Technical report, European Fuel Cell Forum, Morgenacherstrasse.

Bruce, S., Temminghoff, M., Hayward, J., Schmidt, E., Munnings, C., Palfreyman, D., and Hartley, P. (2018). National hydrogen roadmap. *Australia: CSIRO*.

Burheim, O. S. (2017). *Engineering energy storage*. Academic press.

Cambridge Dictionary (2021). Cambridge dictionary. `https://dictionary.cambridge.org/dictionary/english/hub`. Accessed: 2021-11-18.

Cambridge Dictionary (2022). Meaning of *demand* in english. `https://dictionary.cambridge.org/dictionary/english/demand`. Accessed: 2022-02-28.

Cluster, O. (2020). Hydrogen and ammonia infrastructure safety and risk information and guidance. *Lloyd's Register: London, UK*.

Commonwealth of Australia (2018). Hydrogen for Australia's future. *Hydrogen Strategy Group*, 57(1):1–57.

Concawe (2016). Marine fuel facts. `https://www.concawe.eu/wp-content/uploads/2017/01/marine_factsheet_web.pdf`. Accessed: 2022-05-20.

Dale, T. (2020). Development of simplified methods for ship powering performance calculations. Master's thesis, NTNU.

Dawood, F., Anda, M., and Shafiullah, G. (2020). Hydrogen production for energy: An overview. *International Journal of Hydrogen Energy*, 45(7):3847–3869.

De Groot, S. (1982). The impact of laying and maintenance of offshore pipelines on the marine environment and the north sea fisheries. *Ocean Management*, 8(1):1–27.

Decker, L. (2019). Liquid hydrogen distribution technology. In *Hyper Closing Seminar, Brussels, Belgium, Nov*, volume 27.

Deloitte, C. (2020). Fueling the future of mobility.

DNV (2019). Produksjon og bruk av hydrogen i norge. *2019-0039*, 138(Rev. 1):1–138.

DNV (2020). Pathway to net zero emissions. *Energy Systems and Maritime*, 1:1–94.

DNV-GL (2022). Sulphur limit in ECAs - increased risk of psc deficiencies and detentions. `https://www.dnv.com/news/sulphur-limit-in-ecas-increased-risk-of-psc-deficiencies-and-detentions-142911`. Accessed: 2022-02-24.

E24 (2021). Eit skritt nærmare for hydrogenfabrikk på mongstad. `https://e24.no/det-groenne-skiftet/i/x305kB/eit-skritt-naermare-for-hydrogenfabrikk-paa-mongstad`. Accessed: 2021-10-10.

E4Tech (2020). The fuel cell industry review 2020. `https://fuelcellindustryreview.com/`. Accessed: 2021-10-09.

Elgohary, M. M., Seddiek, I. S., and Salem, A. M. (2015). Overview of alternative fuels with emphasis on the potential of liquefied natural gas as future marine fuel. *Proceedings of the Institution of Mechanical Engineers, Part M: Journal of Engineering for the Maritime Environment*, 229(4):365–375.

Enova (2020). Ombygging av mf hidle til hydrogendrift. `https://www.enova.no/om-enova/om-organisasjonen/teknologiportefoljen/ombygging-av-mf-hidle-til-hydrogendrift/`. Accessed: 2021-10-10.

Erikstad, S. O. and Levander, K. (2012). System based design of offshore support vessels. In *Proceedings 11th International Marine Design Conference—IMDC201*.

Finansdepartementet (2022). Endring av prop. 1 ls (2021–2022) - skatter, avgifter og toll 2022. *Forslag til lovvedtak og stortingsvedtak*, 1(1):25–26.

Gilbert, P., Walsh, C., Traut, M., Kesieme, U., Pazouki, K., and Murphy, A. (2018). Assessment of full life-cycle air emissions of alternative shipping fuels. *Journal of Cleaner Production*, 172:855–866.

Havyard (2021). Havyard hydrogen. `https://www.havyard.com/brands--solutions/havyard-hydrogen/?preview=true`. Accessed: 2021-10-10.

Helbæk, M., Kjelstrup, S., and Helb, M. (2006). *Fysikalsk kjemi*. Fagbokforl.

Hexagon Purus (2021). Hydrogen distribution systems in standard execution. `https://s3.eu-central-1.amazonaws.com/hexagonpurus-website/HexagonPurus_X-Store_Container_Datasheets.pdf`. Accessed: 2022-03-10.

Ianssen, C., Ianssen, E., and Sandblost, T. (2017). Battery/fuel cell fast ferry. *Report Naeringslivets NOx Fond*.

IMO (2022). Prevention of air pollution from ships. `https://www.imo.org/en/OurWork/Environment/Pages/Air-Pollution.aspx`. Accessed: 2022-02-27.

International Energy Agency (2021). Tracking transport 2021. `https://www.iea.org/reports/tracking-transport-2021`. Accessed: 2022-02-22.

International Maritime Organization (2021). Nitrogen oxides (nox) – regulation 13. `https://www.imo.org/en/OurWork/Environment/Pages/Nitrogen-oxides-(NOx)-%E2%80%93-Regulation-13.aspx`. Accessed: 2021-10-07.

Jafarzadeh, S. and Schjølberg, I. (2017). Emission reduction in shipping using hydrogen and fuel cells. *International Conference on Ocean, Offshore and Arctic Engineering*, 9(1):1–9.

Jensen, H. J. (2021). The domestic bulk fleet's zero-emission potential based on hydrogen infrastructure development. Master's thesis, Norwegian University of Science and Technology, Trondheim, Norway.

Johansson, L., Jalkanen, J.-P., and Kukkonen, J. (2017). Global assessment of shipping emissions in 2015 on a high spatial and temporal resolution. *Atmospheric Environment*, 167:403–415.

Khotseng, L. (2019). *Fuel Cell Thermodynamics*. Department of Chemistry, University of the Western Cape, Cape Town, South Africa.

Körner, A., Tam, C., Bennett, S., and Gagné, J. (2015). Technology roadmap-hydrogen and fuel cells. *International Energy Agency (IEA): Paris, France*.

Łebkowski, A. and Wnorowski, J. (2021). A comparative analysis of energy consumption by conventional and anchor based dynamic positioning of ship. *Energies*, 14(3):524.

Letafat, A., Rafiei, M., Ardeshiri, M., Sheikh, M., Banaei, M., Boudjadar, J., and Khooban, M. H. (2020). An efficient and cost-effective power scheduling in zero-emission ferry ships. *Complexity*, 2020.

Li, X. (2006). *Principles of Fuel Cells*, pages 5–37. Taylor and Francis Group, New York, NY.

Linde (2021). Extending the reach of the hydrogen value chain. *From Source to Service. Every Step of the Way*, 8(1):4–4.

Lindstad, H. E., Eskeland, G. S., and Rialland, A. (2017). Batteries in offshore support vessels–pollution, climate impact and economics. *Transportation Research Part D: Transport and Environment*, 50:409–417.

Maritimt Forum (2021). Norled bestiller flytende hydrogen og hydrogenlagring fra linde [picture]. `https://www.maritimt-forum.no/stavangerregionen/nyheter/2021/norled-bestiller-flytende-hydrogen-og-hydrogenlagring-fra-linde`. Accessed: 2021-10-10.

Mazloomi, K. and Gomes, C. (2012). Hydrogen as an energy carrier: Prospects and challenges. *Renewable and Sustainable Energy Reviews*, 16(5):3024–3033.

McCarty, R. D., Hord, J., and Roder, H. M. (1981). *Selected properties of hydrogen (engineering design data)*, volume 168. US Department of Commerce, National Bureau of Standards.

Midilli, A., Ay, M., Dincer, I., and Rosen, M. A. (2005). On hydrogen and hydrogen energy strategies: I: current status and needs. *Renewable and sustainable energy reviews*, 9(3):255–271.

Myklebust, T. A. and Ådnanes, A. K. (2011). Parallel hybrid propulsion for ahts. *Electric propulsion in offshore supply vessels*, 5(1):2–3.

Nedstack (2022). Pemgen mt-fcpi-500. `https://nedstack.com/en/pemgen-solutions/maritime-power-installations/pemgen-mt-fcpi-500`. Accessed: 2022-05-12.

NEL (2019). Status and q&a regarding the kjørbo incident.

Nerem, T. (2018). Assessment of marine fuels in a fuel cell on a cruise vessel. Master's thesis, Norwegian University of Science and Technology, Trondheim, Norway.

Norges Bank (2022). Exchange rates. `https://www.norges-bank.no/en/topics/Statistics/exchange_rates/?tab=currency&id=USD`. Accessed: 2022-05-16.

Norges Rederiforbund (2015). Norwegian offshore shipping companies - local value creation, global success. *Reports*, 1(1):9–10.

North Sea Wind Power Hub (2021). Towards the first hub-and-spoke project. `https://northseawindpowerhub.eu/knowledge/towards-the-first-hub-and-spoke-project`. Accessed: 2021-09-03.

Norwegian Shipowner's Association (2021). Quarterly report - shipping and mobile offshore activities. *Journal of Cleaner Production*, 3:4.

NRK (2019). Eksplosjon ved hydrogenstasjon. `https://www.nrk.no/norge/eksplosjon-ved-hydrogenstasjon-1.14582914`. Accessed: 2021-12-13.

Nygård, J. H. and Strømgren, T. (2017). Sluttrapport forprosjekt gkp7h2. *DNV-GL Grønt Kystfartsprogram*.

Office of Energy Efficiency and Renewable Energy (2020). Hydrogen storage. `https://www.energy.gov/eere/fuelcells/hydrogen-storage`. Accessed: 2021-10-11.

Ognedal, T. S. (2021). Battery hybrid propulsion systems for ahts vessels. B.S. thesis, NTNU.

Pettersen, S. S. (2015). Designing flexible offshore construction vessels to handle future uncertainty. Master's thesis, NTNU.

Regjeringen (2019). Plan for fossilfri kollektivtrafikk i 2025. *Handlingsplan*, 64:4–5.

Research and Markets (2021). Global industrial gas market report 2021. `https://www.globenewswire.com/en/search/organization/Research%2520and%2520Markets`. Accessed: 2022-03-05.

Risholm, A. and Amon Maritime (2020). 2030 offshore market nh3 fuel demand. *HyInfra*, 1:1–21.

Samferdselsdepartementet (2019). Handlingsplan for infrastruktur for alternative drivstoff i transport. *Handlingsplan*, 1:55–56.

Ship & Bunker (2022). Average bunker prices. `https://shipandbunker.com/prices/av`. Accessed: 2022-05-12.

Skatteetaten (2022). Nox-avgift. `https://www.skatteetaten.no/bedrift-og-organisasjon/avgifter/saravgifter/om/nox/`. Accessed: 2022-03-17.

Solstad Offshore (2022). Maress. `maress.no`. Accessed: 2022-02-22.

SSB (2021). Utslipp til luft. `https://www.ssb.no/natur-og-miljo/forurensning-og-klima/statistikk/utslipp-til-luft`. Accessed: 2021-12-13.

Strande, T. N. (2018). Anchor handling tug supply: Is there a correlation between fuel consumption and rate levels? Master's thesis, University of South-Eastern Norway.

Strømgren, T., Aarskog, F. G., Danebergs, J., and Ulleberg, Ø. (2020). Energy and cost analysis of a hydrogen driven high speed passenger ferry. *International Shipbuilding Progress*, 67(1):97–123.

Sundvor, I., Thorne, R. J., Danebergs, J., Aarskog, F., and Weber, C. (2021). Estimating the replacement potential of norwegian high-speed passenger vessels with zero-emission solutions. *Transportation Research Part D: Transport and Environment*, 99:103019.

Tarasov, B., Lototskii, M., and Yartys, V. (2007). Problem of hydrogen storage and prospective uses of hydrides for hydrogen accumulation. *Russian journal of general chemistry*, 77(4):694–711.

Teknisk Ukeblad (2022). Nullutslippsdrivstoff – noen retninger peker seg ut. `https://www.tu.no/artikler/nullutslippsdrivstoff-noen-retninger-peker-seg-ut/518900?key=3q3t0Fcr`. Accessed: 2022-04-26.

The Economist (2021). Hydrogen: Fuel of the future? - The economist. `https://www.youtube.com/watch?v=fkX-H24Chfw&ab_channel=TheEconomist`. Accessed: 2021-10-09.

The Norwegian Government (2020). The norwegian government's hydrogen strategy. `https://www.regjeringen.no/en/dokumenter/the-norwegian-governments-hydrogen-strategy/id2704860/`. Accessed: 2021-10-19.

Thompson, S. T., James, B. D., Huya-Kouadio, J. M., Houchins, C., DeSantis, D. A., Ahluwalia, R., Wilson, A. R., Kleen, G., and Papageorgopoulos, D. (2018). Direct hydrogen fuel cell electric vehicle cost analysis: System and high-volume manufacturing description, validation, and outlook. *Journal of Power Sources*, 399:304–313.

Toyota (2022). 2022 mirai, full specs. `https://www.toyota.com/mirai/features/mpg/3002`. Accessed: 2021-12-14.

Tronstad, T., Åstrand, H. H., Haugom, G. P., and Langfeldt, L. (2017). Study on the use of fuel cells in shipping. *EMSA European Maritime Safety Agency*, pages 1–108.

UMOE Advanced Composites (2022). Transport modules for hydrogen. `https://www.uac.no/container-transportation-solutions/hydrogen/`. Accessed: 2022-03-10.

United Nations (2022). What are the sustainable development goals? `https://www.undp.org/`. Accessed: 2022-03-03.

United Nations Industrial Development Organization (2018). Towards hydrogen societies: Expert group meeting. *Current advancements in hydrogen technology and pathways to deep decarbonisation*, 12(1):5–6.

U.S Department of Energy (2017). Hydrogen storage. *Energy Efficiency and Renewable Energy*, 2(1):1–2.

US Drive (2016). Hydrogen delivery technical team roadmap. *Driving Research and Innovation*.

Valland, A. (2020). End-user assessment for hydrogen as fuel. *OHC HyInfra*, 1:1–17.

Veson Nautical (2022). Nautical distance tables. `https://www.veslink.com/distances/`. Accessed: 2022-04-26.

Vesselfinder (2022). Vessels database. `https://www.vesselfinder.com/vessels`. Accessed: 2022-03-01.

Wilhelmsen (2020). Wilhelmsen's topeka hydrogen project awarded nok 219 million. `https://www.wilhelmsen.com/media-news-and-events/press-releases/2020/wilhelmsens-topeka-hydrogen-project-awarded-nok-219-million/`. Accessed: 2021-10-10.

Zumdahl, S. S. (2009). *Chemical Principles*. Cengage Learning.

Appendix A

Characteristics for vessels in database

Table A.1: OCV characteristics from database.

Num.	Year	GT [ton]	dwt [ton]	Length [m]	Width [m]
OCV1	2003	6689	4577	90	23
OCV2	2018	14908	9734	138	27
OCV3	2010	4323	6128	90	19
OCV4	2009	5903	4582	82	22
OCV5	2007	7617	4000	106	21
OCV6	2001	4456	4850	84	20
OCV7	2005	3187	3355	74	16
OCV8	2007	3203	3224	74	16
OCV9	2012	5773	4857	94	20
OCV10	2010	8246	5750	109	24
OCV11	2001	7941	5090	104	24
OCV12	2011	15183	9000	142	27
OCV13	2019	14957	12513	140	28
OCV14	2009	3131	3550	80	16
OCV15	2000	4641	3722	93	20
OCV16	2009	6802	3600	106	21
OCV17	2008	9074	6000	121	23
OCV18	2011	7386	3729	107	21
OCV19	2017	5883	2970	93	20
OCV20	2010	15183	9000	142	27
OCV21	2006	4454	4150	86	20
OCV22	2014	16954	13000	157	27
OCV23	2015	15008	9000	143	25
OCV24	2014	7885	5520	108	22
OCV25	2006	14506	9511	124	28
OCV26	1999	5913	5292	95	24
OCV27	2015	15008	9200	143	25
OCV28	2001	10979	9976	128	27
OCV29	2014	8973	4750	121	23
OCV30	2007	14161	14180	130	28
OCV31	2013	7403	7054	108	22
OCV32	2017	7652	4200	98	22
OCV33	2003	12913	8018	119	27
OCV34	2013	8594	5000	121	26

Continued on next page

Table A.1 – continued from previous page

Num.	Year	GT [ton]	dwt [ton]	Length [m]	Width [m]
OCV35	2014	8878	5251	121	27
OCV36	2013	8594	5000	121	26
OCV37	2014	8878	5253	121	27
OCV38	2009	4869	4257	94	20
OCV39	2008	11602	8700	120	25
OCV40	2010	10277	4900	122	23
OCV41	2011	8552	7000	98	20
OCV42	2016	5138	2632	88	22
OCV43	2016	5138	2426	88	22
OCV44	2013	7534	4500	91	22
OCV45	1999	7401	6350	103	22
OCV46	2015	19813	13500	147	35
OCV47	2013	11363	5125	107	25
OCV48	2008	9464	6200	109	23
OCV49	2008	6074	4900	95	20
OCV50	2009	4398	2325	85	19
OCV51	2017	23885	13574	160	32
OCV52	2011	11071	7250	120	23
OCV53	2009	9494	7800	132	22
OCV54	2008	18367	11366	157	28
OCV55	2014	18666	12182	146	31
OCV56	2011	16511	11300	157	27
OCV57	2008	5275	4665	104	20
OCV58	2012	4902	4857	94	20
OCV59	2012	4902	4857	94	20
OCV60	2009	6838	4925	94	23
OCV61	2007	6038	4900	95	21
OCV62	2008	6596	3900	106	21
OCV63	2015	5395	3100	93	19
OCV64	2020	11387	5866	123	25
OCV65	2008	12223	8200	116	25
OCV66	2014	6983	4600	103	21
Avg.	**2010**	**9264**	**6375**	**111**	**23**

Table A.2: PSV characteristics from database.

Num.	Year	GT [ton]	dwt [ton]	Length [m]	Width [m]
PSV1	2006	3760	4131	89	19
PSV2	2006	3760	4127	81	19
PSV3	2012	3966	4574	88	19
PSV4	2003	3285	4100	84	20
PSV5	2011	3959	4700	88	19
PSV6	2009	4469	5005	95	20
PSV7	2011	5054	5054	95	20
PSV8	2013	4365	2896	82	17
PSV9	2012	3958	4700	88	19
PSV10	2012	3588	3594	82	17
PSV11	2008	4859	4423	97	21
PSV12	2012	3788	3100	82	17

Continued on next page

Table A.2 – continued from previous page

Num.	Year	GT [ton]	dwt [ton]	Length [m]	Width [m]
PSV13	2003	3482	3933	86	20
PSV14	2005	3790	4847	86	19
PSV15	2008	4293	4678	91	19
PSV16	2006	3922	4779	89	19
PSV17	2012	4058	4400	89	19
PSV18	2008	2341	3205	73	17
PSV19	2006	2321	3230	73	17
PSV20	2006	2529	2927	73	17
PSV21	2009	2537	2930	73	17
PSV22	2009	495	581	50	11
PSV23	2019	3370	3821	84	18
PSV24	2015	3601	5154	87	19
PSV25	2015	1424	2068	61	15
PSV26	2008	1111	1674	58	15
PSV27	2015	1424	2049	61	15
PSV28	2007	1111	1783	58	15
PSV29	2019	4125	4200	86	18
PSV30	2014	1445	2049	61	15
PSV31	2009	2177	3279	74	16
PSV32	2014	1445	2068	61	15
PSV33	2017	1634	2252	67	15
PSV34	2015	3601	5116	87	19
PSV35	2019	4125	4200	86	18
PSV36	2019	4125	4200	86	18
PSV37	2018	3370	3948	84	17
PSV38	2016	1634	2252	67	15
PSV39	2019	4125	4545	86	18
PSV40	2004	1243	817	66	14
PSV41	2013	1445	2049	61	15
PSV42	2016	1634	2252	67	15
PSV43	2019	1634	2252	67	15
PSV44	2012	3601	5131	87	19
PSV45	2012	3601	5145	87	19
PSV46	2016	3638	4122	83	18
PSV47	2012	5280	4900	94	20
PSV48	2011	4258	4500	85	20
PSV49	2013	5335	4800	90	21
PSV50	2009	5211	5944	94	21
PSV51	2013	3527	4000	82	18
PSV52	2012	3527	4000	82	18
PSV53	2013	3527	4000	82	18
PSV54	2012	4590	5300	94	20
PSV55	2014	4007	4700	88	19
PSV56	2014	4007	4700	89	19
PSV57	2014	4007	4700	88	19
PSV58	2014	4007	4700	89	19
PSV59	2014	3455	4000	82	17
PSV60	2011	4258	4500	85	20
PSV61	2012	3527	4000	82	18
PSV62	2008	4755	5127	93	21
PSV63	2012	5370	5800	92	22
PSV64	2008	4755	5200	93	21
PSV65	2012	4059	4706	88	19
PSV66	2013	4059	4697	88	19

Continued on next page

Table A.2 – continued from previous page

Num.	Year	GT [ton]	dwt [ton]	Length [m]	Width [m]
PSV67	2014	3585	4078	85	18
PSV68	2015	3585	4054	85	18
PSV69	2015	3585	4089	85	18
PSV70	2015	3585	4103	85	18
PSV71	2017	3585	4078	85	18
PSV72	2017	3585	4065	85	18
PSV73	2018	3585	4045	85	18
PSV74	2018	3585	4052	85	18
PSV75	2018	3585	4049	85	18
PSV76	2014	5179	5263	97	20
PSV77	2014	5179	5263	97	20
PSV78	2006	2218	3250	73	16
PSV79	2008	2218	3250	73	16
PSV80	2013	3933	4700	88	19
PSV81	2014	3933	4700	88	19
PSV82	2015	5321	5071	89	19
PSV83	2014	4768	5500	89	19
PSV84	2016	4768	5500	89	19
PSV85	2012	3719	5125	87	19
PSV86	2012	3404	3691	76	18
PSV87	2005	2045	3462	77	17
PSV88	2015	3927	4662	84	18
PSV89	2009	2999	4820	85	18
PSV90	2009	2999	4725	85	18
PSV91	2004	3045	4381	85	18
PSV92	2009	2933	3790	79	18
PSV93	2012	4424	4976	93	20
PSV94	2011	3022	3683	80	18
PSV95	2008	4309	4800	94	20
PSV96	2009	3062	4100	80	18
PSV97	2013	4258	5509	84	20
PSV98	2015	3804	4000	82	18
PSV99	2013	3464	4000	82	17
PSV100	2013	3708	5053	87	19
PSV101	2016	3804	4000	82	18
PSV102	2014	5165	5098	97	20
PSV103	2008	6111	6200	92	21
PSV104	2012	5381	6150	90	24
PSV105	2012	5381	6150	90	21
PSV106	2009	6111	6200	92	21
PSV107	2004	6545	6200	92	20
PSV108	2013	4870	4944	92	21
PSV109	2007	3706	4081	86	20
PSV110	2009	3693	4000	86	20
PSV111	2011	4518	5100	95	20
PSV112	2014	4800	5733	90	20
PSV113	2014	4800	5761	90	20
PSV114	2011	3140	3000	80	16
PSV115	2012	5197	5066	94	20
PSV116	2014	3315	3750	84	17
PSV117	2012	4676	4750	96	20
PSV118	2012	4676	4750	96	20
PSV119	2014	5068	5300	97	20
PSV120	2015	5068	5300	97	20

Continued on next page

Table A.2 – continued from previous page

Num.	Year	GT [ton]	dwt [ton]	Length [m]	Width [m]
PSV121	2009	4608	4100	93	20
PSV122	2007	4382	4100	93	20
Avg.	**2012**	**3727**	**4231**	**84**	**18**

Table A.3: AHTS characteristics from database.

Num.	Year	GT [ton]	dwt [ton]	Length [m]	Width [m]
AHTS1	2014	6490	4000	84	23
AHTS2	2015	6490	4168	80	22
AHTS3	2010	6798	4252	90	23
AHTS4	2010	6798	4223	90	23
AHTS5	2006	5470	4029	89	21
AHTS6	2019	10181	4912	95	25
AHTS7	2017	10181	4905	95	25
AHTS8	2017	10181	4905	95	25
AHTS9	2018	10181	4912	95	25
AHTS10	2018	10181	4906	95	25
AHTS11	2008	4998	3411	73	20
AHTS12	2008	4678	3509	73	20
AHTS13	2009	4678	3518	73	20
AHTS14	2009	4678	3492	73	20
AHTS15	2011	7099	4700	95	24
AHTS16	2015	7334	4299	94	22
AHTS17	2010	8164	5750	109	24
AHTS18	2012	3181	3000	74	17
AHTS19	2006	3519	2600	80	18
AHTS20	2011	3181	3195	75	17
AHTS21	2007	3519	2600	80	18
AHTS22	2009	6838	4925	94	23
AHTS23	2013	8269	4000	94	24
AHTS24	2012	7099	4700	95	24
AHTS25	2010	2771	2250	74	17
AHTS26	2016	7334	4756	94	22
AHTS27	2007	3519	2600	81	18
AHTS28	2014	7334	4299	94	22
AHTS29	2004	3360	2240	76	18
AHTS30	2004	3360	2240	76	18
AHTS31	2013	2343	2100	69	15
AHTS32	2004	3254	2450	78	18
AHTS33	2006	2310	2100	67	15
AHTS34	2010	2343	2100	69	15
AHTS35	2006	2310	2396	67	15
AHTS36	2013	3208	3107	81	17
AHTS37	2013	3208	3124	81	17
AHTS38	2011	1678	1321	59	15
AHTS39	2011	1678	1337	59	15
AHTS40	2011	1678	1324	59	15
AHTS41	2012	1678	1327	59	15
AHTS42	2012	1678	1314	59	15

Continued on next page

Table A.3 – continued from previous page

Num.	Year	GT [ton]	dwt [ton]	Length [m]	Width [m]
AHTS43	2015	2281	1969	65	16
AHTS44	2010	8053	4724	95	24
AHTS45	2010	8053	4611	95	24
AHTS46	2007	7934	4559	89	22
AHTS47	2010	7480	4559	91	22
AHTS48	2009	6107	3900	87	21
AHTS49	2014	6170	4000	87	21
AHTS50	2013	6170	4028	87	21
AHTS51	2014	6170	3954	87	21
AHTS52	2009	6107	3880	87	21
AHTS53	2001	3170	2805	80	18
AHTS54	2005	2854	2400	78	17
AHTS55	2006	3628	2721	81	18
AHTS56	2007	7176	4800	93	22
AHTS57	2010	6107	3954	87	21
AHTS58	2013	6170	4015	87	21
AHTS59	2014	6641	4449	92	22
AHTS60	2013	6641	4523	92	22
AHTS61	2014	6641	4517	92	22
AHTS62	2014	6641	4518	82	22
AHTS63	2014	6641	4543	92	22
AHTS64	2013	6641	4547	92	22
AHTS65	2011	4566	3332	86	20
AHTS66	2007	2147	2485	66	16
AHTS67	2008	2147	2499	66	16
AHTS68	2008	2147	2306	66	16
AHTS69	2010	2147	2644	66	16
AHTS70	2008	2147	2467	66	16
AHTS71	2009	2147	2496	66	16
AHTS72	2002	2327	2355	69	16
AHTS73	2003	2332	2162	69	16
AHTS74	2002	1864	2116	64	15
AHTS75	2002	1864	2000	64	15
AHTS76	2011	7473	4250	91	22
AHTS77	2011	7473	4250	91	22
AHTS78	2010	7473	4250	91	22
AHTS79	2010	7473	4250	91	22
AHTS80	2009	7473	4250	91	22
AHTS81	2010	7473	4250	91	22
AHTS82	2010	7558	5250	91	22
AHTS83	2016	5733	3700	87	20
AHTS84	2009	5993	5190	106	22
AHTS85	2009	6455	3866	92	22
AHTS86	2011	2744	2488	70	17
AHTS87	2009	1951	1700	68	15
AHTS88	2010	2952	2193	75	17
AHTS89	2011	2763	2525	70	17
AHTS90	1999	2590	2854	74	17
AHTS91	2003	2263	1890	67	16
AHTS92	2011	8360	4800	95	24
AHTS93	2011	8360	4800	95	24
AHTS94	2007	5733	4229	86	22
AHTS95	2007	6335	5172	93	22

Continued on next page

Table A.3 – continued from previous page

Num.	Year	GT [ton]	dwt [ton]	Length [m]	Width [m]
Avg.	**2010**	**5149**	**3498**	**82**	**20**

Appendix B

Installed power as function of GT

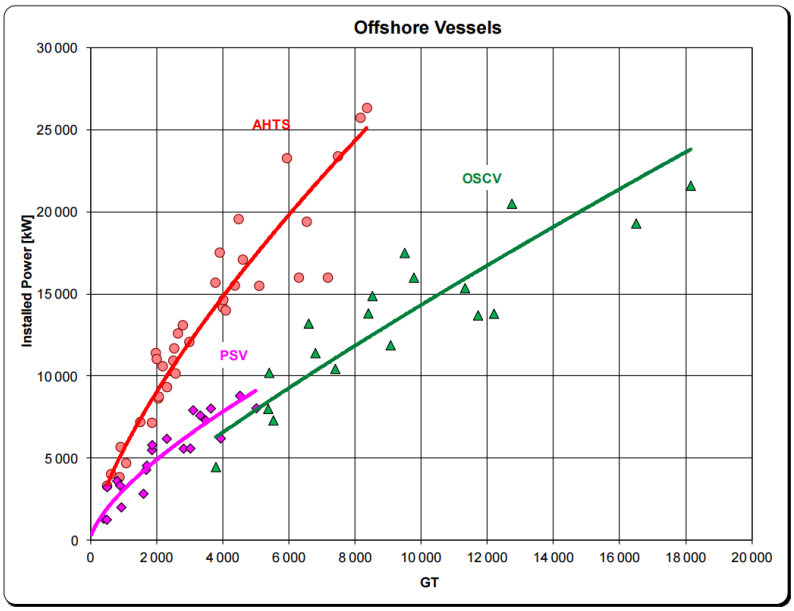

Figure B.1: Installed power as function of gt.

Source: [Erikstad and Levander, 2012]

Appendix C

Historical NOx taxes from 2018 to 2022

Table C.1: Historical NOx taxes from Skatteetaten [2022].

Year	**Tax** [NOK/kg NOx]
2018	21.94
2019	22.27
2020	22.69
2021	23.48
2022	23.79

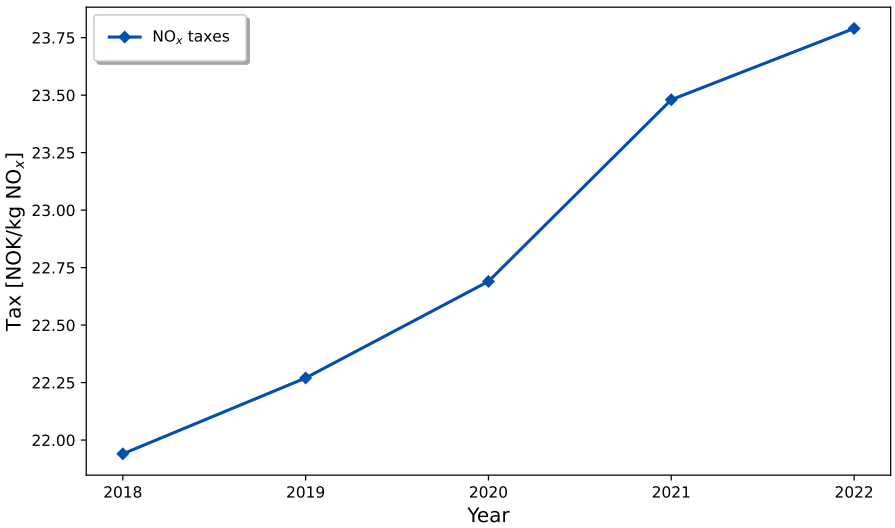

Figure C.1: Development of NOx tax prices from 2018 to 2022.

Appendix D

Analysis of operational profiles

Table D.1: Analysis of time spent in different operational modes from MARESS [Solstad Offshore, 2022].

	DP [%]	**Standby** [%]	**Transit** [%]	**Towing** [%]	**AH** [%]
OCV1	33	22	9	N/A	N/A
OCV2	53	2	24	N/A	N/A
OCV3	91	0	9	N/A	N/A
OCV4	39	2	31	N/A	N/A
OCV5	42	11	19	N/A	N/A
OCV6	21	22	35	N/A	N/A
OCV7	57	7	11	N/A	N/A
OCV8	22	10	27	N/A	N/A
OCV9	45	18	16	N/A	N/A
OCV10	52	12	12	N/A	N/A
Avg.	**46**	**11**	**19**	**N/A**	**N/A**
Std.	**20**	**8**	**9**	**N/A**	**N/A**
PSV1	20	24	37	N/A	N/A
PSV2	8	33	21	N/A	N/A
PSV3	22	30	14	N/A	N/A
PSV4	12	38	21	N/A	N/A
PSV5	26	24	20	N/A	N/A
PSV6	18	38	31	N/A	N/A
PSV7	20	26	34	N/A	N/A
PSV8	21	34	20	N/A	N/A
PSV9	10	46	21	N/A	N/A
PSV10	26	21	28	N/A	N/A
Avg.	**18**	**31**	**25**	**N/A**	**N/A**
Std.	**6**	**8**	**7**	**N/A**	**N/A**
AHTS1	8	30	19	1	9
AHTS2	4	13	15	1	14
AHTS3	10	10	20	2	6
AHTS4	4	39	19	6	5
AHTS5	8	32	13	11	7
AHTS6	14	33	24	0	7
AHTS7	12	41	23	2	3
AHTS8	9	41	17	2	11
AHTS9	28	24	19	8	9

Continued on next page

Table D.1 – continued from previous page

	DP [%]	Standby [%]	Transit [%]	Towing [%]	AH [%]
AHTS10	8	43	26	1	6
Avg.	**11**	**31**	**20**	**3**	**8**
Std.	**7**	**12**	**4**	**4**	**3**

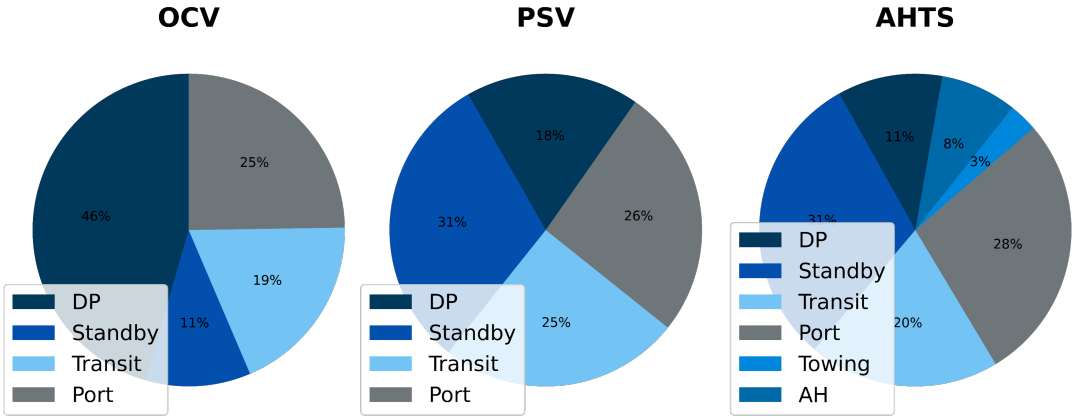

Figure D.1: Annual operational profile OSVs with time in port.

Appendix E

Analysis of specific fuel consumption

Table E.1: SFC for 15 arbitrary OCVs from MARESS, data from 2020 to 2022 Solstad Offshore [2022].

Vessel num.	**DP** [ton/day]	**Standby** [ton/day]	**Transit (11 kn)** [ton/day]
OCV1	16.21	14.34	34.48
OCV2	11.69	8.55	19.19
OCV3	8.47	7.77	24.03
OCV4	16.01	9.29	34.07
OCV5	22.13	10.61	27.37
OCV6	12.82	9.43	19.57
OCV7	15.64	14.11	20.48
OCV8	10.39	7.97	19.68
OCV9	14.27	12.40	38.07
OCV10	7.93	6.09	15.95
OCV11	6.86	5.31	15.16
OCV12	9.39	7.15	21.12
OCV13	11.81	11.42	17.00
OCV14	7.15	7.42	9.69
OCV15	9.56	6.86	16.00

Table E.2: SFC for 17 arbitrary PSVs from MARESS, data from 2020 to 2022 Solstad Offshore [2022].

Vessel num.	**DP** [ton/day]	**Standby** [ton/day]	**Transit (11 kn)** [ton/day]
PSV1	7.99	4.28	12.23
PSV2	5.41	3.70	11.06
PSV3	5.75	3.41	12.02
PSV4	8.00	5.01	12.25
PSV5	5.74	3.90	8.96
PSV6	5.74	3.57	9.60
PSV7	6.09	4.23	10.42
PSV8	6.35	4.90	11.17
PSV9	5.50	3.69	8.08
PSV10	6.64	3.65	8.82
PSV11	7.49	3.20	13.81
PSV12	5.67	3.68	11.32
PSV13	4.77	3.47	10.85
PSV14	5.96	4.68	10.94
PSV15	6.43	4.63	10.48
PSV16	7.27	5.03	14.02
PSV17	5.63	3.85	10.77

Table E.3: SFC for 12 arbitrary AHTS vessels from MARESS, data from 2020 to 2022 Solstad Offshore [2022].

Vessel num.	**DP** [ton/day]	**Standby** [ton/day]	**Transit (11 kn)** [ton/day]	**Towing** [ton/day]	**AH** [ton/day]
AHTS1	9.91	6.62	25.58	28.78	16.89
AHTS2	11.00	8.38	26.31	44.99	17.85
AHTS3	14.95	8.06	24.18	20.17	20.38
AHTS4	18.65	5.95	20.90	39.38	22.10
AHTS5	10.51	4.47	19.98	28.60	17.07
AHTS6	9.00	4.80	16.26	7.35	17.66
AHTS7	9.47	4.69	22.86	33.87	21.60
AHTS8	11.26	5.32	15.35	27.14	16.26
AHTS9	11.53	6.34	22.56	17.91	21.37
AHTS10	15.26	6.53	14.08	14.57	17.59
AHTS11	14.89	7.87	18.05	16.92	23.63
AHTS12	10.65	6.91	25.27	26.60	17.84

Appendix F

Analysis of tank sizes

Table F.1: Analysis of tank sizes.

Vessel num.	**Tanksize** [m3]
OCV1	1850
OCV2	3520
OCV3	2400
OCV4	1650
OCV5	1450
OCV6	2701
OCV7	3278
OCV8	1864
OCV9	2400
OCV10	1110
OCV11	1210
Avg.	**2130**
PSV1	1134
PSV2	1331
PSV3	1675
PSV4	877
PSV5	902
PSV6	1100
PSV7	897
PSV8	1098
PSV9	1400
PSV10	1300
PSV11	1076
Avg.	**1163**
AHTS1	1994
AHTS2	2006
AHTS3	1200
AHTS4	1210
AHTS5	1076
AHTS6	957
AHTS7	1213
AHTS8	985
AHTS9	957
AHTS10	998
AHTS11	1152

Continued on next page

Table F.1 – from prev. page

Vessel num.	**Tanksize [m3]**
Avg.	**1250**

Appendix G

Hydrogen storage characteristics from the industry

Table G.1: 40 ft container hydrogen storage characteristics from the industry [UMOE Advanced Composites, 2022] [Hexagon Purus, 2021].

Pressure [Bar]	**Total Storage Volume [m3]**	**Storage Capacity [kg]**	**Molar Volume [kmol/m3]**
		UMOE	
200	30.6	457	7.41
250	30.6	555	9.00
300	30.6	647	10.5
350	30.6	734	11.9
		Hexagon Purus	
300	39.9	847	10.5
318	39.9	889	11.1
381	39.9	1029	12.8

Appendix H

Resistance plots

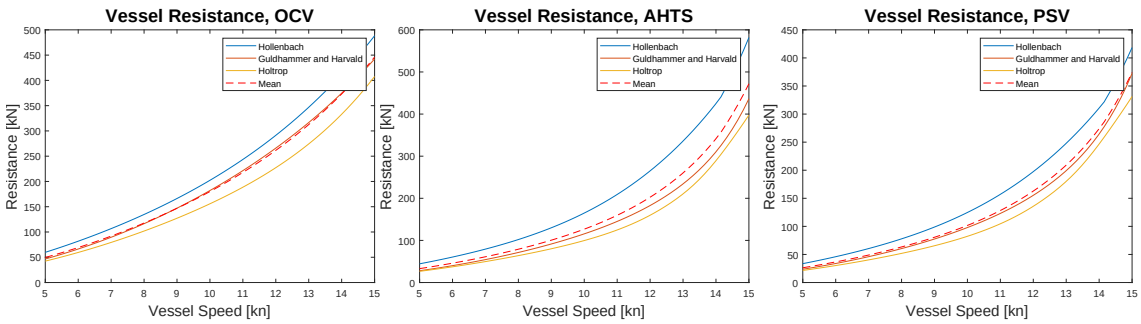

(a) OCV (b) AHTS (c) PSV

Figure H.1: Resistance as function of vessel speed.

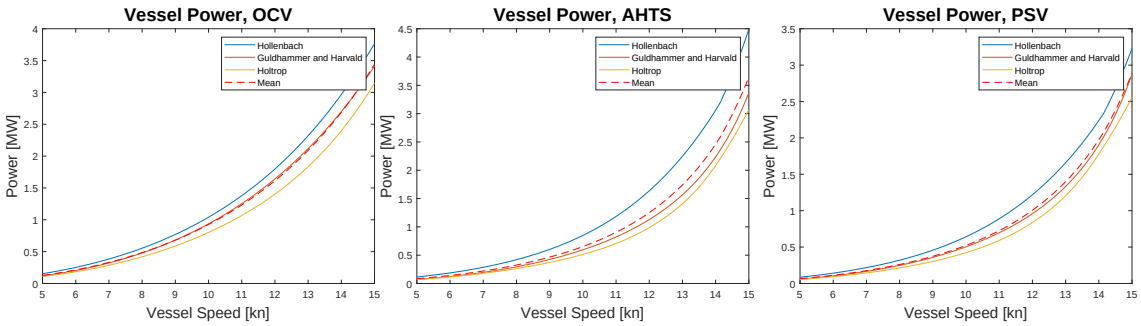

(a) OCV (b) AHTS (c) PSV

Figure H.2: Power as function of vessel speed.

Appendix I

Python functions to analyze AIS data

I.1 Open database and clean data

```python
# ==============================================================================

# Function that opens the database containing the AIS data. Input is the name of the database and the name of the vessel. Output is the data of the chosen vessel as a panda dataframe (df).

def readDatabase(dbName, vesselIn=None):
    # Connect to database
    dbPath = './Database/'  # The database has to be stored in
    # C:\Users\andre\OneDrive { NTNU\9. semester\projectThesis\Database!
    con = sqlite3.connect(dbPath + dbName)
    cur = con.cursor()

    # Check table names in db
    cur.execute('SELECT name from sqlite_master where type= "table"')
    vessels = cur.fetchall()
    print('There are ' + str(len(vessels)) + ' unique vessels in the database:')
    for vessel in vessels:
        v = functools.reduce(operator.add, vessel)
        print(' - ' + v)
    print('----------------------------')

    if vesselIn == None:
        # Ask user for which vessel to create heatmap from
        choice = selectVessel(vessels)  # Own function that asks user for input
        choice = functools.reduce(operator.add, choice)
    else:
        choice = vesselIn  # Possible to use MMSi number as input if desirable
    print('\n- You choosed: ' + str(choice))

    # Read data from selected table into a pandas dataframe
    string = 'SELECT * FROM ' + choice
    df = pd.read_sql(string, con)
    print('\n- Size of dataframe: ' + str(df.shape) + '\n')
```

```python

    # Changing the dtype from "object" to "datetime64"
    df['dt'] = pd.to_datetime(df['dt'])

    # Clean data: Lat and Lon values must be between -90 and 90, and -180 and 180.
    rows1 = df.shape[0]
    df.drop(df.index[df['lat'] <= -90.0 + 0.25], inplace=True)  # 0.25: isOnLand() function is searching an area of +/-
    df.drop(df.index[df['lat'] >= 90.0 - 0.25], inplace=True)   # 0.25 lat/lon around each input point!
    df.drop(df.index[df['lon'] <= -180.0 + 0.25], inplace=True)
    df.drop(df.index[df['lon'] >= 180.0 - 0.25], inplace=True)

    df.dropna()  # Deleting possible rows with zero data
    df.drop_duplicates()  # Deleting possible duplicate rows

    rows2 = df.shape[0]
    print('- Number of rows neglected: ' + str(rows1 - rows2) +
          ' (duplicates, zero-values, lat: [-90, 90], lon: [-180, 180])')

    del df['index']  # Remove the extra index column
    df.sort_values(by='dt', inplace=True)  # have to be sure that the data is sorted by date
    df.reset_index(drop=True, inplace=True)  # Reset the indexes

    return df, choice

# ==============================================================================
```

I.2 Speed profile

```python
# ==============================================================================

# Function that will take in a list of dataframes (each dataframe represents one route) and give a new updated
# list of dataframes as output. The updated list of dataframes is the same as input, but with extra columns added,
# speed, distance and deltaT.
def addSpeedDistanceColumn(listDFin):
    listDFout = list()  # create an empty list for output

    for dfi in listDFin:  # loop through all dataframes in the input list of dataframes

        d_vec = np.zeros(len(dfi.lat) - 1)    # preallocate vector to store distances for each dataframe (route)
        dt_vec = [None] * (len(dfi.lat) - 1)  # preallocate vector to store time between two data points
        for i in range(len(dfi.lat) - 1):  # Loop through all data points in the dataframe (Route), except the last one
            coord1 = dfi.lat[i], dfi.lon[i]
            coord2 = dfi.lat[i + 1], dfi.lon[i + 1]
```

```python

            # Calculate distance between data points in meters
            d_vec[i] = distance(coord1, coord2).m

            # Calculate time between data points
            deltaT = dfi.dt[i + 1] - dfi.dt[i]
            dt_vec[i] = deltaT.total_seconds()  # [s]

        # Now we have two vectors with distance and time between the points
        # then we can calculate the speed profile. Distance in meters and time in
        # seconds.
        v_vec = np.zeros(len(dfi.lat) - 1)     # preallocate vector to store speed as kn
        dt_vec_h = np.zeros(len(dfi.lat) - 1)  # preallocate vector to store time step as hours
        d_vec_nm = np.zeros(len(dfi.lat) - 1)  # preallocate vector to store distances in nm
        for i in range(len(dt_vec)):
            a = d_vec[i] / 1852      # [nm]
            b = dt_vec[i] / 60 / 60  # [h]
            dt_vec_h[i] = b
            d_vec_nm[i] = a
            v = a / b
            v_vec[i] = v

        v_vec = np.append(v_vec, 0)
        d_vec_nm = np.append(d_vec_nm, 0)
        dt_vec_h = np.append(dt_vec_h, 0)

        # Adding the new data as new columns in the dataframe
        dfi['Speed'] = v_vec        # [kn] Adding the calculated speeds to the new output dataframe as new column
        dfi['Distance'] = d_vec_nm  # [nm] Adding the distance to the new output dataframe as a new column
        dfi['deltaT'] = dt_vec_h    # [h] Adding the time between each datapoint into the dataframe as new column

        # Adding the new dataframe to the output list of dataframes
        listDFout.append(dfi)

    return listDFout

# ==============================================================================
```

I.3 Clean data

```python
# ==============================================================================

# This function will take in a list of dataframes and use the following columns:
# route number ('Route'), time ('dt') and speed ('Speed'). It will drop all data
```

```python
# rows with speeds larger than 25 kn and lower than 0 kn. After rows are
# neglected it will use another function, 'removeLargeTimeIntervals(dfi)', which
# loops through the dataframe again to see if it has intervals larger than 36000
# seconds (10 h). If large time intervals are found, the output will be:
# removeDataframe=True, False otherwise. When removeDataframe=True, the
# dataframe will be neglected and will not be used further in the analysis. A
# new dataframe will be created, (routeLenDF), this will contain the route
# number, length of the route, mean speed of the vessel on this route and the
# duration of the route as both a string and in seconds. In addition to this
# the function will have some additional outputs:
#   - numRoutes: Number of routes identified in AIS data set after cleanup is
#     finished.
#   - numRowsNeglectedSpeed: Number of rows neglected from the dataset because
#     of unrealistic speeds.
#   - numRoutesNeglectedTime: Number of routes neglected due to large time
#     intervals within the routes.
#   - listDFOut: Updated list of DF where large time intervals and unnatural
#     speeds are neglected.
def cleanSpeedDataframe(listDFspeed):
    listSizeStart = len(listDFspeed)
    print('- Size of listDF before speed- and time interval cleaning: ' + str(listSizeStart))
    listDFout = list()

    # Dataframe to store the lengths of the different routes
    routeLenDF = pd.DataFrame(
        columns=['route', 'length', 'meanSpeed', 'routeDuration', 'routeDuration_s'])

    # route:          [int]
    # length:         [nautical miles]
    # meanSpeed:      [knots]
    # RouteDuration:  [hours]

    numRowsSpeed = 0
    dfWithHighSpeed = 0
    for dfi in listDFspeed:
        # Find the route number for dataframe dfi
        routeNum = dfi.Route[0]
        numRowsBeforeSpeed = len(dfi)
        dfi = dfi[dfi.Speed < 25]  # Remove rows with speed values larger than 25 kn
        dfi = dfi[dfi.Speed >= 0]  # Remove rows with speed values lower than 0 kn
        numRowsAfterSpeed = len(dfi)
        rowsNeglected = (numRowsBeforeSpeed - numRowsAfterSpeed)
        if rowsNeglected > 0:
            dfWithHighSpeed += 1
        numRowsSpeed = numRowsSpeed + rowsNeglected   # Check how many rows neglected because of speed

        # Have to check the new time intervals, if they are too big the route is neglected
        removeDataframe = removeLargeTimeIntervals(dfi)

```

```
        # Calculate the duration of each route
        startTime = dfi['dt'].iloc[0]   # time
        endTime = dfi['dt'].iloc[-1]
        routeDuration = endTime - startTime
        totSeconds = routeDuration.total_seconds()
        days = routeDuration.days
        seconds = routeDuration.seconds
        hours = seconds//3600
        routeDurationString = str(days) + ' days, ' + str(hours) + ' hours'

        if removeDataframe == False:
            # Store route in a dataframe
            routeLenDF = routeLenDF.append({'route': routeNum, 'length': dfi['Distance'].sum(),
                                            'meanSpeed': dfi.Speed[:-1].mean(), 'routeDuration': routeDurationString,
                                            'routeDuration_s': totSeconds}, ignore_index=True)

            dfi.reset_index(drop=True, inplace=True)  # Need to reset the index for the dataframe

            # Adding the new dataframe to the output list of dataframes
            listDFout.append(dfi)

    # Sort the dataframe with the largest routes on top
    numRoutes = len(routeLenDF)
    listSizeEnd = len(listDFout)
    if numRoutes > 0:
        routeLenDF = routeLenDF.nlargest(numRoutes, 'length')
        print('- The speed cleanup [0kn, 20kn] neglected ' + str(numRowsSpeed) + ' row(s), from a total of '
              + str(listSizeStart) + ' different routes.')
        print('- The time interval cleanup neglected ' + str(listSizeStart - listSizeEnd) + ' route(s).')
    else:
        print('- All routes neglected in speed- and time interval cleanup! No more routes to investigate!')

    numRoutesNeglectedTime = listSizeStart - listSizeEnd  # Number of rows neglected because of too large time interval between datapoints

    routeLenDF.reset_index(drop=True, inplace=True)  # Need to reset the index for each dataframe

    return listDFout, routeLenDF, numRoutes, numRowsSpeed, numRoutesNeglectedTime

# ==========================================================================
```

I.4 Remove large time intervals

```python
# ==========================================================================

# Function that will take in a sorted dataframe containing a route and check if
# the data points does not have too large intervals between them. If dataframe
# has points with more than 10 hours between --> removeDataframe = True
def removeLargeTimeIntervals(routeDF):
    removeDataframe = False
    s = routeDF['dt'].diff().apply(lambda x: x/np.timedelta64(1, 's')).fillna(0).astype('int64')
    if (s > 43200).any():  # 6 hours = 21600 seconds, 10 hours = 36000, 24 hours = 86400, 48 hours = 172800
        removeDataframe = True
    return removeDataframe

# ==========================================================================
```

I.5 Classification of data points

```python
# ==========================================================================

# Function that will take in the AIS data and evaluate all points and classify
# them into two categories: offshore and nearshore points.
def classifyPoints(df):
    offshoreMat = []   # the first zero-row is deleted after for-loop!
    nearshoreMat = []  # the first zero-row is deleted after for-loop!
    classify = []

    # Loop through dataframe and check every point if it is nearshore or offshore
    for row in df.itertuples():
        lat = getattr(row, 'lat')
        lon = getattr(row, 'lon')

        if isOnLand(lat, lon):  # See function isOnLand()
            nearshoreMat.append([lat, lon])
            classify.append("Nearshore")
        else:
            offshoreMat.append([lat, lon])
            classify.append("Offshore")

    # Adding the information of the point in the original dataframe
    df['Class'] = classify
    nearshoreDF = pd.DataFrame(nearshoreMat, columns=['lat', 'lon'])
    offshoreDF = pd.DataFrame(offshoreMat, columns=['lat', 'lon'])

    return df, nearshoreDF, offshoreDF


# ==========================================================================
```

I.6 Identify nearshore points

```python
# ==============================================================================

# Function that takes in coordinates (lat, lon) and evaluates if a point is
# nearshore or offshore. The nearshore distance is defined as a circle around
# the original point with radius of 0.25 degrees. n is the number of points
# on the circle to be checked. If one of the points on the circle is on land
# the point will be defined as a nearshore point --> isNearShore = True
def isOnLand(lat, lon, r=0.25, n=8):
    pMat = np.zeros((n, 2))  # col1 = Latitude, col2 = Longitude
    isNearShore = False
    dTheta = np.pi*2/n
    startTheta = 0

    # Create n points in circle with radius r around input point
    for i in range(n):
        pMat[i][0] = lat + np.sin(startTheta)*r  # Lat
        pMat[i][1] = lon + np.cos(startTheta)*r  # Lon
        if globe.is_land(pMat[i][0], pMat[i][1]):  # Check every point in pMat if it is on land
            isNearShore = True
        startTheta += dTheta

    return isNearShore
```

I.7 Establish routes

```python
# ==============================================================================

# Function that will loop through all rows in dataframe and identify the
# different routes.
def findRoutes(df):
    routesDF = pd.DataFrame(columns=['dt', 'lat', 'lon', 'Class', 'Route']) # Creating an empty dataframe to store the startpoints

    startPointVec = []

    numRoutes = 0

    for row in df[:-1].itertuples():  # Loops through the whole dataframe except the last point

        # When the iteration reach a nearshore point we want to find the route it travels until it
        # reaches a nearshore point again
        if row.Class == 'Nearshore' and df.loc[row.Index + 1, 'Class'] == 'Offshore':
            numRoutes += 1  # Every time this is satisfied we get a new route
            startPointVec.append(row.Index)  # Add the index for the startpoint into a vector
            countIndex = row.Index + 1   # Next point
```

```
            nextPointClass = df.loc[countIndex, 'Class']

            # Store route in a dataframe
            routesDF = routesDF.append({'dt': row.dt, 'lat': row.lat, 'lon': row.lon, 'Class': row.Class, 'Route': numRoutes}, ignore_index=True)

            # Now we want to loop from the indexcount until we get a new nearshore point, this will be one route
            while nextPointClass == 'Offshore' and countIndex < len(df.index)-1:
                routesDF = routesDF.append({'dt': df.loc[countIndex, 'dt'], 'lat': df.loc[countIndex, 'lat'], 'lon': df.loc[countIndex, 'lon'], 'Class': df.loc[countIndex, 'Class'], 'Route': numRoutes},
                                           ignore_index=True)

                countIndex += 1
                nextPointClass = df.loc[countIndex, 'Class']

            routesDF = routesDF.append({'dt': df.loc[countIndex, 'dt'], 'lat': df.loc[countIndex, 'lat'], 'lon': df.loc[countIndex, 'lon'], 'Class': df.loc[countIndex, 'Class'], 'Route': numRoutes}, ignore_index=True)

    # Create a dataframe for each route and store them in a list of dataframes
    listDF = list()
    grouped = routesDF.groupby(routesDF.Route)
    for i in (n+1 for n in range(numRoutes)):  # i = 1,2,3 ... numRoutes
        dfIn = grouped.get_group(i)
        dfIn.reset_index(drop=True, inplace=True)  # Need to reset the index for each dataframe
        if len(dfIn) > 20:  # Need more than 20 points to be called a route
            listDF.append(dfIn)

    # Going through all dataframes to check that every route starts and stops with a nearshore point
    listDFout = list()
    for dfi in listDF:
        if dfi['Class'].iloc[0] == 'Nearshore' and dfi['Class'].iloc[-1] == 'Nearshore':
            listDFout.append(dfi)

    return listDFout  # List of dataframes with lat,lon,class and route classification


# ==============================================================================
```

I.8 Theoretical sailing distance

```
# ==============================================================================

# Function that calculates the theoretical maximum sailing distance for each
```

```python
# vessel type, based on fuel type, transit speed and tank capacity.
def sailingDistance(largestDist=1000, vesselType='OCV'):

    # Ask user for what plots he/she wants
    values = selectDistancePlots()

    # Plotting colors
    colors = ['#00395C', '#024FAD', '#73C3F5', '#6E767A', '#0087DB', '#0069A8', '#4D5763']

    # Getting the necessary information from csv-files.
    # These functions opens the different csv files.
    fuelMat = fuelParameters()
    transPowMat = transitPower()
    tanksizeMat = tankSize()
    loadProfileMat = loadProfiles()
    operationalProfilesMat = operationalProfiles()

    # Assume a efficiency of FuelCell and Diesel Engine
    effFuelCell = 0.5  # From Aarskog et al.
    effEngine = 0.37   # From Aarskog et al.

    # Use loss in energy due to storage of hydrogen
    eta1loss = 1.00     # [-] Loss in energy due to compressing hydrogen to 1MPa
    eta10loss = 0.95    # [-] Loss in energy due to compressing hydrogen to 1MPa
    eta100loss = 0.95   # [-] Loss in energy due to compressing hydrogen to 10MPa
    eta300loss = 0.90   # [-] Loss in energy due to compressing hydrogen to 30MPa
    eta400loss = 0.89   # [-] Loss in energy due to compressing hydrogen to 40MPa
    eta700loss = 0.85   # [-] Loss in energy due to compressing hydrogen to 70MPa
    etaLiqloss = 0.70   # [-] Loss in energy due to storing hydrogen as liquid

    # Placement in 3D matrix:
    """
    0. hydr_1bar
    1. hydr_10bar
    2. hydr_100bar
    3. hydr_300bar
    4. hydr_400bar
    5. hydr_700bar
    6. hydr_liq
    7. MDO
    """

    numFuelTypes = len(fuelMat)  # 8
    numSpeeds = len(transPowMat)  # 6

    # Adding all matrices into 3D matrix
    distanceMat = np.zeros((numFuelTypes, numSpeeds, 3))  # 8 [6x3] matrices | Speed | Max Dist. OCV |
    # Max Dist. PSV | Max Dist. AHTS |
    tankSizes = [1, 2, 3]
```

```
    for i in range(numFuelTypes):  # Going through all fuel types
        for j in range(numSpeeds):  # Going through all vessel speeds
            for k in tankSizes:  # Going through vessel types
                if i == 0:  # hydr_1bar
                    distanceMat[i, j, k - 1] = (tanksizeMat[0][k] * fuelMat[i][1] * effFuelCell * eta1loss *
                        transPowMat[j][0] * operationalProfilesMat[2][k]) / ((transPowMat[j][k] * operationalProfilesMat[2][k] +
                                loadProfileMat[1][k] * operationalProfilesMat[1][k] +
                                loadProfileMat[0][k] * operationalProfilesMat[0][k]) * (60 * 60))
                elif i == 1:  # hydr_10bar
                    distanceMat[i, j, k - 1] = (tanksizeMat[0][k] * fuelMat[i][1] * effFuelCell * eta10loss *
                                transPowMat[j][0] * operationalProfilesMat[2][k]) / ((transPowMat[j][k] * operationalProfilesMat[2][k] +
                                loadProfileMat[1][k] * operationalProfilesMat[1][k] +
                                loadProfileMat[0][k] * operationalProfilesMat[0][k]) * (60 * 60))
                elif i == 2:  # hydr_100bar
                    distanceMat[i, j, k - 1] = (tanksizeMat[0][k] * fuelMat[i][1] * effFuelCell * eta100loss *
                                transPowMat[j][0] * operationalProfilesMat[2][k]) / ((transPowMat[j][k] * operationalProfilesMat[2][k] +
                                loadProfileMat[1][k] * operationalProfilesMat[1][k] +
                                loadProfileMat[0][k] * operationalProfilesMat[0][k]) * (60 * 60))
                elif i == 3:  # hydr_300bar
                    distanceMat[i, j, k - 1] = (tanksizeMat[0][k] * fuelMat[i][1] * effFuelCell * eta300loss *
                                transPowMat[j][0] * operationalProfilesMat[2][k]) / ((transPowMat[j][k] * operationalProfilesMat[2][k] +
                                loadProfileMat[1][k] * operationalProfilesMat[1][k] +
                                loadProfileMat[0][k] * operationalProfilesMat[0][k]) * (60 * 60))
                elif i == 4:  # hydr_400bar
                    distanceMat[i, j, k - 1] = (tanksizeMat[0][k] * fuelMat[i][1] * effFuelCell * eta400loss *
                                transPowMat[j][0] * operationalProfilesMat[2][k]) / ((transPowMat[j][k] * operationalProfilesMat[2][k] +
```

```
                                        loadProfileMat[1][k] * operationalProfilesMat[1][k] +
                                        loadProfileMat[0][k] * operationalProfilesMat[0][k]) * (60 * 60))
                elif i == 5:  # hydr_700bar
                    distanceMat[i, j, k - 1] = (tanksizeMat[0][k] * fuelMat[i][1] * effFuelCell * eta700loss *
                                        transPowMat[j][0] * operationalProfilesMat[2][k]) / ((transPowMat[j][k] * operationalProfilesMat[2][k] +
                                        loadProfileMat[1][k] * operationalProfilesMat[1][k] +
                                        loadProfileMat[0][k] * operationalProfilesMat[0][k]) * (60 * 60))
                elif i == 6:  # hydr_liquid
                    distanceMat[i, j, k - 1] = (tanksizeMat[0][k] * fuelMat[i][1] * effFuelCell * etaLiqloss *
                                        transPowMat[j][0] * operationalProfilesMat[2][k]) / ((transPowMat[j][k] * operationalProfilesMat[2][k] +
                                        loadProfileMat[1][k] * operationalProfilesMat[1][k] +
                                        loadProfileMat[0][k] * operationalProfilesMat[0][k]) * (60 * 60))
                else:  # MDO_diesel
                    distanceMat[i, j, k - 1] = (tanksizeMat[0][k] * fuelMat[i][1] * effEngine *
                                        transPowMat[j][0] * operationalProfilesMat[2][k]) / ((transPowMat[j][k] * operationalProfilesMat[2][k] +
                                        loadProfileMat[1][k] * operationalProfilesMat[1][k] +
                                        loadProfileMat[0][k] * operationalProfilesMat[0][k]) * (60 * 60))

    return distanceMat

# ==========================================================================

# Function that gets all necessary information about different vessel fuels from csv-files
def fuelParameters():
    # The source for these values is Aarskog et al. and own calculations

    # Read data from CSV file
    dfFuel = pd.read_csv('fuelParameters.csv')
    fuelMat = dfFuel.to_numpy()  # | fueltype | MJ/m3 |
    return fuelMat

# ==========================================================================
```

```python

# Function that collects all necessary information about the transit power consumption for all vessel types
def transitPower():
    # The resistance is calculated by using the mean of Holtrop-, Hollenbach- and Guldhammer method in combination
    # with values from background study

    # Read data from CSV file
    dfTransitPower = pd.read_csv('transitPower.csv')
    transPowMat = dfTransitPower.to_numpy()  # | Speed [kn] | OCV [MW] | PSV [MW] | AHTS [MW] |

    return transPowMat

# ==============================================================================

# Function that collects the load profiles of each vessel type from csv files
def loadProfiles():
    # The source for the values in the csv files are gathered from an analysis in the MARESS database from
    # Solstad Offshore

    # Read data from CSV file, OCV
    dfLoadProfile = pd.read_csv('loadProfile.csv')
    loadProfileMat = dfLoadProfile.to_numpy()  # | Mode | Power OCV [MW] | Power PSV [%] | Power AHTS [%] |

    return loadProfileMat

# ==============================================================================
# Function that gets all necessary information about the operational profiles for the different vessel types
# from csv-files
def operationalProfiles():
    # The source for the values in the csv files are gathered from an analysis in the MARESS database from
    # Solstad Offshore

    # Read data from CSV file
    dfOperationalProfiles = pd.read_csv('operationalProfile.csv')
    operationalProfilesMat = dfOperationalProfiles.to_numpy()  # | Mode | OCV Time [%] | PSV Time [%] | AHTS Time [%] |
    return operationalProfilesMat

# ==============================================================================

# Function that takes in the fueltank sizes of the different vessel types
def tankSize():

    # Read data from CSV file
    dfTanksize = pd.read_csv('tankSizes.csv')
    tanksizeMat = dfTanksize.to_numpy() # | Index | OCV [m3] | PSV [m3] | AHTS [m3] |
    return tanksizeMat
```

Appendix J

Input files for calculating theoretical sailing distance

J.1 fuelParameters.csv

Table J.1: Fuel parameters used to calculate D_{max}.

Fueltype	MJ/m^3
Hydrogen,1bar	9.3
Hydrogen,10bar	91.7
Hydrogen,100bar	871
Hydrogen,300bar	2340
Hydrogen,400bar	2970
Hydrogen700bar	4540
Hydrogen,liquid	8000
MDO	36100

J.2 transitPower.csv

Table J.2: Transit power for calculating D_{max}.

Speed [kn]	**OCV** [MW]	**PSV** [MW]	**AHTS** [MW]
5	0.4	0.19	0.36
7	1.1	0.49	0.93
9	2.2	1.0	2.0
11	4.0	2.0	3.8
13	6.8	3.9	7.3
15	11	8	15

J.3 loadProfile.csv

Table J.3: Load profiles used for calculating D_{max}.

Mode	**Power OCV** [MW]	**Power PSV** [MW]	**Power AHTS** [MW]
DP	2.3	1.1	2.2
Standby	1.7	0.74	1.2
Towing	N/A	N/A	4.7
AH	N/A	N/A	3.5

J.4 operationalProfile.csv

Table J.4: Operational profiles used for calculating D_{max}.

Mode	**OCV Time** [-]	**PSV Time** [-]	**AHTS Time** [-]
DP	0.60	0.25	0.15
Standby	0.14	0.42	0.43
Transit	0.26	0.33	0.27
Towing	N/A	N/A	0.05
AH	N/A	N/A	0.11

J.5 tanksizes.csv

Table J.5: Tank sizes for calculating D_{max}.

OCV [m^3]	**PSV** [m^3]	**AHTS** [m^3]
2130	1163	1250

Appendix K

Speed profiles of database

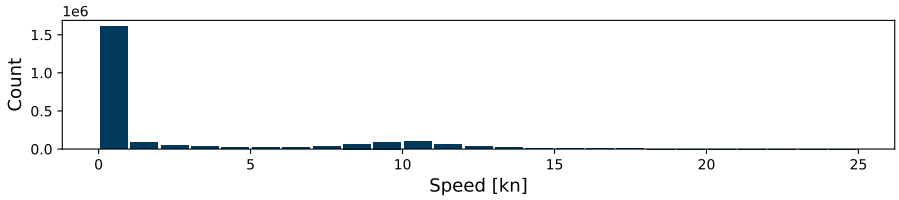

(a) OCV

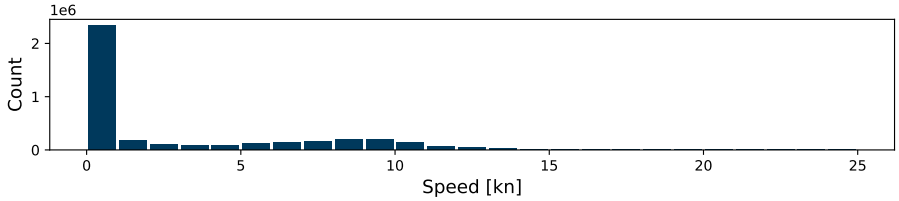

(b) PSV

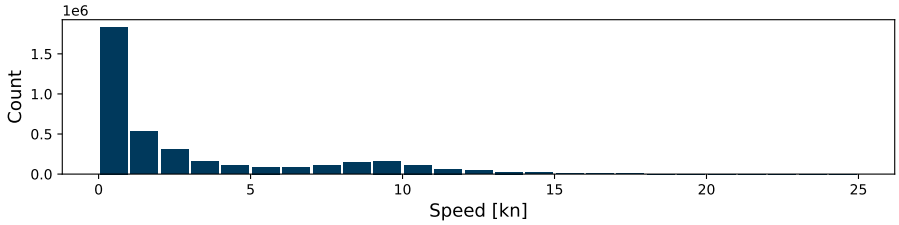

(c) AHTS

Figure K.1: Total speed profiles for the different vessel types.

Appendix L

Theoretical sailing distances - fuel types

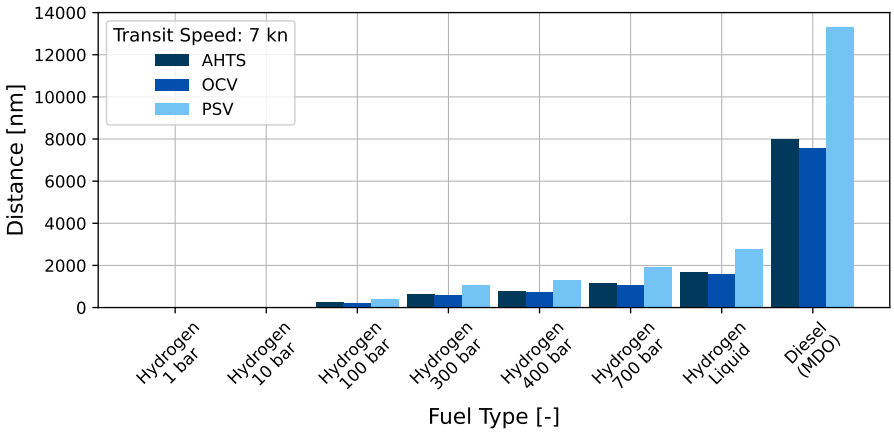

Figure L.1: D_{max} with transit speed of 7 kn.

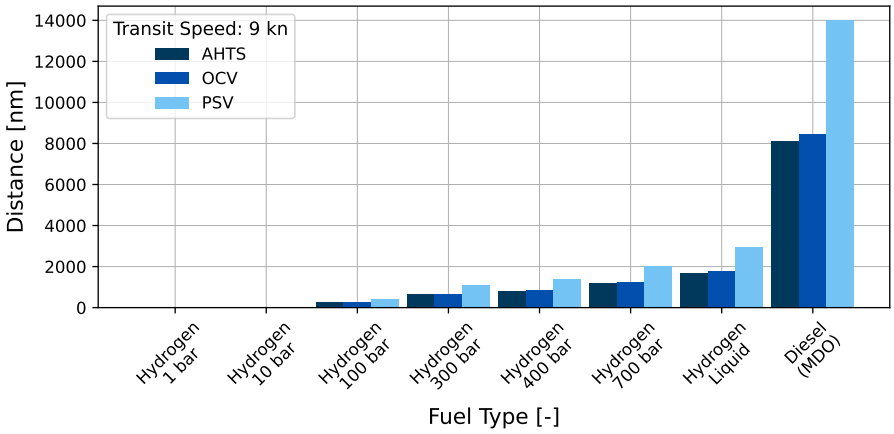

Figure L.2: D_{max} with transit speed of 9 kn.

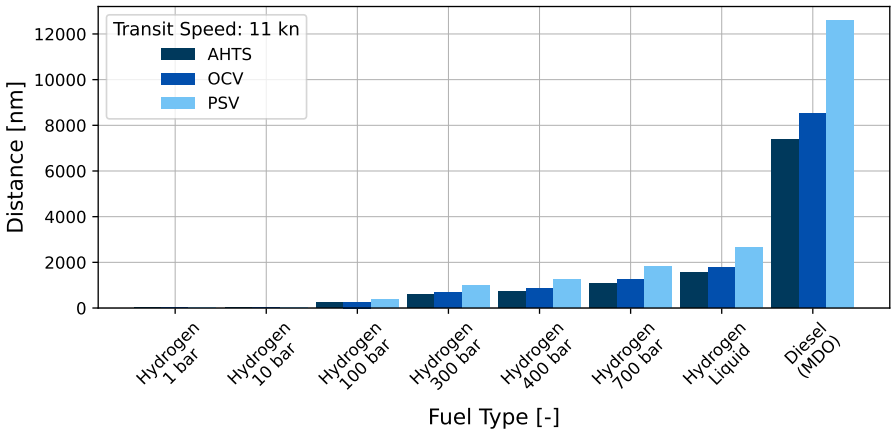

Figure L.3: D_{max} with transit speed of 11 kn.

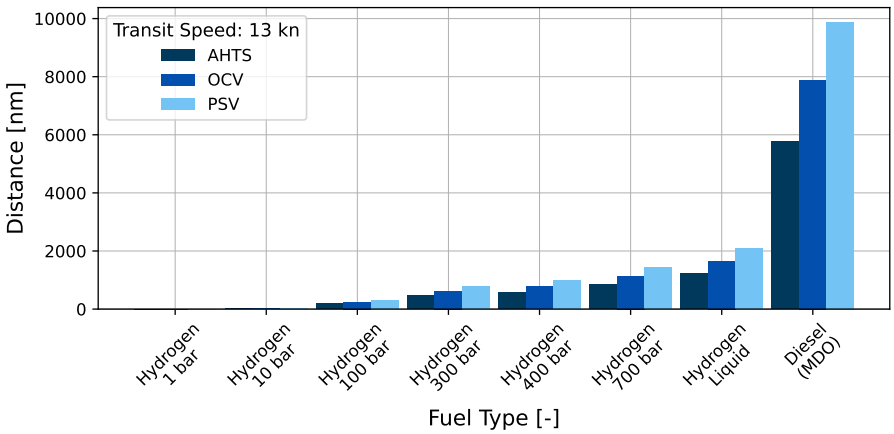

Figure L.4: D_{max} with transit speed of 13 kn.

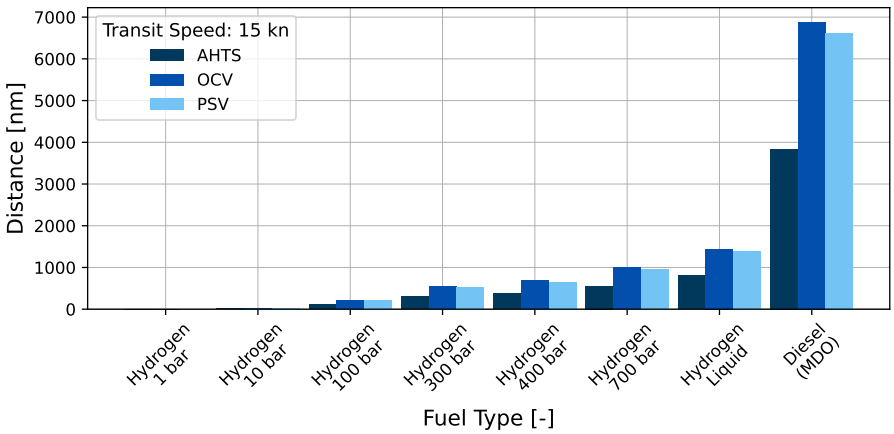

Figure L.5: D_{max} with transit speed of 15 kn.

Appendix M

Theoretical sailing distances - transit speeds

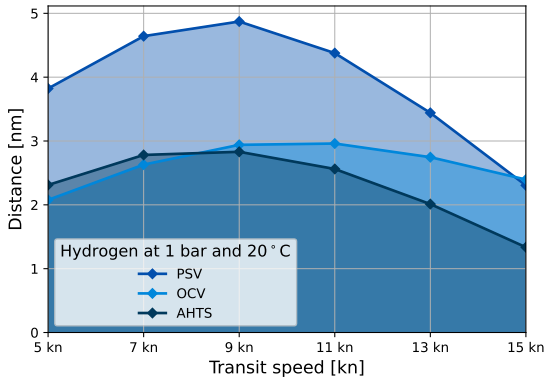

(a) Hydrogen 1 bar.

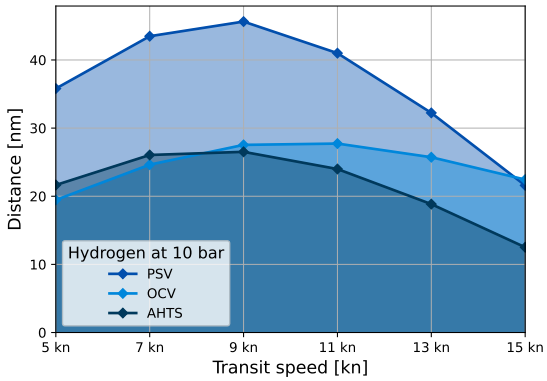

(b) Hydrogen 10 bar.

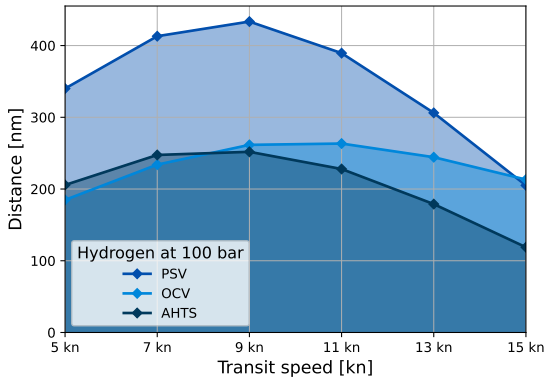

(c) Hydrogen 100 bar.

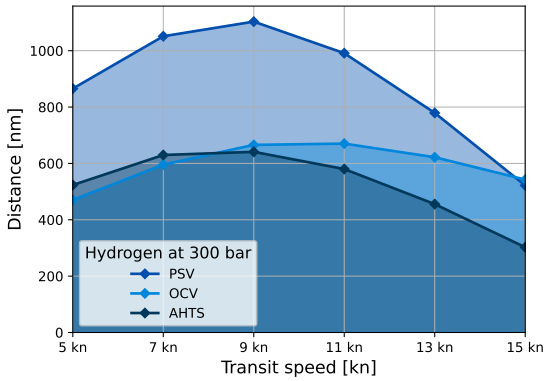

(d) Hydrogen 300 bar.

Figure M.1: D_{max} as function of transit speed (1).

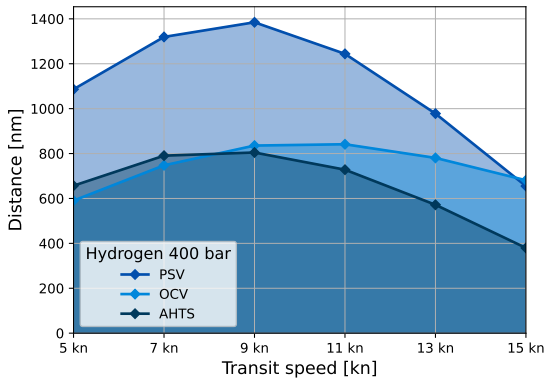

(a) D_{max} for hydrogen at 400 bar.

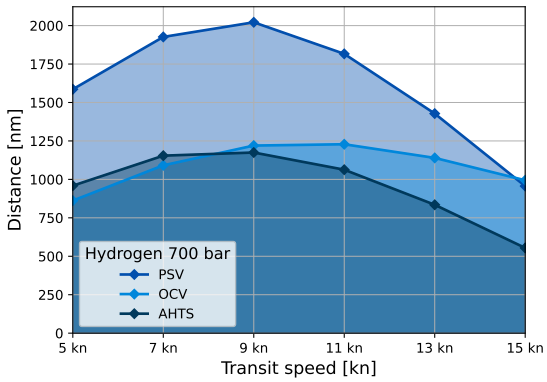

(b) D_{max} for hydrogen at 700 bar.

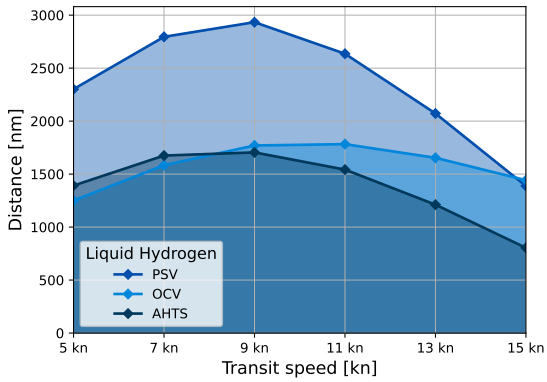

(c) D_{max} for LH_2.

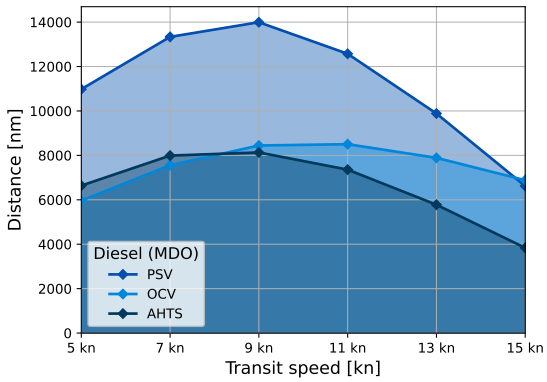

(d) D_{max} for diesel (MDO).

Figure M.2: D_{max} as function of transit speed (2).

Appendix N

AIS data coverage - Method 1

Table N.1: Route coverage with transit speed of 7 kn.

	OCV	**PSV**	**AHTS**
hydr. 1 bar	0.0%	0.0%	0.0%
hydr. 10 bar	0.0%	0.0%	0.0%
hydr. 100 bar	3.0%	45.1%	12.6%
hydr. 300 bar	31.8%	80.3%	42.1%
hydr. 400 bar	39.4%	83.6%	54.7%
hydr. 700 bar	59.1%	91.0%	70.5%
hydr. liq.	62.1%	95.1%	78.9%
MDO	100.0%	100.0%	100.0%

Table N.2: Route coverage with transit speed of 9 kn.

	OCV	**PSV**	**AHTS**
hydr. 1 bar	0.0%	0.0%	0.0%
hydr. 10 bar	0.0%	0.0%	0.0%
hydr. 100 bar	4.5%	46.7%	13.7%
hydr. 300 bar	34.8%	82.0%	43.2%
hydr. 400 bar	43.9%	84.4%	55.8%
hydr. 700 bar	59.1%	91.0%	70.5%
hydr. liq.	71.2%	95.1%	78.9%
MDO	100.0%	100.0%	100.0%

Table N.3: Route coverage with transit speed of 11 kn.

	OCV	**PSV**	**AHTS**
hydr. 1 bar	0.0%	0.0%	0.0%
hydr. 10 bar	0.0%	0.0%	0.0%
hydr. 100 bar	4.5%	39.3%	12.6%
hydr. 300 bar	34.8%	78.7%	38.9%
hydr. 400 bar	43.9%	82.8%	48.4%
hydr. 700 bar	59.1%	88.5%	68.4%
hydr. liq.	71.2%	95.1%	74.7%
MDO	100.0%	100.0%	100.0%

Table N.4: Route coverage with transit speed of 13 kn.

	OCV	**PSV**	**AHTS**
hydr. 1 bar	0.0%	0.0%	0.0%
hydr. 10 bar	0.0%	0.0%	0.0%
hydr. 100 bar	3.0%	24.6%	11.6%
hydr. 300 bar	33.3%	71.3%	30.5%
hydr. 400 bar	40.9%	78.7%	38.9%
hydr. 700 bar	59.1%	84.4%	55.8%
hydr. liq.	66.7%	91.8%	70.5%
MDO	100.0%	100.0%	98.9%

Appendix O

AIS data coverage - Method 2

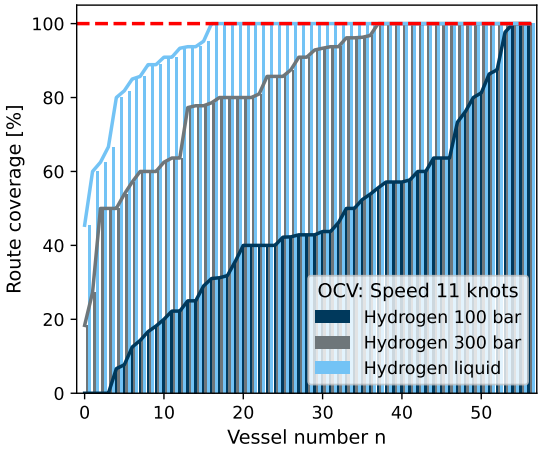

(a) OCV

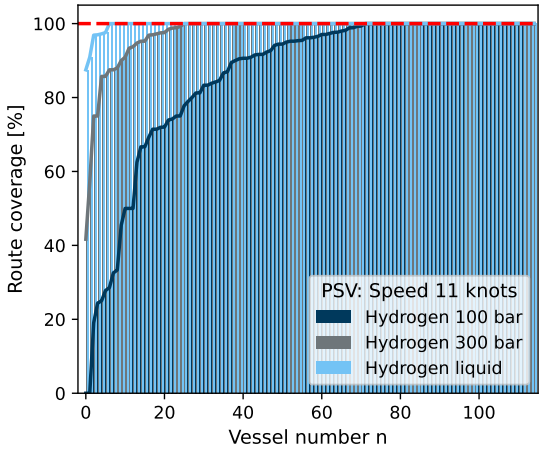

(b) PSV

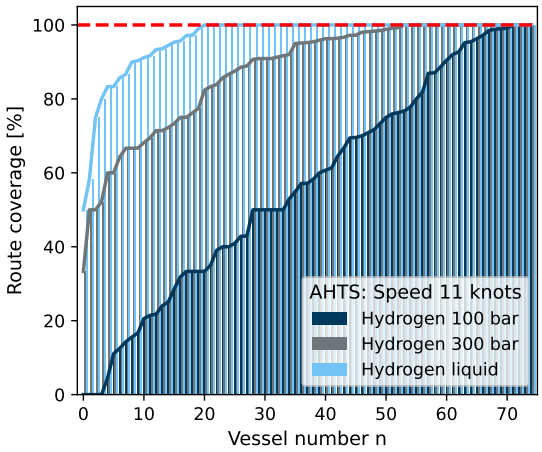

(c) AHTS

Figure O.1: Route coverage with transit speed of 11 knots and hydrogen at 100 bar, 300 bar and liquid.

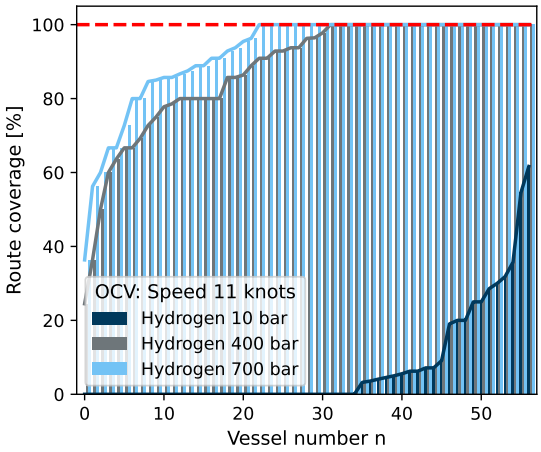

(a) OCV

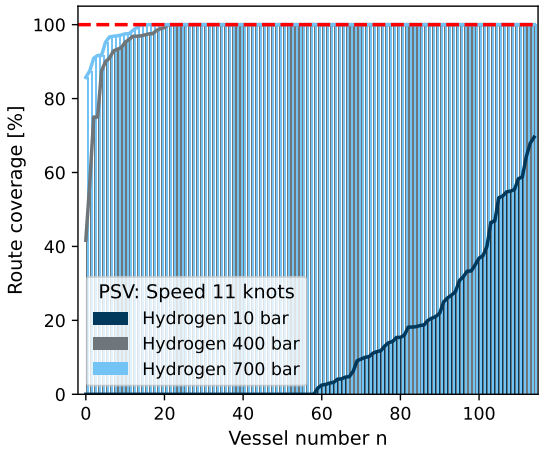

(b) PSV

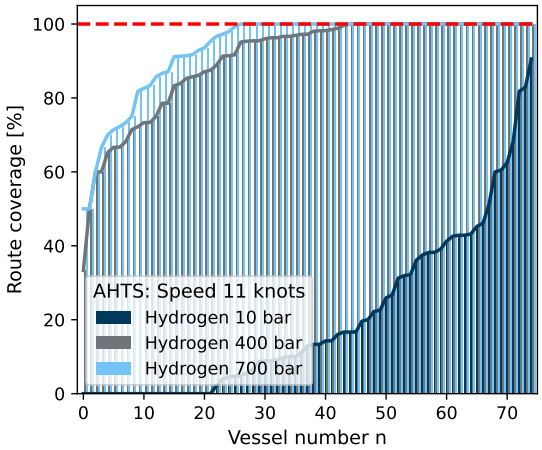

(c) AHTS

Figure O.2: Route coverage with transit speed of 11 knots and hydrogen at 10, 400 and 700 bar.

Andreas Isaksen

NTNU

Norwegian University of
Science and Technology